CRYSTAL STRUCTURE

OF AN

AMINOGLYCOSIDE 6'-*N*-ACETYLTRANSFERASE

By

LEANNE WYBENGA-GROOT, B.Sc.

A Thesis

Submitted to the School of Graduate Studies

in Partial Fulfillment of the Requirements

for the Degree

Master of Science

McMaster University

MASTER OF SCIENCE (1999) McMaster University
(Biochemistry) Hamilton, Ontario

TITLE: Crystal Structure of an Aminoglycoside 6'-*N*-Acetyltransferase

AUTHOR: Leanne Wybenga-Groot, B.Sc. (McMaster University)

SUPERVISOR: Dr. Albert M. Berghuis

NUMBER OF PAGES: xi, 116

Abstract

The overwhelming increase in antibiotic resistant bacterial strains poses a serious public health problem, with multiply-resistant strains becoming an important cause of mortality in hospitals. The predominant mechanism of resistance to aminoglycoside antibiotics involves enzymatic modification of the drug, rendering it ineffective. The crystal structure of the aminoglycoside-modifying enzyme aminoglycoside acetyltransferase(6')-Ii (AAC(6')-Ii) in complex with its cofactor, acetyl coenzyme A (AcCoA), was determined at 2.7 Å resolution by the multiwavelength anomalous diffraction technique. The resolution of this structure was subsequently extended to 2.15 Å by molecular replacement, with no significant changes in the topology of the complex. The enzyme was found to exhibit a novel CoA-binding fold, with the cofactor bound in a cleft between the N- and C-terminal arms of the protein molecule. Although the enzyme packs as a monomer in the $I4_132$ crystal form, the most probable physiological dimer of the complex was determined through analysis of a number of symmetry-related molecules.

The crystal structure of the AAC(6')-Ii•AcCoA complex was compared to the structures of three members of a large superfamily of GCN5-related *N*-acetyltransferases (GNATs), namely yeast histone acetyltransferase HAT1, *N*-myristoyltransferase, and aminoglycoside acetyltransferase(3)-Ia. Despite negligible sequence similarity between

these GNAT superfamily members, a distinct folding pattern is conserved in all four structures. This establishes AAC(6')-Ii as a structural homolog of enzymes with protein acetylating activity, supporting the hypothesis that the enzyme may possess another physiological function in *Enterococcus faecium*.

Acknowledgements

I would like to thank my supervisor, Dr. Albert Berghuis, for his support, assistance, and encouragement during my time in his laboratory. I appreciated his 'open-door policy' and enjoyed learning in a relaxed atmosphere. Dank U wel! I would also like to acknowledge my committee members, Drs. Gil Privé and Richard Epand, for their valuable input. Thank you also to Dr. Gerry Wright for his interest in my research; I appreciated his optimism and excitement. Thank you to my labmates, Byron De La Barre, Desirée Fong, Adelaine Leung, Laura Rossi, and Jeff Schwartzenhauer for their support, especially on trying and tiring synchrotron trips, and for being patient with me and my assertive personality. Thank you especially to Byron, not only for giving up synchrotron time for me, but also for the numerous times he offered his assistance and advice. I'm glad we ended on the same wavelength. Thank you also to Kari-ann Draker for keeping me up to speed on her research, and for helpful discussions. Best of luck with the continuation of the project!

I would also like to thank my parents for encouraging me to develop my God-given talents and teaching me to take pride in my work. Finally, thank you to my husband, Paul, for his continuous support and for taking my mind off Science more than once.

List of Abbreviations

AAC	aminoglycoside acetyltransferase
AcCoA	acetyl coenzyme A
AGAC	aminoglycoside-aminocyclitol
ANT	aminoglycoside nucleotidyltransferase
APH	aminoglycoside phosphotransferase
BNL	Brookhaven National Laboratory
CCD	charge coupled device
CCP4	collaborative computational project, number 4
CHESS	Cornell High-Energy Synchrotron Source
CoA	coenzyme A
DTDP	4,4'-dithiodipyridine
DTT	dithiothreitol
EDTA	ethylenediamine tetraacetic acid
GNAT	GCN5-related *N*-acetyltransferase
GRASP	Graphical Representation and Analysis of Surface Properties
HAT	histone acetyltransferase
HEPES	N-2-hydroxyethylpiperazine-N'-2-ethane sulfonic acid
LB	Luria broth
MAD	multiwavelength anomalous diffraction
MIC	minimal inhibitory concentration
MRSA	methicillin-resistant *Staphylococcus aureus*
NMT	*N*-myristoyl transferase
NSLS	National Synchrotron Light Source
OD	optical density
PMSF	phenylmethylsulfonyl fluoride
SDS-PAGE	sodium dodecyl sulfate polyacrylamide gel electrophoresis
SeMet	selenomethionyl
SHARP	Statistical Heavy Atom Refinement and Phasing
VRE	vancomycin resistant enterococcus

Table of Contents

List of Figures

Chapter 1

Chapter 2

Chapter 3

Chapter 4

List of Tables

Chapter 1 Introduction

1.1 Bacterial Resistance to Aminoglycoside Antibiotics

The overwhelming increase in antibiotic resistant bacterial strains poses an important public health problem. The development of antibiotic-resistant strains appears to be accelerating, and although the lack of global, and in many cases national, surveillance systems hampers quantification of the problem, the trend of increasing prevalence is evident (Travis, 1994; Williams & Heymann, 1998; Haley et al., 1982). Not only has the frequency and spectrum of antimicrobial-resistant infections increased in hospitals and communities (Cohen, 1992), but so has the number of bacteria that are resistant to multiple antibiotics (Williams & Heymann, 1998; Jacoby, 1996). The emergence of multiple-drug resistant bacterial strains such as *Serratia marcescens* (Schaberg et al., 1976), *Mycobacterium tuberculosis*, *Streptococcus pneumoniae*, *Staphylococcus aureus*, and *Enterococcus*, have left many drugs ineffective, resulting in essentially untreatable infections (Cohen, 1992; Murray, 1990). Consequently, epidemics have begun to occur both in the developing world and in institutional settings in the Western world (Cohen, 1992; Schaberg et al., 1976; Eliopoulos et al., 1988; Kingman, 1994). The problem is further complicated by the fact that a number of multiple-drug resistant organisms can be transmitted through indirect contact, such as

transient carriage on the hands of hospital personnel (Schaberg et al., 1976; Zervos et al., 1987). Interhospital transmission has been observed for multiply resistant *S. marcescens* (Schaberg et al., 1976), aminoglycoside-resistant Gram-negative bacilli (Weinstein & Kabins, 1981), methicillin-resistant *S. aureus* (MRSA) (Haley et al., 1982), and both gentamicin-resistant (Horodniceanu et al., 1979; Zervos et al., 1987) and vancomycin-resistant enterococci (VRE) (Jacoby, 1996). These nosocomial or hospital acquired pathogens are difficult to control, with MRSA endemic in many hospitals (Cohen, 1992). Both MRSA and enterococci often cause opportunistic infections, such as bacteremias, surgical wound infections, and urinary tract infections (Cohen, 1992; Murray, 1990). Since both pathogens are resistant to numerous antibiotics, an initial small infection could turn lethal for lack of effective drugs (Travis, 1994). As the morbidity and mortality rates, as well as health-care costs, increase as a result of antimicrobial-resistant infections, some members of the community fear that society is entering the post-antibiotic era (Williams & Heymann, 1998). For this reason it is essential that the problem be contained through the prudent use of existing agents, the control of spread, education, and the development of new, more effective agents (Williams & Heymann, 1998; Cohen, 1992; Neu, 1992; Travis, 1994).

Resistance to one type of antibiotic, the aminoglycoside-aminocyclitols (AGACs), has increased to the extent that resistance has been detected in all known hospital bacteria (Davies, 1991). These antibiotics, commonly referred to as aminoglycosides, constitute a large family of water soluble, cationic molecules that are relatively diverse in structure

except for the incorporation of a six-member aminocyclitol ring (Figure 1.1) (Wright et al., 1999). Members of the group are divided into three structural classes; the 4,5-disubstituted deoxystreptamines, the 4,6-disubstituted deoxystreptamines, and others (Table 1.1) (Davies, 1991). Accordingly, the first two types of compounds incorporate a 2-deoxystreptamine ring that can be substituted at positions 4 and 5 or 4 and 6, respectively, while the third group of compounds does not contain a 2-deoxystreptamine ring. Substituents on the 6-aminohexose attached by a glycosidic linkage to the 4-position are typically numbered 1' to 6', whereas the hexose or pentose ring linked to position 5 or 6 is designated by a double prime (reviewed in Davies, 1991 and Wright et al., 1999). The majority of AGACs are natural products produced primarily by actinomycetes (bacteria) of the *Streptomyces* genus. However, a few are produced by *Micromonospora* spp. or *Bacillus* spp., while several others, such as amikacin and netilmicin, are actually semisynthetic derivatives of naturally occurring compounds (Table 1.1) (reviewed in Davies, 1991 and Wright et al., 1999).

4,5-Disubstituted Deoxystreptamines	4,6-Disubstituted Deoxystreptamines	Others
Butirosin	Amikacin*	Apramycin
Lividomycin	Dideoxykanamycin B*	Fortimicin
Neomycin	Gentamicins C_{1a}, C_1, C_2	Hygromycin
Paromomycin	Isepamicin*	Streptomycin
Ribostamycin	Kanamycins A, B, C	Spectinomycin
	Netilmicin*	
	Sisomicin	
	Tobramycin	

Table 1.1 Classes of aminoglycoside-aminocyclitol antibiotics.
*Semisynthetic (not naturally occurring). Information obtained from references Davies, 1991 and Wright et al., 1999.

(a)

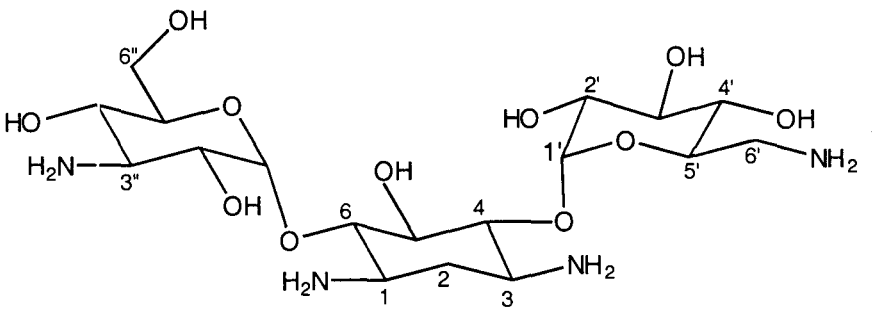

(b)

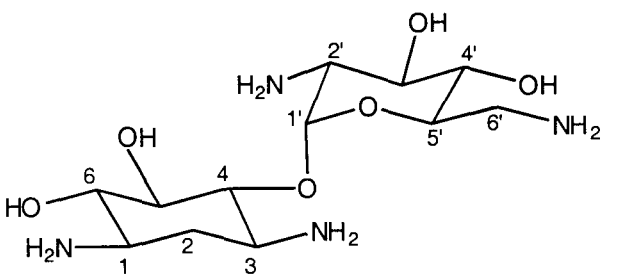

(c)

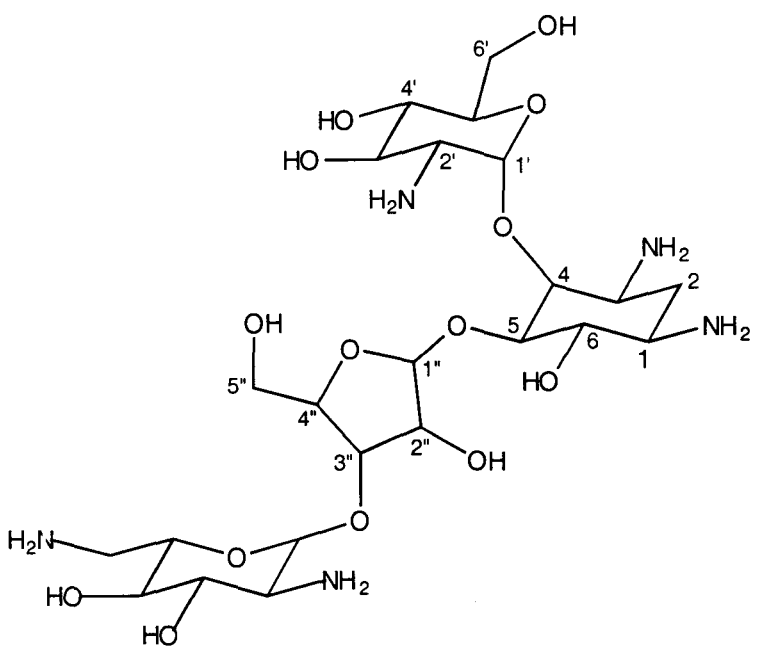

Figure 1.1 Structures of representative aminoglycoside-aminocyclitols. The structures of (a) kanamycin A, (b) neamine, and (c) paromomycin are shown. Information obtained from references Davies, 1991 and Wright et al., 1999, and http://www.chemfinder.com

The primary target for the action of the AGAC antibiotics is the ribosome. Specifically, chemical footprinting experiments indicate that most aminoglycosides bind to the tRNA binding (A-site) region of the 16S rRNA of the 30S ribosomal subunit (Moazed & Noller, 1987; Woodcock et al., 1991). Consequently, misreading or mistranslation results (Davies et al., 1964; Gorini, 1974), as well as inhibition of protein synthesis (Kaji & Kaji, 1965). The aminoglycosides induce a number of other physiological effects, such as loss of cell membrane integrity and impairment of respiration (Dubin et al., 1963). It has been suggested that these secondary effects are the basis of the killing or bactericidal action of the AGAC antibiotics (Davies, 1991). The lethal action of aminoglycosides has been discussed in several reviews and textbooks (see Davis, 1988; Davies, 1991; Wright et al., 1999).

The clinical usefulness of aminoglycosides was immediately realized upon their discovery over fifty years ago. When streptomycin was first isolated from *Streptomyces griseus* in 1944, most of the antibiotic substances known at the time, such as penicillin, acted primarily upon Gram-positive bacteria (Schatz et al., 1944). Thus, the bactericidal activity of streptomycin against both Gram-positive and Gram-negative organisms was of particular interest (Schatz et al., 1944). Within a year of its discovery, streptomycin was found to be effective in the treatment of *Mycobacterium tuberculosis* (Hinshaw & Feldman, 1945), for which it is still widely used today (Musser, 1995). Aminoglycosides have also been the choice drugs in the treatment of Gram-negative bacillary infections, such as intra-abdominal infections, for many years (Hunter, 1947; Ho & Barza, 1987).

Furthermore, the therapeutic strategy for Gram-positive enterococcal infections typically involves the use of an aminoglycoside in combination with an agent that inhibits cell wall synthesis, such as penicillin (Mandell et al., 1970; Moellering et al., 1971c). The combination of the two drugs results in enhanced or synergistic killing of the pathogen and thus elimination of the infection (Jawetz et al., 1950). However, if the organism has acquired high-level resistance to the aminoglycoside being used, this synergism is lost, and the infection allowed to continue (Standiford et al., 1970; Moellering et al., 1971b). As enterococci become increasingly resistant to AGACs and prevalent as nosocomial pathogens, the potential for untreatable infections increases (Spera & Farber, 1994).

The usefulness of combined aminoglycoside-penicillin therapy for the treatment of enterococcal infections has been recognized since 1947. Hunter found that a strain of *Enterococcus faecalis*, isolated from a patient with bacterial endocarditis, appeared to be more susceptible *in vitro* to a mixture of penicillin and streptomycin than to either drug alone (Hunter, 1947). Treatment with both antibiotics in combination resulted in recovery of the patient and the recommendation that for "clinically resistant cases of endocarditis caused by organisms which show some *in vitro* sensitivity to both penicillin and streptomycin, a course of therapy with both drugs together should be tried" (Hunter, 1947). The increased effect of using penicillin in conjunction with streptomycin was found to be due to antibiotic synergism, as indicated by the fact that the rate of bactericidal action of the mixture was greater than that for either penicillin or streptomycin alone (Jawetz et al., 1950). Whereas the effects of penicillin on enterococci

are mainly bacteriostatic, even at very high concentrations (Moellering et al., 1971c, Mandell et al., 1970; Jawetz et al., 1950), and most enterococci are resistant to clinically achievable concentrations of streptomycin (Toala et al., 1969; Standiford et al., 1970), the mixture is bactericidal in combinations which can readily be obtained clinically (Moellering et al., 1971c). For this reason, the synergistic combination of penicillin and streptomycin became the recommended therapy for eradicating infections caused by enterococci (Mandell et al., 1970). Since this marked synergistic killing effect against enterococci occurs only when AGACs are combined with agents that inhibit cell wall synthesis, such as vancomycin or penicillin, the natural low-level resistance of enterococci to aminoglycosides appears to be the result of the cell wall or envelope acting as a relative permeability barrier to intracellular uptake (Moellering et al., 1970; Moellering et al., 1971c; Standiford et al., 1970). Thus, agents which inhibit cell wall synthesis essentially breach this barrier, thereby allowing the aminoglycoside to penetrate the cell wall and produce a bactericidal effect (Moellering et al., 1970; Moellering et al., 1971c). In support of this hypothesis, the exposure of enterococcal cells to penicillin or other agents that impair bacterial cell wall synthesis has been shown to increase the uptake of ^{14}C-labeled streptomycin by enterococci (Moellering et al., 1970; Moellering & Weinberg, 1971a; Moellering et al., 1980).

The effectiveness of combined therapy soon faltered, however, as enterococcal strains resistant to penicillin-aminoglycoside synergism began to appear more frequently. For instance, strains of *E. faecalis* exhibiting resistance to penicillin-streptomycin and

penicillin-kanamycin synergism emerged (Standiford et al., 1970), as did strains of *Enterococcus faecium* that were resistant to combinations of penicillin and kanamycin, tobramycin, netilmicin, or sisomicin (Moellering et al., 1971b; Moellering et al., 1973). The presence or absence of synergism in forty-nine strains of *E. faecalis* was found to correlate with the minimal inhibitory concentration (MIC) of the strain for the aminoglycoside. While strains with MICs of 250 μg/mL or less were susceptible to synergism, strains resistant to synergism required 6250 μg/mL or more of the aminoglycoside for inhibition (Standiford et al., 1970). Likewise, loss of penicillin-kanamycin synergism in strains of *E. faecium* was attributed to high-level resistance to kanamycin (Moellering et al., 1971b). However, although the correlation between MIC and susceptibility to synergism appeared to be valid for both organisms, strains of *E. faecium* were consistently more resistant to antimicrobial synergism (Moellering et al., 1979). While combinations of penicillin and netilmicin, sisomicin, tobramycin, or kanamycin typically remained effective against *E. faecalis* (Moellering et al., 1973; Moellering et al., 1979), these mixtures failed to produce synergism against strains of *E. faecium* at clinically achievable concentrations (Moellering et al., 1979). This greater resistance to synergism in strains of *E. faecium* was credited to its elevated MICs for both penicillin and all aminoglycosides tested excluding gentamicin, amikacin and streptomycin (Moellering et al., 1979). Fortunately, combined treatment with penicillin-gentamicin remained effective against both *E. faecalis* and *E. faecium*, and thus became the optimal therapy for the treatment of severe enterococcal infections, such as endocarditis (Moellering et al., 1973; Weinstein & Moellering, 1973). Therefore, when

strains of both *E. faecalis* and *E. faecium* that were highly resistant to gentamicin began to emerge (Horodriceanu et al., 1979; Eliopoulos et al., 1988), the successful treatment of enterococcal infections became a worldwide health concern.

Unfortunately, the treatment of bacterial infections caused by enterococci still presents a major problem. Not only is the prevalence of high-level resistance to gentamicin among clinical isolates of enterococci increasing, but so is the number of hospital-acquired infections due to enterococci (Schaberg et al., 1991; Hoffmann & Moellering, 1987; Spera & Farber, 1992). In fact, over 50% of clinical isolates of enterococci are resistant to penicillin-gentamicin synergy in some centers (Zervos et al., 1987). In addition, enterococci caused 12% of nosocomial infections between 1986 and 1989, second only to *Escherichia coli* in incidence (Schaberg et al., 1991). Furthermore, in 1993, 13.6% of isolates reported to the Centers for Disease Control and Prevention from intensive care unit patients were found to be vancomycin-resistant enterococci (reviewed in Jacoby, 1996). Since VRE are often *E. faecium* and therefore highly resistant to penicillins and aminoglycosides, therapeutic options for patients infected with VRE are quite limited (Spera & Farber, 1992; Jacoby, 1996). Considering enterococci often cause infections in seriously ill or immunocompromised patients, like those in intensive care or burn units, or those recently having undergone surgery, such multiply-resistant strains of enterococci have become important causes of mortality in hospitals (Zervos et al., 1987; Jones et al., 1986; Hoffmann & Moellering, 1987; Jacoby, 1996; Murray, 1990). Many excellent reviews discuss the frightening development of

multidrug-resistant *E. faecium* and its impact on therapeutic options, referring to the organism as the untreatable, "nosocomial pathogen of the 1990s" (Spera & Farber, 1992; Spera & Farber, 1994; Moellering, 1991).

Several different mechanisms appear to be responsible for the high-level resistance to aminoglycoside antibiotics observed in enterococci. For instance, very high-level resistance to streptomycin and subsequent loss of penicillin-streptomycin synergism in enterococci can be ribosomally mediated (Zimmermann et al., 1971). Specifically, ribosomes purified from highly resistant strains were found to be insensitive to streptomycin-induced misreading, although they remained susceptible to paromomycin-induced misreading (Zimmermann et al., 1971). Furthermore, in one instance, defective uptake of gentamicin in the presence of penicillin resulted in a loss of synergism and thus persistence of an enterococcal endocarditis infection (Moellering et al., 1980). However, the most common mechanism of high-level resistance in enterococci is mediated by the production of aminoglycoside-modifying enzymes (Krogstad et al., 1978b; Courvalin et al., 1978; Horodniceanu et al., 1979; Chen & Williams, 1985). The enzymatic modification of the aminoglycoside effectively inactivates the antibiotic so that it no longer inhibits ribosomal protein synthesis (Krogstad et al., 1978b; Courvalin et al., 1978). Consequently, synergism is lost and the enterococcal infection is allowed to persist (Krogstad et al., 1978b).

The aminoglycoside-inactivating enzymes are organized into three classes according to the type of chemical transformation they catalyze: the phosphotransferases (APHs), the adenylyl- or nucleotidyltransferases (ANTs), and the acetyltransferases (AACs) (Shaw et al., 1993). The enzymes are further classified as follows: 1, 3', 2'', etc. for their specific site of modification; I, II, III, etc. for their unique aminoglycoside resistance profile; and a, b, c, etc. for their unique protein designation (Shaw et al., 1993). Since many of the genes encoding AGAC-modifying enzymes are plasmid-borne or associated with transposable genetic elements, they are readily transferable (Krogstad et al., 1978a; Courvalin et al., 1978; Shaw et al., 1993). Consequently, rapid dissemination of the genes within a wide variety of bacterial species is possible, as well as the presence of multiple resistance-encoding genes in a given strain (Shaw et al., 1993).

1.2 Introduction to Aminoglycoside Acetyltransferase(6')-Ii

As mentioned above, strains of *E. faecium* are consistently resistant to synergism when exposed to penicillin in combination with kanamycin, tobramycin, sisomicin, or netilmicin, while strains of *E. faecalis*, for the most part, remain susceptible to these antimicrobial mixtures (Moellering et al., 1973; Moellering et al., 1979). The unique resistance profile of *E. faecium* strains is credited to the presence of a chromosomally encoded acetyltransferase which catalyzes the acetylation of AGACs with an unprotected amino group at the 6' position, such as kanamycins A and B, neomycin, netilmicin, sisomicin, and tobramycin (Figure 1.2) (Wennersten & Moellering, 1980; Chen & Williams, 1985; Costa et al., 1993). The gene encoding this 6'-*N*-acetyltransferase,

aac(6')-Ii, is chromosomal and specific for *E. faecium*, as it could not be detected in strains belonging to 13 other enterococcal species (Costa et al., 1993). The gene codes for a protein of 182 amino acid residues, with a calculated molecular mass of 20,666 Da, an apparent molecular mass of 23,000 Da by 15% SDS-PAGE (Costa et al., 1993), and an accurate mass of 20,710.0 Da by electrospray mass spectrometry (Wright & Ladak, 1997). (The enzyme overexpressed and purified by Wright and Ladak is identical to that characterized by Costa *et al.*, except for a valine to glutamate mutation at residue 127.)

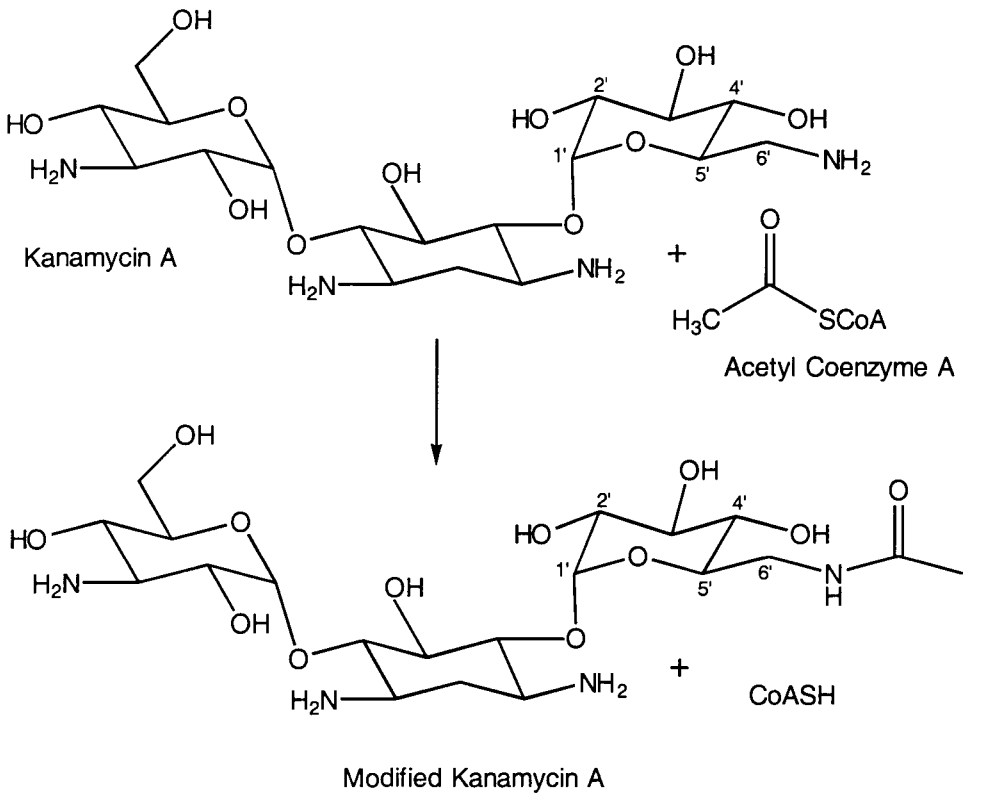

Figure 1.2 Acetylation reaction catalyzed by aminoglycoside 6'-*N*-acetyltransferase. The acetyl group of acetyl coenzyme A is transferred to the 6' amino group of an aminoglycoside, producing CoASH and a modified AGAC.

The AAC(6')-Ii enzyme has a broad substrate specificity, with neamine representing its minimal AGAC substrate (Figure 1.1) (Wright & Ladak, 1997; DiGiammarino et al., 1998). Furthermore, AAC(6')-Ii can utilize both acetyl- and propionyl-coenzyme A (CoA) as substrates for acyl transfer (Figure 1.3) (Wright & Ladak, 1997). Interestingly, the enzyme appears to be produced at low-levels that are barely detectable unless highly productive variants are selected by growth on increasing concentrations of AGAC (Wennersten & Moellering, 1980; Costa et al., 1993). In addition, AAC(6')-Ii confers only low-level aminoglycoside resistance, with MICs less than 50 μg/mL (Wright & Ladak, 1997). However, despite its inability to confer high-level resistance to AGACs, the rate of modification of aminoglycosides by AAC(6')-Ii is sufficient to abrogate aminoglycoside-penicillin synergism, thereby making infections produced by *E. faecium* strains even more refractory to treatment (Moellering et al., 1979).

Comparison of AAC(6')-Ii to other aminoglycoside-inactivating enzymes indicates that the enzyme is a relatively inefficient detoxifying catalyst. First, the enzyme displays relatively low specificity constants (k_{cat}/K_m) for a number of AGACs (Wright & Ladak, 1997). Similarly, whereas efficient detoxifying catalysts exhibit a positive correlation between MIC and V_{max}/K_m, indicating maximal efficiency at low aminoglycoside concentrations (Radika & Northrop, 1984), AAC(6')-Ii demonstrates a positive correlation between MIC and k_{cat}, the rate at a saturating AGAC concentration (Wright & Ladak, 1997). These results imply that AAC(6')-Ii is not optimally evolved

for aminoglycoside inactivation, and thus may possess another physiological function in *E. faecium* (Wright & Ladak, 1997).

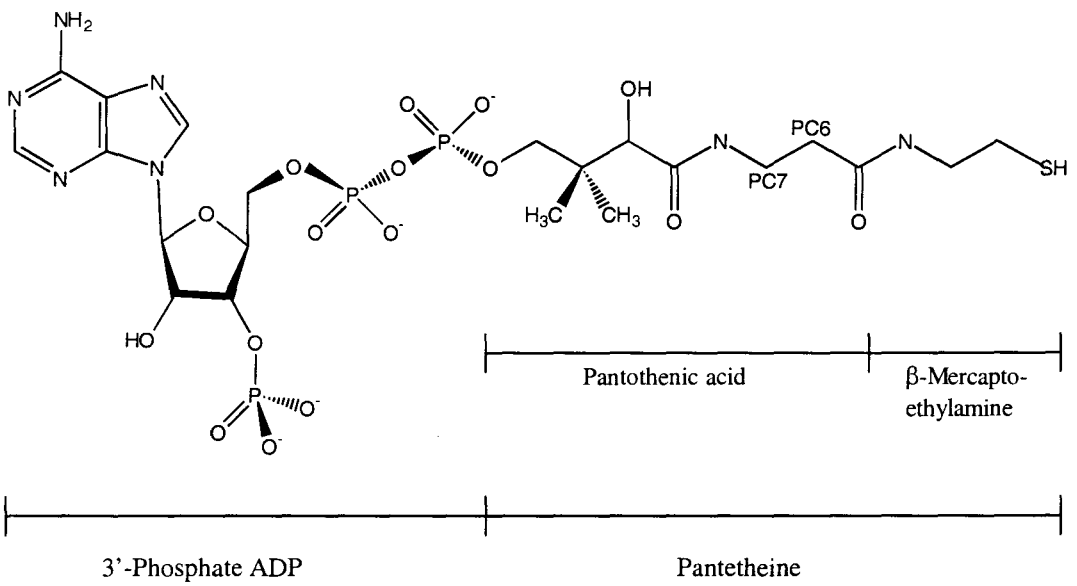

Figure 1.3 Schematic drawing of Coenzyme A. Figure adapted from Engel & Wierenga, 1996.

Sequence alignment results are consistent with the theory that AAC(6')-Ii may have a function other than antibiotic modification in *E. faecium*. Pairwise comparison of primary structures reveals a significant similarity between AAC(6')-Ia, which is 42.2% identical to AAC(6')-Ii, AAC(3)-Ia, streptothricin acetyltransferase (STAT), phosphinothricin acetyltransferase (PHAT), puromycin acetyltransferase (PUAT), and a ribosomal protein acetyltransferase, RimI, which acetylates the N-terminal alanine of the S18, 30S ribosomal protein (Piepersberg et al., 1988). This significant sequence

similarity, particularly in the C-terminal halves of the enzymes, along with the fact that the proteins are of similar length, suggests that the enzymes may share a common evolutionary origin (Piepersberg et al., 1988). That is, aminoglycoside resistance genes may have evolved from bacterial genes that encode enzymes involved in normal cellular control (Piepersberg et al., 1988). Although the validity of these alignment results has been questioned (Shaw, 1993), similar findings were recently published by Neuwald and Landsman (1997). An extensive sequence alignment performed by these two authors identified a large superfamily of GCN5-related *N*-acetyltransferases (GNATs) (Neuwald & Landsman, 1997). This superfamily spans all kingdoms of life and "comprises more than a dozen protein families associated with diverse functions and phenotypes, and which often lack pairwise sequence similarity to each other" (Neuwald & Landsman, 1997). The superfamily is characterized by four conserved regions, A-D, spanning over 100 residues, with motif A being universally conserved (Neuwald & Landsman, 1997). Interestingly, AAC(6')-Ia, AAC(3)-Ia, STAT, PHAT, PUAT, and RimI are all members of this superfamily, supporting the hypothesis that these proteins evolved from a common ancestral *N*-acetyltransferase (Neuwald & Landsman, 1997).

1.3 Structural Analysis of AAC(6')-Ii

Prior to the development of a purification scheme for AAC(6')-Ii, knowledge regarding the protein's structure was restricted to that obtained from sequence homology and mutagenesis studies. For instance, an extensive protein sequence alignment performed by Shaw *et al.* revealed three distinct AAC(6') subfamilies: (i) AAC(6')-Ib,

AAC(6')-IIa, AAC(6')-IIb, and the AAC(6') portion of an AAC(6')+APH(2'') bifunctional protein; (ii) AAC(6')-Ic, AAC(6')-Id, and AAC(6')-If; and (iii) AAC(6')-Ia (Shaw et al., 1993). AAC(6')-Ii, AAC(6')-Il, and AAC(6')-Iq were later added to the Ia subfamily based on sequence homology (Costa et al., 1993; Hannecart-Pokorni et al., 1997; Centron & Roy, 1998). Two regions appear to be relatively conserved across the three families of proteins. The larger region at positions 85 to 98 of AAC(6')-Ii contains a highly conserved leucine residue at position 91. When the equivalent leucine was mutated to serine in AAC(6')-Ic, amikacin resistance was lost, while resistance to other aminoglycosides remained the same, implying that this region is involved in the active site (Shaw et al., 1993). The second motif, which corresponds to pentapeptide LHPLV at positions 73 to 77 in AAC(6')-Ii, is also thought to influence substrate binding and specificity (Rather et al., 1992; Shaw et al., 1993). In AAC(6')-I proteins, which are capable of modifying amikacin and gentamicin C_{1a} and C_2, the fourth residue of this pentapeptide is a leucine. However, in AAC(6')-II proteins, which can acetylate all gentamicin C compounds but not amikacin, the fourth residue is a serine (Rather et al., 1992). Rather *et al.* shifted the resistance profile of AAC(6')-Ib to that of AAC(6')-IIa by mutating this leucine to a serine residue, indicating that the second conserved region is likely in the aminoglycoside binding domain (Rather et al., 1992).

The recent establishment of an overexpression and purification protocol for AAC(6')-Ii permitted initiation of structural studies on the enzyme. In particular, NMR spectroscopy, combined with molecular modeling, was used to determine the

conformations of two enzyme-bound aminoglycosides (DiGiammarino et al., 1998). These studies indicate that butirosin A adopts a single conformation in the AAC(6')-Ii•CoA•butirosin A ternary complex, while isepamicin binds in two different conformations, one of which may represent an unproductive binding mode. Since amikacin has also been shown to bind to APH(3')-IIIa in two different conformations (Cox & Serpersu, 1997), the authors suggest that the formation of unproductive enzyme-substrate complexes may explain why isepamicin and amikacin remain as two of the more effective aminoglycosides (DiGiammarino et al., 1998; Miller et al., 1997). Furthermore, aminoglycosides with 4,5- and 4,6-disubstituted 2-deoxystreptamine rings bind to AAC(6')-Ii in different fashions (DiGiammarino et al., 1998), as was first suggested by Wright and Ladak (1997).

Insight regarding conformational changes in AAC(6')-Ii upon substrate binding has also been obtained since the development of a purification protocol for the enzyme (Draker et al., 1999). Subtilisin digestion experiments and NMR experiments with uniformly ^{15}N-labelled AAC(6')-Ii indicate that ligand binding induces the enzyme to close and become more ordered (Draker et al., 1999). Specifically, a significant conformational change appears to take place upon binding of either acetyl-CoA (AcCoA) or paromomycin, and again upon formation of the ternary complex, although the main change occurs upon formation of the binary complex. Whereas circular dichroism spectra support notable reorganization of the structure upon acetyl-CoA binding, Trp fluorescence studies combined with mutagenesis results suggest that such structural

changes upon ligand binding involve the C-terminus in particular (Draker et al., 1999). These conformational changes in AAC(6')-Ii associated with ligand binding may constitute a requirement for catalysis or explain why the enzyme can modify such a broad range of aminoglycoside substrates (Draker et al., 1999).

Purification of AAC(6')-Ii has also allowed for its crystallization in preparation for determination of the enzyme's three-dimensional structure. Crystallization of the wild-type protein in the presence of its cofactor, AcCoA, was accomplished as part of an undergraduate thesis project (Wybenga, 1997). The encouraging results obtained from x-ray diffraction experiments on the F2 beamline at the Cornell High-Energy Synchrotron Source (CHESS) prompted the construction of a selenomethionyl derivative of the enzyme. This was achieved by transformation of the *Escherichia coli* methionine auxotroph B834(DE3)/pLysS with the pPLaac-1 plasmid containing the *aac(6')-Ii* gene (Wybenga, 1997). Crystals of this selenomethionine-substituted protein can be used in multiwavelength anomalous diffraction (MAD) experiments to solve the phase problem for AAC(6')-Ii and thus facilitate determination of its atomic structure.

1.4 Thesis Objective

As bacteria continue to develop resistance to every antibiotic in the medical armamentarium, the need for new, more effective, antimicrobial agents increases (Williams & Heymann, 1998; Neu, 1992). Whereas the majority of the drugs in use today were discovered by random screening methods, a more novel approach to

developing drugs uses detailed structural and mechanistic information about a target enzyme to assist in the design of therapeutic agents (Navia & Peattie, 1993). Since aminoglycoside-modifying enzymes confer high-level resistance to aminoglycosides in a number of nosocomial pathogens, such as enterococci, *S. aureus*, staphylococci, and Gram-negative organisms (Krogstad et al., 1978b, Lovering et al., 1988; Shaw et al., 1993), this class of enzymes is an excellent target for rational drug design studies. To this end, the three-dimensional structure of aminoglycoside phosphotransferase(3')-IIIa was determined by Hon *et al.* (1997).

The objective of this study is to determine the structure of aminoglycoside acetyltransferase(6')-Ii by x-ray crystallographic techniques. It is anticipated that the structural and functional information obtained from this structure and those of other aminoglycoside modifying enzymes, in conjunction with details obtained from mutagenesis and kinetic experiments, will facilitate development of inhibitors of these enzymes in order to combat aminoglycoside antibiotic resistance.

Chapter 2 General Experimental Procedures

2.1 Aminoglycoside Acetyltransferase Activity

2.1.1 Materials and Buffers

Acetyl coenzyme A was obtained from Pharmacia Biotech. Buffer components are generally reagent grade and purchased from Sigma. The assay buffer consists of 25 mM HEPES and 1 mM EDTA, pH 7.5.

2.1.2 Methods

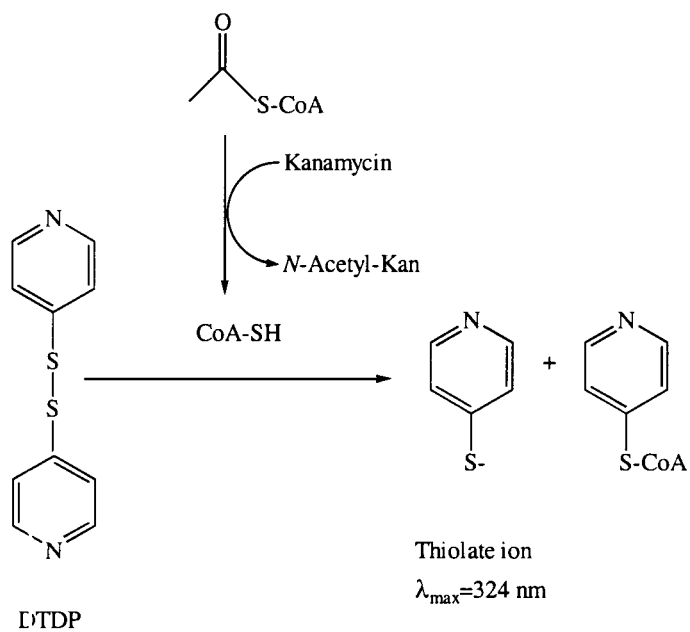

Figure 2.1 Reaction employed by AAC activity assay. Modification of kanamycin by an active aminoglycoside acetyltransferase produces CoASH, which reacts with DTDP to produce a thiolate ion.

Kanamycin-dependent acetyltransferase activity was assayed by *in situ* titration of free coenzyme A with 4,4'-dithiodipyridine (DTDP) as described previously (Williams & Northrop, 1978). Briefly, acetylation of kanamycin by the enzyme produces CoASH, which then reacts with DTDP to produce a thiolate ion, which exhibits maximum absorbance at 324 nm, with an extinction coefficient of 19,800 $M^{-1}cm^{-1}$. Thus, by monitoring the optical density at 324 nm (OD_{324}) with respect to time, the AAC activity of the protein sample can be measured. Assay conditions were similar to those described previously (Wright & Ladak, 1997). (See Appendix 1 for detailed protocol.)

2.2 Aminoglycoside Acetyltransferase(6')-Ii Production and Purification

2.2.1 Materials

Reagents for the Bradford or Bio-Rad Protein Assay were purchased from Bio-Rad, as were the SDS-PAGE low range markers. The remaining chemicals are reagent grade and can generally be purchased from Sigma. *E. coli* W3110/pPLaac-1, the cell strain containing the overexpression system for AAC(6')-Ii, was kindly provided by Dr. Gerard D. Wright, McMaster University. The cell strain *E. coli* B834(DE3)/pLysS was kindly provided by Dr. A. Edwards, McMaster University (currently University of Toronto).

The buffers employed are as follows:

Buffer A: 25 mM HEPES (N-2-hydroxyethylpiperazine-N'-2-ethane sulfonic acid), 2 mM EDTA (ethylenediamine tetraacetic acid), pH 7.5

Buffer B: 25 mM HEPES, 2 mM EDTA, 1 M NaCl, pH 7.5

Lysis Buffer: 25 mM HEPES, 2 mM EDTA, 0.2 M NaCl, 0.1 mM DTT (dithiothreitol), pH 7.5, 1 mM PMSF (phenylmethyl sulfonyl fluoride) (add just before lysis from an 100 mM stock in EtOH)

Assay Buffer: 25 mM HEPES, 1 mM EDTA, pH 7.5

The media employed are as follows:

Luria Broth: 10 g pancreatic digest of casein, 5 g yeast extract, 10 g NaCl, 1 L deionized/distilled water; autoclave 45 minutes.

LeMaster's Media: Add the following to 1 L of dd H_2O, pH to 7.5, and autoclave:

0.50 g L-alanine	0.10 g L-proline
0.60g D,L-arginine-HCl	2.00 g D,L-serine
0.40 g L-aspartate	0.23 g L-threonine
0.03 g L-cystine	0.17 g L-tyrosine
0.70 g L-glutamate	0.23 g D,L-valine
0.33 g L-glutamine	0.50 g uridine
0.54 g glycine	1.50 g sodium acetate
0.06 g L-histidine	1.50 g succinic acid
0.23 g D,L-isoleucine	1.50 g ammonium chloride
0.23 g L-leucine	1.20 g sodium hydroxide
0.42 g L-lysine-HCl	10.5 g di-potassium hydrogen orthophosphate
0.13 g L-phenylalanine	

Filter sterilize 10 g glucose, 0.25 g magnesium sulfate (hydrate), 5 mg ferrous sulfate (hydrate), 8 µL sulfuric acid (conc.), and 100 mL dd H_2O and add to cooled medium. Supplement medium with 5 µg/mL thiamine, 100 µg/mL ampicillin, 30 µg/mL chloramphenicol, and 50 µg/mL L-selenomethionine. Remove 25 mL aliquot from this solution for overnight culture; use remainder as 1 L aliquot.

2.2.2 Purification of Native Enzyme

The overexpression and purification of wild-type aminoglycoside acetyltransferase(6')-Ii was performed as described previously (Wright & Ladak, 1997). Briefly, purification of the enzyme involves an anion exchange column, a gel filtration step, and an affinity column. (See Appendix 1 for detailed protocol.)

2.2.3 Purification of Selenomethionyl AAC(6')-Ii

The purification scheme employed for the selenomethionyl derivative of AAC(6')-Ii was similar to that described for native enzyme, with the following exceptions:

i. A single colony of *E. coli* B834 (DE3)/pLysS/pPLaac-1 cells was used to inoculate the 1 mL overday culture.

ii. All growth media were supplemented with 100 μg/mL ampicillin, as well as 30 μg/mL chloramphenicol.

iii. A modified version of the media described by LeMaster and Richards (1985) was used in place of the 25 mL and 1 L Luria broth aliquots. Major modifications included replacement of methionine with L-selenomethionine and adjustment of pH to 7.5. (See LeMaster's media recipe above.)

2.3 Crystallization

2.3.1 Materials

Crystal Screens I and II and Additive Screens I and II were obtained from Hampton Research (Laguna Niguel, CA). Linbro tissue culture multi-well plates were obtained from ICN (Aurora, Ohio). Coverslips were purchased from Fisher Scientific. Dimethyldichlorosilane solution purchased from BDH is used to siliconize the coverslips prior to use.

2.3.2 General Crystallization Techniques Employed

Crystallization of AAC(6')-Ii in the presence of various substrates was performed using the hanging drop method. One of the most common crystallization techniques, this method is based on the principle of vapor diffusion. Typically, a small volume of highly purified protein is added to an equal volume of a solution known to precipitate protein, such as ammonium sulfate or polyethylene glycol, on a siliconized coverslip. The coverslip is then suspended over a well of a sterile tissue culture tray, which contains the precipitant solution, and a seal formed around the mouth of the well with vacuum grease. Water diffusion then occurs within this closed system until the final concentration of the precipitant in the protein solution is nearly equal to that in the reservoir. Thus, if the concentration of the precipitant solution in the well is optimal, it is anticipated that crystallization will occur (reviewed in Rhodes, 1993).

In general, the sparse matrix approach to crystallization was used to obtain initial crystallization conditions. This approach samples a wide range of effective crystallization conditions in a rapid and efficient manner. Two commercially available screening kits were employed (Hampton Research), each one containing 48-50 unique solutions known for their ability to crystallize macromolecules. Once initial crystallization conditions were found, parameters such as protein concentration, precipitant concentration, and pH were refined until diffraction quality crystals were obtained. Refinement often involved the use of two commercially available additive screens (Hampton Research), each containing 24 unique additive solutions composed of a variety of small molecules. This approach takes advantage of the fact that small molecules can affect the crystallization of proteins by manipulating protein-protein and protein-solvent interactions in such a way that the stability of the macromolecule is altered. If the change in stability is favourable to crystallization, the quality and size of the protein crystals can be improved.

Ordinarily, crystallization trials were performed with 2 μL of protein solution and 2 μL of well solution, mixing was performed by pipetting, and trays were grown at 22 °C in a low temperature incubator. Trays were normally left undisturbed for four to seven days before being monitored by light microscopy for crystal growth. When crystallization trials using the additive screens were performed, the method of crystallization was altered slightly; the final droplet contained 3 μL of protein solution, 2 μL of well solution, and 1 μL of additive solution, added to the coverslip in that order.

2.4 Refinement of Atomic Models

Once an atomic model has been fit to its electron density map, the model is refined in reciprocal-space. That is, computerized attempts are made to improve the agreement of the atomic model with the observed diffraction data. Traditionally, the quality of this fit is measured by the R value:

$$R = \frac{\Sigma_{hkl} \left| \left| \mathbf{F}_{obs}(hkl) - k \left| \mathbf{F}_{calc}(hkl) \right| \right| \right|}{\Sigma_{hkl} \left| \mathbf{F}_{obs}(hkl) \right|} \qquad (1)$$

where h, k, l are the reciprocal lattice points of the crystal, $|\mathbf{F}_{obs}(hkl)|$ and $|\mathbf{F}_{calc}(hkl)|$ are the observed and calculated structure factor amplitudes, respectively, and k is a scale factor. However, since R can be made arbitrarily small by increasing the number of model parameters, a low R value does not necessarily correspond to an accurate model. In order to overcome this problem, Brünger defined a free R value based on the method of statistical cross-validation (Brünger, 1992a; Brünger, 1993). This statistic measures the degree to which the model predicts the diffraction data for a test set of reflections that is omitted in the modeling and refinement process (Brünger, 1992a). R free is calculated in the same manner as the conventional R factor, using only reflections in the test set. Since R free is highly correlated with the accuracy of the atomic model phases, it represents a reliable and unbiased parameter by which to assess improvement of the model during the course of refinement and to evaluate whether overfitting has occurred (Brünger, 1992a; Kleywegt & Brünger, 1996).

Refinement of the AAC(6')-Ii structures described in this study was performed using X-PLOR (Brünger, 1992b) version 3.843. This program system is based on an energy function approach, such that an energy function is minimized by a variety of gradient descent and simulated annealing procedures (Brünger, 1992b). The energy function combines both chemical and effective energy terms:

$$E_{total} = E_{chem} + w\, E_{x\text{-}ray} \qquad (2)$$

where E_{chem} comprises empirical information about covalent-bonding geometry, hydrogen-bonded and nonbonded interactions and $E_{x\text{-}ray}$ represents energy terms that use experimental information (Brünger et al., 1990; Brünger, 1992b). If the computed data agrees with the observed data, then $E_{x\text{-}ray}$ is equal to zero (Brünger et al., 1990). Therefore,

$$E_{x\text{-}ray} = \Sigma_{hkl} (\left| \mathbf{F}_{obs} (hkl) \right| - k \left| \mathbf{F}_{calc} (hkl) \right|)^2 \qquad (3)$$

The w term in equation (2) represents a weight factor that can be adjusted to place more or less emphasis on the $E_{x\text{-}ray}$ term during minimization of the target function.

The general refinement strategy employed for the various AAC(6')-Ii structures is illustrated in the form of a flow-chart (Figure 2.2). First, a test set of reflections is obtained by randomly selecting ten percent of the observed reflections (Brünger, 1992a; Brünger, 1992b). Since by definition the same test set must be maintained throughout the fitting procedure, this step is only necessary in the first round of refinement. Next, a molecular structure file is generated from the coordinates of the atomic model. This file contains information like atom names, atom charges, bond terms, and angle terms and is

used in conjunction with the coordinate file and reflection file throughout refinement. Improvement of the agreement between $|\mathbf{F}_{calc}|$ and $|\mathbf{F}_{obs}|$ begins by calculating structure factors for the bulk solvent in the crystal and including these terms in subsequent refinement (Jiang & Brünger, 1994). After bulk solvent correction, the ideal weight between E_{chem} and E_{x-ray} is calculated (equation (2)) (Brünger et al., 1987; Brünger et al., 1990; Brünger, 1992a) and employed in positional refinement. This step uses a conjugate gradient type minimization to minimize E_{total} by adjusting the atomic positions of the model (Powell, 1977). Following positional refinement, individual restrained isotropic B-factors are refined for each atom by the same minimization method. Such B-factors, or temperature factors, account for the fact that atoms are not static entities, but actually vibrate or oscillate around the position specified in the model. The extent of vibration depends on the temperature at which data was collected, the mass of the atom, and the degree to which the atom is interacting with surrounding atoms. Since this variation in atomic position affects diffraction, adding the effects of motion to a model makes it more realistic and thus more likely to fit the experimental data precisely (Rhodes, 1993). After B-factor refinement, a new ideal weight is calculated and positional refinement repeated. (If the decrease in the R factors is significant at this point, i.e. ~10%, the cycle may be repeated from the bulk solvent correction stage.) Alternation between positional and B-factor refinement continues until no further improvement of the R factors is observed. At this point, new electron density maps are computed using $|\mathbf{F}_{calc}|$ values calculated from the new model, $|\mathbf{F}_{obs}|$ values from the original diffraction data, and the new, improved phase estimates (Read, 1986; Kleywegt & Brünger, 1996). These maps, generally $\mathbf{F}_o$-$\mathbf{F}_c$

or $2F_o$-F_c maps, can then be used to improve the fit of the atomic model in real space, using a graphical program like O (Jones et al., 1991). Iterative refinement and model adjustment against a new electron density map is carried out until the free R appears unaffected.

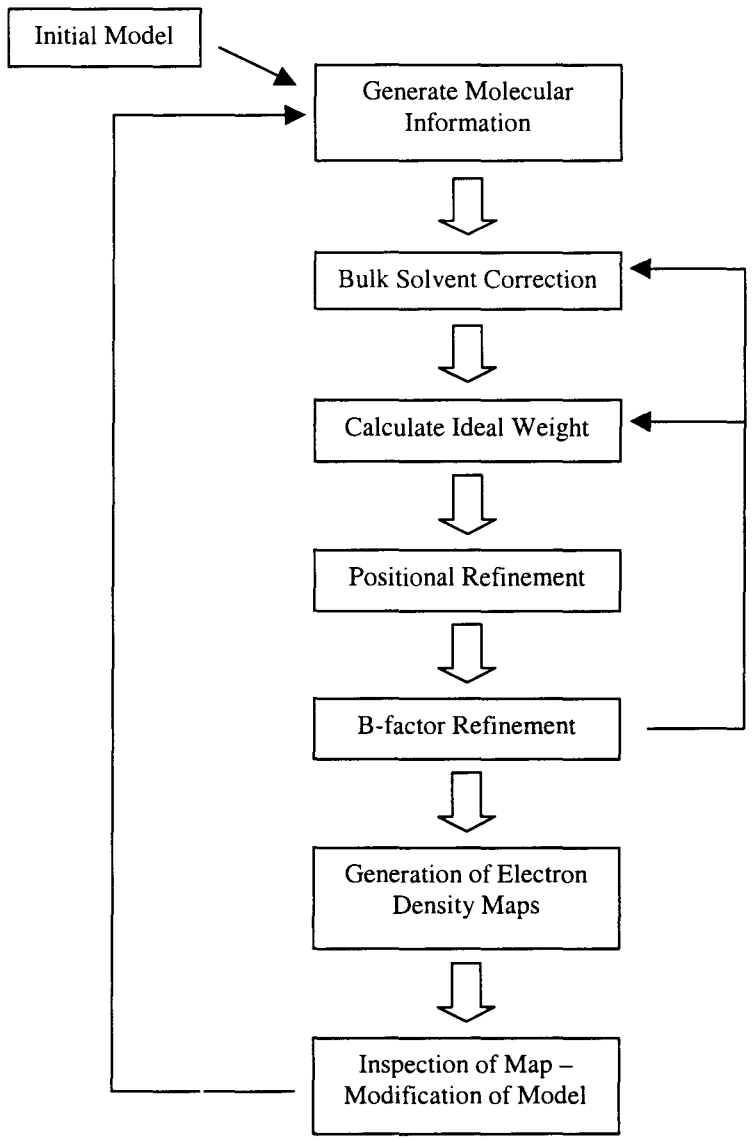

Figure 2.2 General refinement scheme employed for AAC(6')-Ii structures, using X-PLOR version 3.843.

Chapter 3 Aminoglycoside Acetyltransferase(6')-Ii•Acetyl Coenzyme A Complex

3.1 Introduction to the Multiwavelength Anomalous Diffraction Method

The goal of x-ray crystallography is to obtain a contour map of the electron density in a crystal so that the three-dimensional structure of the crystal can be determined. This requires solving the phases of the protein crystal, which, for macromolecular structures, generally involves at least one of the following three techniques. First, molecular replacement requires that the unknown structure is similar to an already known structure, thus enabling the phases of the known structure to be used as initial estimates of phases for the new protein. In the heavy-atom or isomorphous replacement method, a small number of heavy atoms are added to the protein crystal. This results in a slight perturbation in the diffraction pattern of the crystal, which can be employed to estimate initial phase angles for the protein. The third technique, which was used to determine phases for AAC(6')-Ii, is the multiwavelength anomalous diffraction (MAD) method. This powerful technique relies on the presence of anomalously scattering atoms in the protein structure to solve the phase problem, and has been the subject of many excellent reviews and chapters. Thus, only a simple, brief introduction to MAD will be presented here. (See Rhodes, 1993; Drenth, 1994; Hendrickson, 1991; and Hendrickson & Ogata, 1997 for more detailed information.)

The magnitude of x-ray absorption by an element increases with increasing x-ray wavelength and then drops sharply just below the element's characteristic emission wavelength. This sudden decrease in absorption as a function of wavelength, called an absorption edge, is dependent on an element's atomic number. When the frequency of incident radiation used in x-ray diffraction experiments is removed from an element's absorption edge, the x-rays are scattered in an elastic manner. Under these conditions, Friedel's law dictates that Bijvoet or Friedel pairs $\mathbf{F}_{hkl}$ and $\mathbf{F}_{-h-k-l}$ have the same length or intensity, as well as opposite phase angles. However, when the energy of an incident x-ray approaches an element's absorption edge, resonant absorption of the radiation occurs. Anomalous scattering or dispersion results, whereby a fraction of the radiation is emitted with altered phase. Thus, the total scattering factor of the element is:

$$f = f_o + \Delta f + if'' = f' + if'' \qquad (4)$$

where f_o is the normal scattering factor, and f' and f'' are the real and imaginary components of the anomalous scattering, respectively (Hendrickson, 1991). The presence of anomalous scattering causes Friedel's law to break down, such that Friedel pairs are no longer equal in intensity or phase angle. These phase shifts are exploited in order to determine the phase angles of the crystal.

From the practical point of view, the MAD method requires that several conditions be met. First, the protein must contain an element that gives a sufficiently strong anomalous signal. Whereas the absorption edges for the light atoms are not near the wavelength of x-rays used in crystallography, the absorption edges of heavy atoms are

often in this range. Therefore, incorporation of a small number of heavy atoms in the protein structure should result in anomalous scattering if the x-ray data can be collected at a wavelength close to the heavy atom's absorption edge. This often requires the use of tunable synchrotron radiation sources, where the x-ray wavelength can be varied in order to maximize anomalous scattering. Furthermore, data should be collected at multiple wavelengths that optimize both the differences between the structure amplitudes of Bijvoet pairs:

$$\Delta F_{\pm hkl} = \left| {}^{\lambda}\mathbf{F}(hkl) \right| - \left| {}^{\lambda}\mathbf{F}(-h-k-l) \right| \qquad (5)$$

and the dispersive differences:

$$\Delta F_{\Delta\lambda} = \overline{\left| {}^{\lambda_i}\mathbf{F} \right|} - \overline{\left| {}^{\lambda_j}\mathbf{F} \right|} \qquad (6)$$

where $\overline{\left| {}^{\lambda}\mathbf{F} \right|} = [\left| {}^{\lambda}\mathbf{F}(hkl) \right| + \left| {}^{\lambda}\mathbf{F}(-h-k-l) \right|] / 2$ at wavelength λ (Hendrickson, 1991). The difference in Bijvoet pairs is due to the imaginary component of anomalous scattering, whereas dispersive differences are a consequence of the real component of anomalous scattering. Thus, x-ray diffraction data is generally collected at the wavelengths of scattering-factor extrema, namely the peak of absorption or f'' and the inflection point of f'' (which corresponds to the minimal f'), as well as at one or two remote wavelengths above or below the absorption edge (Figure 3.1) (Hendrickson & Ogata, 1997). Ideally, these wavelengths are chosen from an absorption spectrum measured on the crystal itself, since the precise position of the absorption edge depends on the chemical environment of the element.

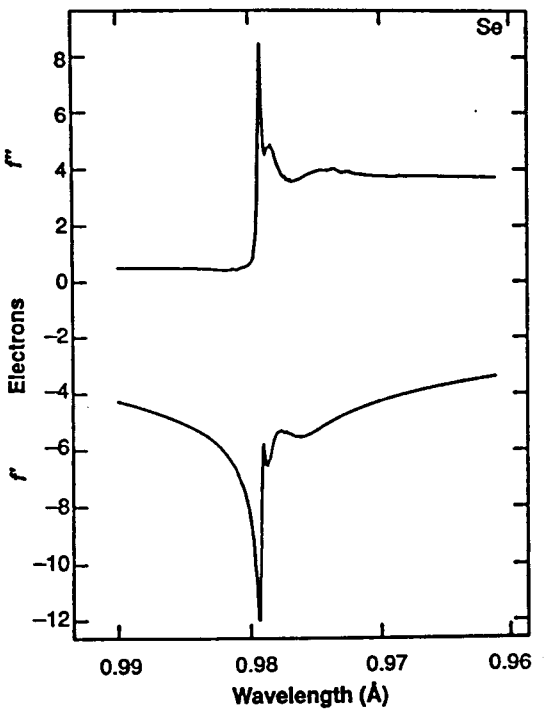

Figure 3.1 Typical anomalous scattering spectrum near the absorption edge of Se. The y-axis has units of number of electrons, with the imaginary component (f'') drawn in the upper portion and the real component (f') in the lower portion. The anomalous scattering factors are shown as a function of wavelength. Figure adapted from Hendrickson, 1991.

3.2 Experimental Procedures

3.2.1 Purification and Crystallization of Selenomethionyl AAC(6')-Ii•AcCoA

At initiation of this study, no model structures were available for determination of aminoglycoside acetyltransferase(6')-Ii by molecular replacement. Therefore, a selenomethionyl derivative of aminoglycoside acetyltransferase(6')-Ii (SeMet-AAC(6')-Ii) was purified from *E. coli* B834 (DE3)/pLysS/pPLaac-1 cells, which are auxotrophic for methionine and carry a plasmid containing the *aac(6')-Ii* gene (GenBank accession

code L12710) (Wright and Ladak, 1997; Wybenga, 1997). Electrospray mass spectrometry analysis of purified wild-type and selenomethionyl-derivatized enzymes revealed that all four methionine residues were fully substituted by selenomethionine (Figure 3.2). Thus, it was anticipated that this SeMet derivative would provide a sufficiently strong anomalous signal for determination of the enzyme's structure by the multiwavelength anomalous diffraction technique (Hendrickson, 1991).

To this end, SeMet-AAC(6')-Ii was crystallized by the hanging drop vapour diffusion technique in the presence of a five-fold molar excess of acetyl coenzyme A under similar conditions as those described for wild-type AAC(6')-Ii (Wybenga, 1997). Reproducible, diffraction quality crystals were obtained by suspending a 6 μL drop, containing 8.5 mg/mL of protein, 2 mM acetyl CoA, 5% (w/v) D(+)-sucrose, and 0.7 M ammonium sulfate, over a 1 mL reservoir of 2.05 M ammonium sulfate. Small, cube-like crystals were typically observed after 1-3 week's growth at 22 °C (Figure 3.3).

In preparation for x-ray analysis, crystals were frozen, and then stored, in liquid nitrogen. This was accomplished by picking up a single crystal from its droplet with a fiber loop, briefly soaking the crystal in a 2.5 M ammonium sulfate solution saturated with D-glucose, and flash freezing the loop in liquid nitrogen.

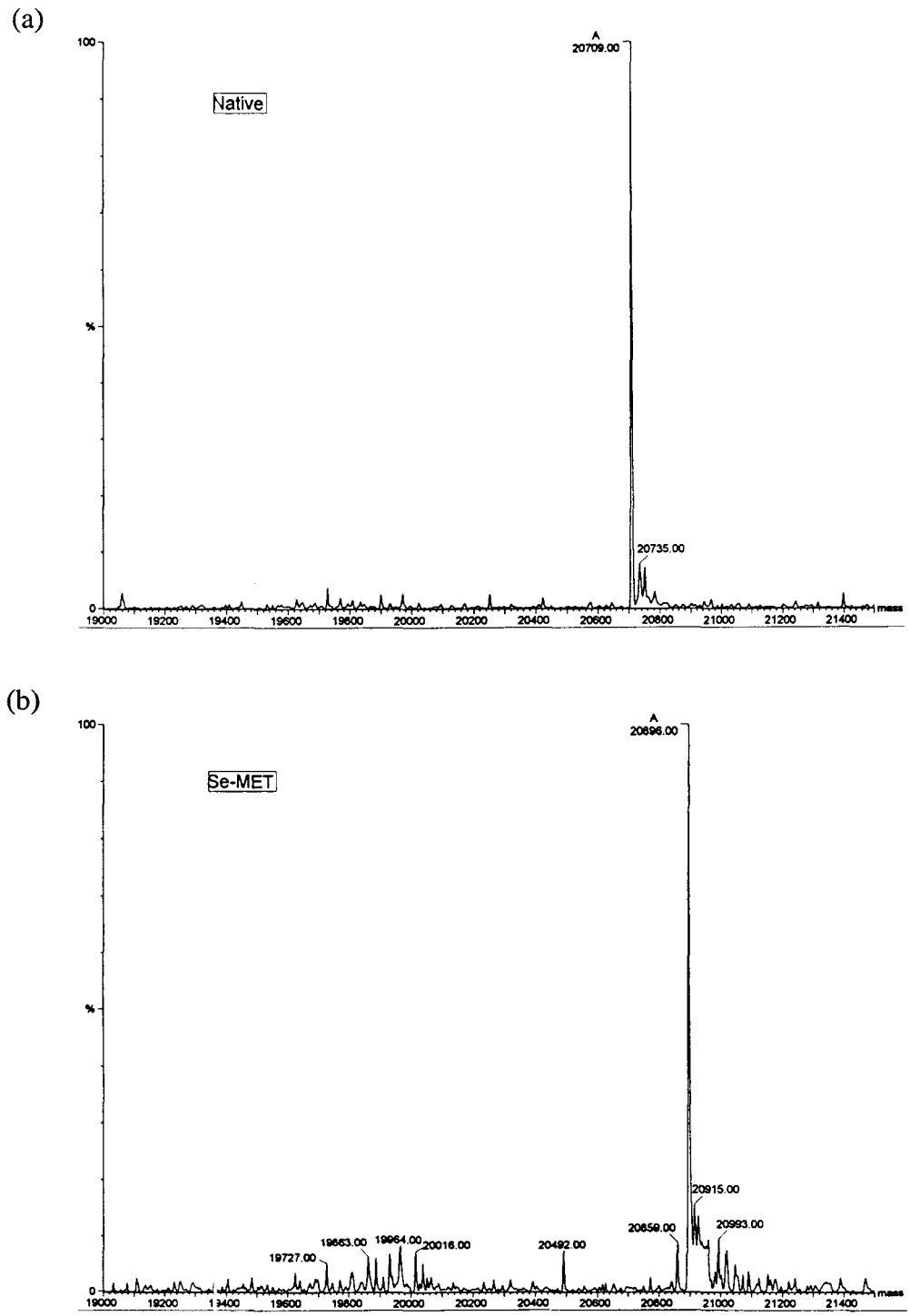

Figure 3.2 Electrospray mass spectrometry analysis of AAC(6')-Ii. (a) Analysis of native enzyme and (b) SeMet-AAC(6')-Ii. Analyses were performed by Dr. Jian Chen, Department of Chemistry, University of Waterloo, Waterloo, Ontario.

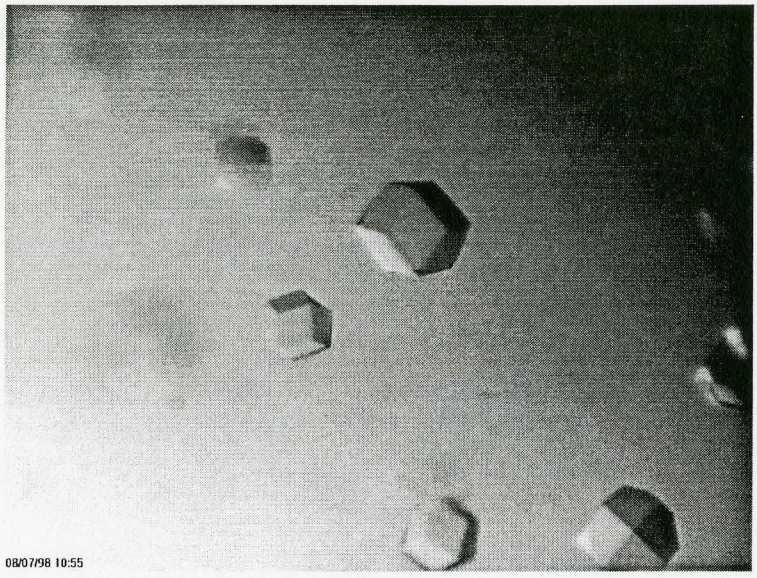

Figure 3.3 Typical cube-like crystals of aminoglycoside acetyltransferase(6')-Ii grown in the presence of acetyl coenzyme A.

3.2.2 Data Collection and Processing

X-ray diffraction experiments were performed on the F2 beamline at the Cornell High-Energy Synchrotron Source (CHESS) using a Quantum 4 ADSC charge coupled device (CCD) detector. Experiments were conducted under cryo-conditions in order to minimize radiation damage to the crystal upon exposure to x-rays. Expendable SeMet-AAC(6')-Ii•AcCoA crystals were mounted and exposed to x-rays with wavelengths in the vicinity of the absorption edge of selenium. The x-ray fluorescence from the sample was monitored and used to produce an x-ray absorption spectrum specific for SeMet-AAC(6')-Ii (Figure 3.4). Although this reference scan did not exhibit a sharp peak or "white-line" feature, the scan was of sufficient quality to identify four wavelengths at which to collect diffraction data. Data was first collected at the wavelength

corresponding to the energy maximum for the imaginary component of the anomalous scattering (λ_{peak}), then at the energy minimum for the real component of the anomalous scattering (λ_{infl}), and finally at wavelengths above (λ_{high}) and below (λ_{low}) the Se absorption edge. All four data sets were collected on a single crystal using the oscillation method, with oscillation angles of one degree.

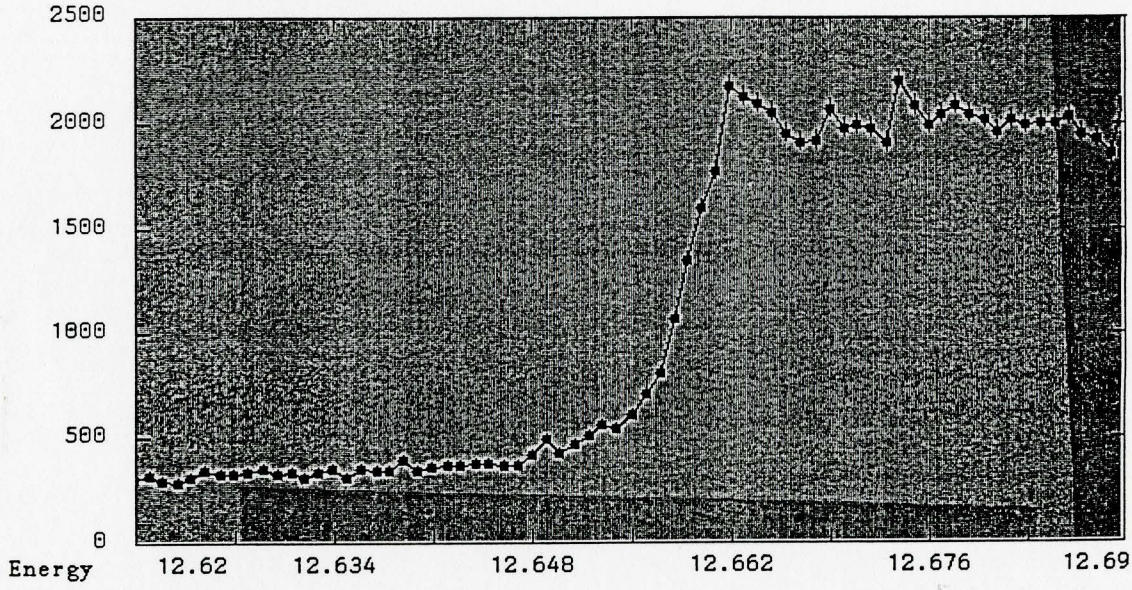

Figure 3.4 X-ray (fluorescence) absorption spectrum specific for SeMet-AAC(6')-Ii, as a function of energy (unit: keV). The y-axis represents the fluorescence of the sample, which is related to the absorption of the sample. The energy of radiation increases as the wavelength decreases, according to the formula: E (keV) = 12.3985 / λ (Å) (Hendrickson & Ogata, 1997).

The complete four-wavelength MAD data set was processed to a resolution of 2.7 Å. In general, data processing consists of three stages. First, the crystal's possible spacegroup, orientation, and cell parameters must be determined. Second, a list of reflections or *hkl* indices is generated and the images integrated, such that every observed *hkl* index is assigned an intensity value and a standard deviation. Both these steps were performed with the data reduction program Mosflm (Leslie, 1990). The crystal orientation, spacegroup, and cell parameters were determined for the λ_{peak} data set, and then the same parameters used in processing the remaining three data sets. The third stage of data processing, which involves scaling and merging the observed intensities, was performed by Scala, a program from the Collaborative Computational Project, number 4 (CCP4) program suite (CCP4, 1994). At this stage the raw intensity measurements are corrected for experimental errors like crystal decay and air absorption. The corrected or scaled intensity measurements are then merged, such that redundant observations are averaged and their standard deviations determined. The level of agreement among symmetry-related reflections after scaling is measured by an $R_{symmetry}$ value:

$$R_{sym}(I) = \frac{\sum_{hkl} \sum_i \left| I_i(hkl) - \overline{I(hkl)} \right|}{\sum_{hkl} \sum_i \overline{I(hkl)}} \qquad (7)$$

where $I_i(hkl)$ is the observed intensity of the *hkl* reflection and $\overline{I(hkl)}$ is the average intensity of the i observations of symmetry-related reflections.

The SeMet crystal was found to belong to the same spacegroup ($I4_132$) as the wild-type crystals, with essentially identical cell dimensions ($a = b = c = 146.96$ Å) (Table 3.1). Using a method proposed by Matthews, (Matthews, 1968), it was estimated that the enzyme packs as a monomer in the $I4_132$ crystal form, with only one molecule per asymmetric unit. The mosaicity of the crystal (a measure of the quality or order of a crystal), as well as the R_{sym} value, increased significantly as data collection proceeded (Table 3.1). This increase is likely due to crystal decay since the data was collected over approximately 28 hours on account of frequent loss of the x-ray beam.

Wavelength	λ_{peak}=0.9792	λ_{infl}=0.9795	λ_{high}=0.9770	λ_{low}=0.9809
Mosaicity (°)	0.2	0.2	0.4	0.5
Resolution Limit (Å)	2.7	2.7	2.7	2.8
Unique Reflections	7725	7726	7637	6085
Redundancy	6.5	6.5	4.4	1.8
Completeness (%) *	99.8 (100.0)	99.9 (100.0)	99.1 (98.5)	89.7 (88.9)
R_{sym} *†	0.072 (0.170)	0.075 (0.188)	0.097 (0.263)	0.127 (0.332)
$\langle I/\sigma \rangle$ *	9.3 (4.1)	8.8 (3.8)	4.9 (1.5)	4.3 (1.4)

Table 3.1 Statistics from processing four-wavelength MAD data set. * Numbers given in brackets refer to data for the highest resolution shell. † For definition of R_{sym}, see equation (7). Statistics were obtained from results of processing with Mosflm (Leslie, 1990) and Scala (CCP4, 1994).

3.2.3 Phase Determination and Modification

In order to estimate the phase angles of the SeMet crystal, determination of the selenium atom positions in the unit cell is required. Mass spectrometry analysis of purified wild-type and SeMet AAC(6')-Ii indicated that all four methionine residues were

fully substituted by selenomethionine (Figure 3.2). However, positions for only three of the selenium atoms were initially searched for since the N-terminal methionine was not expected to be ordered. The Solve package (Terwilliger, 1997) was employed to determine potential positions for three of the selenium atoms.

Refinement of the selenium atom positions and subsequent calculation of phase angles was achieved by another automated program called Statistical Heavy Atom Refinement and Phasing (SHARP) (de La Fortelle & Bricogne, 1997). First, only the strongest selenium site from Solve was refined by SHARP and used to produce residual map peak lists. From these lists, two additional selenium sites were identified and found to correspond to those located by Solve. Thus, all three selenium atom positions were supplied to SHARP and used to calculate initial phase estimates. Solomon, a solvent-flipping program run automatically through SHARP, was used to improve these initial phases (Abrahams & Leslie, 1996). The improved phases were then used to calculate an experimental electron density map with FFT, a program from the CCP4 program suite (CCP4, 1994). The map proved to be of excellent quality.

3.2.4 Model Building and Refinement

Once an interpretable electron density map is obtained, an atomic model of the protein structure must be manually fit to the density. An atomic model of aminoglycoside acetyltransferase(6')-Ii was built using mainly the *baton* and *move* options in the graphical program O (Jones et al., 1991). The *lego* option was applied frequently in order

to ensure the model contained realistic bond lengths and angles. The majority of the acetyl coenzyme A ligand and 90% of the protein residues were readily traced using the experimental electron density map.

Reciprocal-space refinement with X-PLOR version 3.843 was carried out as described in section 2.4. Only 89.0% of the data from 40-2.7 Å was used for the refinement while the remaining 10.7% was used for structure validation (Brünger, 1992a). The first round of refinement included x-ray data in the resolution range of 8-2.7 Å with $F_{obs} > 2.0\sigma F_{obs}$. Tight restraints were placed on the B-factor refinement, with target sigma values of 0.5, 1.0, 0.5, and 1.0 for bonded backbone, angle-related backbone, bonded side-chain, and angle-related side-chain atoms, respectively. After the first round of refinement, the R factor and free R values had decreased from 46% and 45% to 31.4% and 36.4%, respectively. Following the second round of refinement, for which the resolution range for data inclusion was extended to 40-2.7 Å, the remaining ten N-terminal residues were assigned. Refinement of this more complete model with X-PLOR resulted in a significant decrease in both R factors. Furthermore, location of the fourth selenium atom permitted improved phases to be calculated by SHARP/Solomon (Table 3.2). The new phases were used to calculate a more detailed experimental electron density map that was subsequently employed throughout the model building process (Figure 3.5).

During the fourth round of reciprocal-space refinement, the amplitude cutoff was decreased to $1.0\sigma F_{obs}$ (i.e. 99.7% of all available data), resulting in the utilization of more data in the refinement process. After several additional rounds of iterative refinement and model adjustment, the R factor and R free values had decreased to 22.3% and 26.4%, respectively. At this point, ordered solvent molecules were assigned as water molecules. They were identified as well-defined peaks in the $2\mathbf{F}_o$-$\mathbf{F}_c$ and experimental electron density maps within hydrogen bonding distance (2.7-3.5 Å) of appropriate protein atoms or other solvent atoms. Water molecules were refined as oxygen atoms, with occupancies set to one. The occupancies of protein and ligand atoms were constrained to either zero or one throughout the refinement, and thus their B-factors reflect both thermal motion and disorder. The target values for the temperature factor deviations were made less stringent for the final round of refinement, with sigma levels of 1.5, 2.0, 2.0, and 2.5 for bonded backbone, angle-related backbone, bonded side-chain, and angle-related side-chain atoms, respectively.

The final model contains 181 of the possible 182 residues, one AcCoA molecule and 28 ordered solvent molecules. The electron density surrounding the C-terminal region is relatively poor; consequently, the last residue in the sequence was not modeled and the occupancy of residue 181 was set to zero for all side-chain atoms. Electron density for the side-chain atoms of Glu35 and Lys153 (last three atoms) could not be seen and thus these atoms have their occupancies set to zero as well.

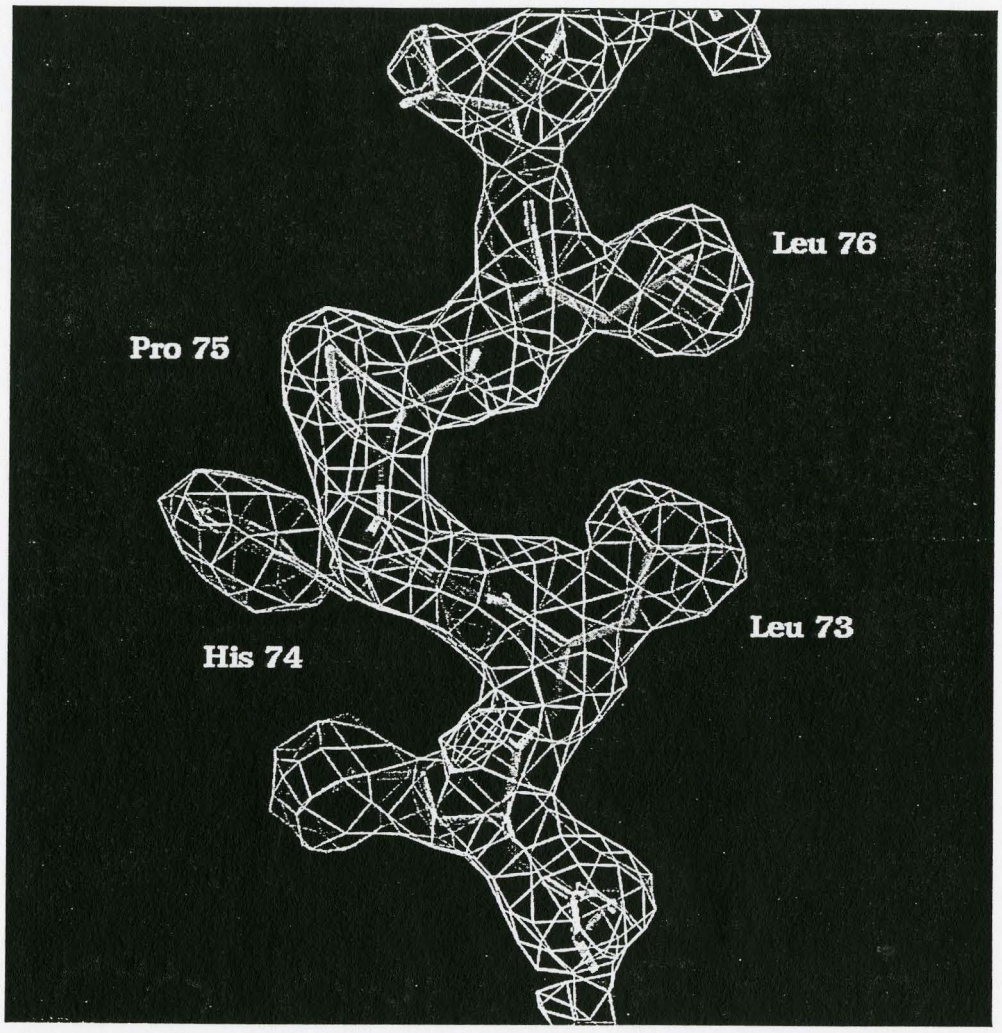

Figure 3.5 Experimental electron density map of the AAC(6')-Ii•AcCoA complex. The electron density map was calculated by FFT (CCP4, 1994) using phases calculated by SHARP given four selenium sites and modified by Solomon (de La Fortelle & Bricogne, 1997; Abrahams and Leslie, 1996). The map is calculated at 2.8 Å, contoured at 1σ, and shows the vicinity of Pro75, which is in the *cis* conformation.

Wavelength (Å)	λ_{peak}=0.9792	λ_{infl}=0.9795	λ_{high}=0.9770	λ_{low}=0.9809
Phasing power (four Se sites)				
Isomorphous centric	-	0.32	0.71	0.45
Isomorphous acentric	-	0.46	0.96	0.49
Anomalous	2.19	1.37	1.09	-
Phasing power (three Se sites)				
Isomorphous centric	-	0.26	0.65	0.41
Isomorphous acentric	-	0.38	0.87	0.44
Anomalous	1.95	1.31	1.06	-

Table 3.2 Phasing power statistics after refinement of heavy atom positions in SHARP. Statistics are provided for the phases derived from the complete heavy-atom model (four Se sites), and for the phases used to trace the initial model (three Se sites). All values were calculated with the SHARP package (de La Fortelle & Bricogne, 1997).

3.3 Results and Discussion

3.3.1 Quality of Aminoglycoside Acetyltransferase(6')-Ii•AcCoA Model

The refined AAC(6')-Ii•AcCoA structure has an R factor of 18.8% and an R free of 23.4%, using data between 40 and 2.7 Å with $F_{obs} > 1\sigma F_{obs}$ (i.e. 99.7% of all available data). These values indicate that the model is likely very accurate. The final model exhibits good stereochemistry as assessed by the program Procheck (Laskowski et al., 1993). In fact, 99% of non-glycine residues are placed within the favourable regions of the Ramachandran plot, with only one residue, Gln53, in the disallowed region of the plot (Figure 3.6). Both the main-chain and side-chain parameters are good, with root mean square deviations (rmsd) from ideality of 0.007 Å for bond lengths and 1.3° for bond angles (Table 3.3). Figure 3.7 illustrates the average isotropic temperature factors for

side-chain and main-chain atoms of each residue. These values are within acceptable ranges, with residues near Asp31 and the C-terminal tail exhibiting the most thermal motion or disorder. Such disorder in the C-terminal tail may explain why the electron density in this region could not be readily interpreted. Statistics for the final refined structure of the AAC(6')-Ii•AcCoA complex are summarized in Table 3.3.

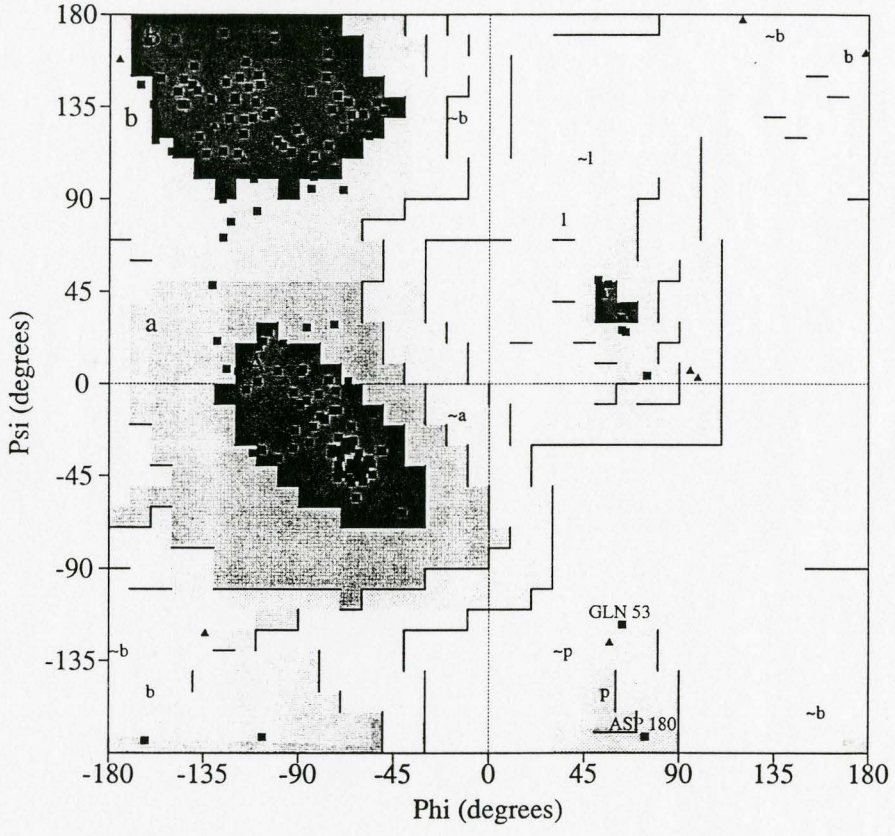

Figure 3.6 Ramachandran plot. The main-chain torsional angle phi (N-C_α bond) is plotted against psi (Cα-C bond) for all residues of aminoglycoside acetyltransferase (6')-Ii. Glycine residues are represented by triangles; all other residues are shown as squares. The shaded or enclosed regions indicate sterically allowed angles, with the most favoured combinations in the darkest region, additionally allowed combinations in the next darkest region, and generously allowed angles in the least shaded region. Figure adapted from output of Procheck (Laskowski et al., 1993).

Refinement Statistics		
Amplitude cutoff	$F_{obs} > 1\sigma F_{obs}$	
Number of reflections used in refinement	7718	
Resolution range (Å)	40-2.7	
Completeness (working + test) (%)	99.7	
R factor (%)[a]	18.8	
R free (%)[a]	23.4	
Number of non-hydrogen atoms used in refinement		
Protein atoms	1452	
AcCoA atoms	51	
Water molecules	28	
Number of atoms with occupancy set to zero	12	
Stereochemistry Statistics		
Rmsd in bond lengths (Å)	0.007	
Rmsd in bond angles (°)	1.3	
Rmsd in dihedral angles (°)	24.9	
Rmsd in improper angles (°)	1.16	
Residues in Ramachandran plot (%)[b]		
Most favourable region	85.9	
Additionally allowed region	12.8	
Generously allowed region	0.6	
Disallowed region	0.6	
	Working set	**Test set**
Luzzati estimated coordinate error (Å)[c]	0.24	0.33
Temperature Factors		
Overall mean B value (Å^2)	11.5	
Isotropic thermal model	Restrained	
Isotropic thermal factor restraints	**RMS**	**SIGMA**
Main-chain bond (Å^2)	2.21	1.50
Main-chain angle (Å^2)	3.30	2.00
Side-chain bond (Å^2)	4.09	2.00
Side-chain angle (Å^2)	5.51	2.50

Table 3.3 Statistics for the final model of the AAC(6')-Ii•AcCoA complex at 2.7 Å resolution. [a] For definitions of R factor and R free, see section 2.4. [b] Values were calculated using Procheck (Laskowski, 1993). [c] Values were calculated by X-PLOR using Luzzati's method for estimating coordinate errors (Luzzati, 1952).

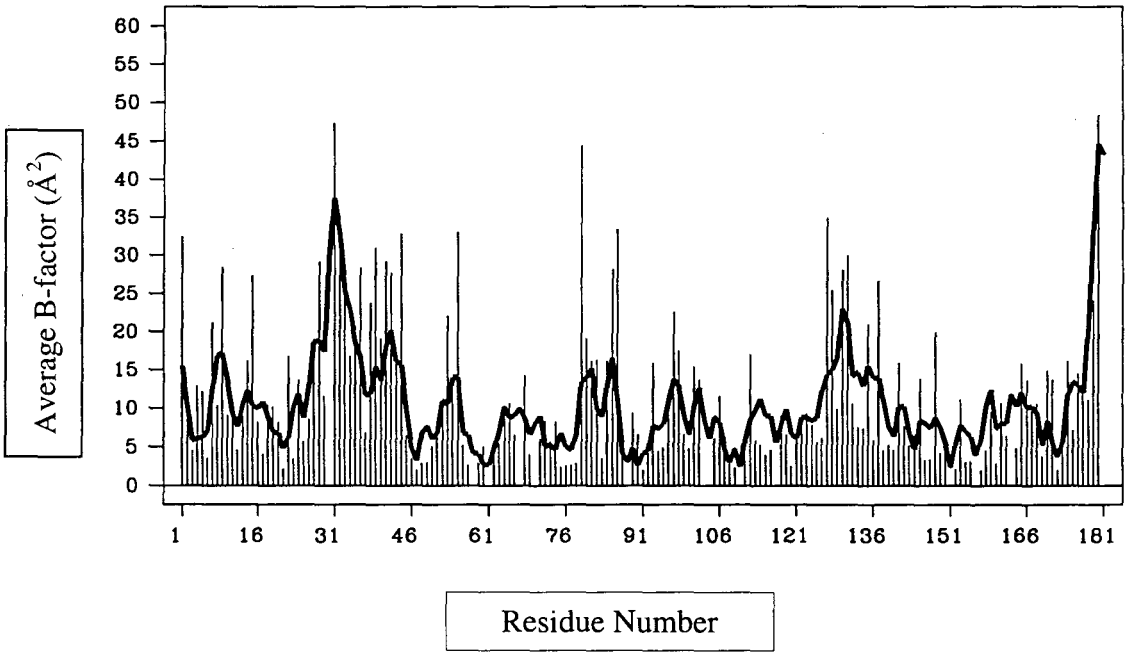

Figure 3.7 Mean values of the main-chain and side-chain isotropic temperature factors for each residue. Main-chain B values are indicated by the dark, thick line. Side-chain B values are represented by vertical spikes. Figure created by Bplot, a program in the CCP4 program suite (CCP4, 1994).

3.3.2 Architecture of Aminoglycoside Acetyltransferase(6')-Ii

The AAC(6')-Ii enzyme is a single domain structure made up of β-strands and α-helices (Figure 3.8). The structure clearly resembles the letter V, with the acetyl CoA ligand bound in between the two arms of the V. Residues one to 103 make up the N-terminal arm, (right arm in Figure 3.8, left panel), the core of which consists of a four stranded antiparallel β sheet (β1-β2-β3-β4) surrounded by three α-helices (α1, α2, and

α3). The first two α-helices are positioned in front of the β sheet, with helix α1 situated along the top of the β sheet and helix α2 roughly parallel to strand β2. The third α-helix is positioned behind the β sheet, close to strands β3 and β4. The C-terminal arm is formed by residues 104 to 182 and contains a three stranded antiparallel β sheet in the order β5-β7-β6 (Figure 3.8). This β sheet is flanked by the enzyme's remaining two α-helices, with helix α4 located on top and helix α5 behind the β sheet.

An intriguing structural feature of the AAC(6')-Ii enzyme is at the bottom of the V, where the N-terminal and C-terminal β sheets merge. In fact, the first five residues in strand β5 (residues 69-73) hydrogen bond with the four N-terminal residues of strand β4 (residues 105-108), so that a mixed parallel/antiparallel β sheet is formed (Figures 3.8 and 3.9). However, after this point the two strands diverge, dividing the mixed sheet into two twisted antiparallel β sheets. This divergence can be accredited to the presence of a classic β bulge formed by His74 N and Pro75 O in strand β4 and Gly61 in strand β3 (Figure 3.9) (Richardson et al., 1978). As defined by Richardson *et al.*, a β bulge is "a region between two consecutive β–type hydrogen bonds which includes two residues on one strand opposite a single residue on the other strand" (Richardson et al., 1978). As a result of this bulge, a bend is introduced into the N-terminal β sheet, significantly increasing its normal right-handed twist (Richardson et al., 1978). Since strand β5 cannot accommodate this twist, the two strands diverge (Figure 3.9). What makes this bulge region even more interesting is first its proximity to the enzyme's active site and

secondly, the presence of a rarely observed *cis*-peptide group between residues His74 and Pro75 (Figures 3.5 and 3.9).

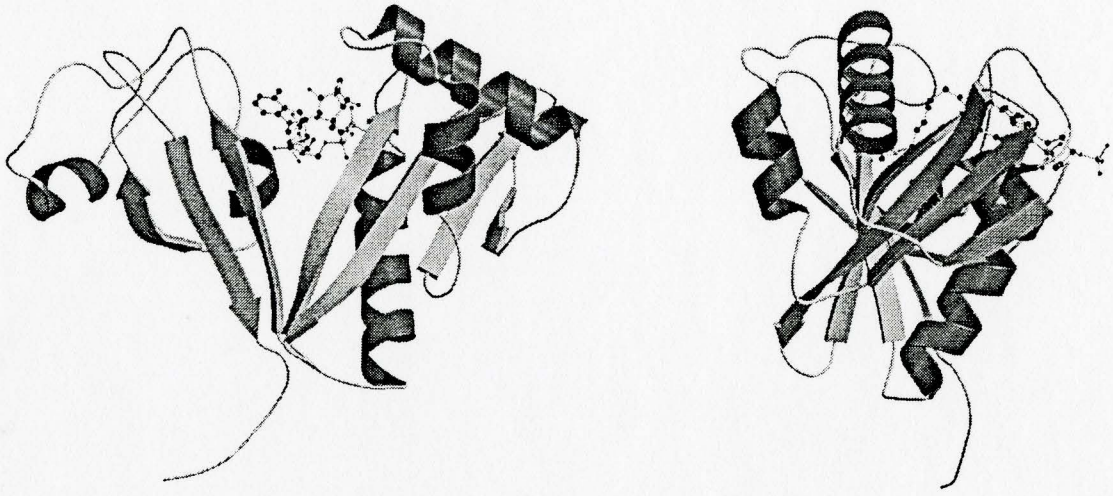

Figure 3.8 Ribbon diagram of the three-dimensional structure of the AAC(6')-Ii•AcCoA complex, highlighting the different secondary structure elements. β strands are shown as arrows, α-helices as spirals, and bound AcCoA in ball-and-stick representation. The right panel is rotated 90° about the vertical axis with respect to the left panel. This figure (and ones to follow) was generated using Bobscript (Kraulis, 1991) and Raster3D (Merritt & Murphy, 1994); secondary structure elements were assigned using the program DSSP (Kabsch & Sander, 1983).

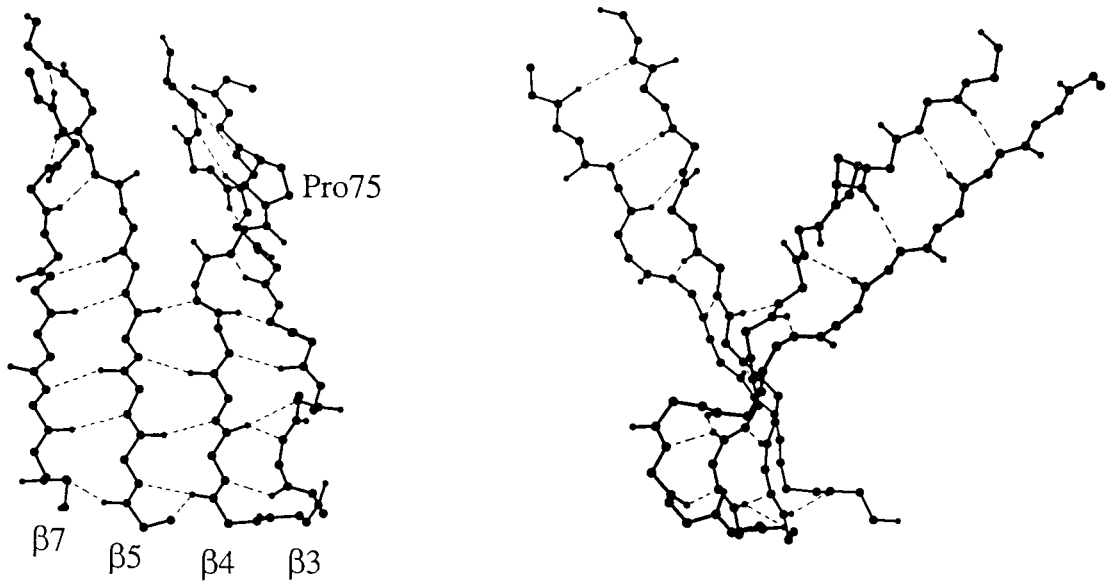

Figure 3.9 Detailed view of region where the N- and C-terminal arms of AAC(6')-Ii•AcCoA complex join, focusing on the β bulge involving *cis* Pro75. Shown are the backbone atoms and hydrogen bonds for β strands β3-β7 and all atoms of Pro75. The two orientations differ from each other by a 90° rotation about the vertical axis.

The C-terminal tail of the enzyme (residues 176-182) does not appear to adopt any rigid conformation or secondary structure, but instead is characterized as a coil by the program DSSP (Kabsch & Sander, 1983). Since the tail extends away from the molecule and forms no intramolecular interactions, it is conceivably very flexible in solution. Thus, the fact that all but the final residue, Gln182, of the tail could be reliably modeled is somewhat surprising. However, examination of crystal packing reveals that residues 176-180 form extensive intermolecular contacts (see section 3.3.4). Such interactions likely reduce the mobility of the C-terminal tail to an extent that it can be interpreted.

3.3.3 Acetyl Coenzyme A Binding and the Active Site

As mentioned above, the acetyl coenzyme A molecule is situated in the cleft between the N- and C-terminal arms of the acetyltransferase enzyme, forming contacts with both arms. In general, the residues involved in AcCoA binding are clustered in two regions of the N-terminal arm; i) the N-terminal half of loop $\alpha1\alpha2$ and ii) strand $\beta4$, loop $\beta4\alpha3$, and the N-terminal end of helix $\alpha3$, and two regions of the C-terminal arm; i) the C-terminal end of strand $\beta5$ and ii) the C-terminal end of loop $\alpha4\alpha5$ and helix $\alpha5$ (Figure 3.8). The cofactor binds in a fairly compact conformation, with a sharp bend at the pyrophosphate group and around the PC6-PC7 position in the pantetheine arm (Figure 1.3). This bent conformation enables the amino group of the adenine ring to form a water-mediated intramolecular hydrogen bond with the pantetheine moiety (Figure 3.10). Coenzyme A has been shown to adopt a similar bent, compact form when binding to enzymes like citrate synthase and enoyl-CoA hydratase, as reviewed by Engel and Wierenga (1996).

The AcCoA molecule is bound to AAC(6')-Ii by both hydrogen bonds and extensive Van der Waals interactions. Numerous hydrogen bonds exist between the cofactor and the enzyme, seven of which involve main-chain atoms, like the carbonyl oxygen of Leu76 and Glu141, or the amide group of Val78 (Figure 3.10). The pyrophosphate group in particular is bound primarily by interactions with main-chain atoms, forming hydrogen bonds with the backbone NH groups of Lys84, Gln86, Gly88,

and Thr89 (Figure 3.10) and water-mediated interactions with Arg82 O, Lys84 O, Asn85 N, and Ile87 N. In addition, the side-chain hydroxyl group of Thr89 forms a hydrogen bond with the α-phosphate group of AcCoA. A similar interaction likely exists between the side-chain hydroxyl group of Tyr147 and the AcCoA sulfur atom (distance 3.7 Å). Furthermore, the side-chain amino group of Lys149 interacts with both the 3'-phosphate group and the adenine ring of the cofactor, via a hydrogen bond/salt bridge and a water-mediated hydrogen bond, respectively (Figure 3.10). Several additional water-mediated hydrogen bonds exist between the carbonyl oxygen of the thioester and nearby polar side-chains, such as Asp112, Glu28, and Tyr29 (Figure 3.10). These hydrogen bonds, in combination with a hydrogen bond formed between the terminal sulphur atom of the β-mercapto-ethylamine and the hydroxyl group of Tyr147, appear to influence positioning of the carbonyl oxygen of the thioester (Figure 3.10). Likewise, the β-methyl of the acetyl group is favourably situated in a hydrophobic pocket formed by the side-chains of Leu73, Pro75, and Leu109, all three of which are absolutely conserved within the AAC(6')-Ii subfamily. Interestingly, this binding pocket appears to be deep enough to accommodate slightly larger groups, which is consistent with the finding that propionyl CoA is a suitable cofactor for AAC(6')-Ii (Wright & Ladak, 1997). A number of other hydrophobic residues (i.e. Thr24, Trp25, Leu76, Val78, Pro143, and Phe146) surround the pantetheine arm of AcCoA, likely forming hydrophobic interactions and Van der Waals contacts with the hydrophobic regions of the ligand (Figure 3.10).

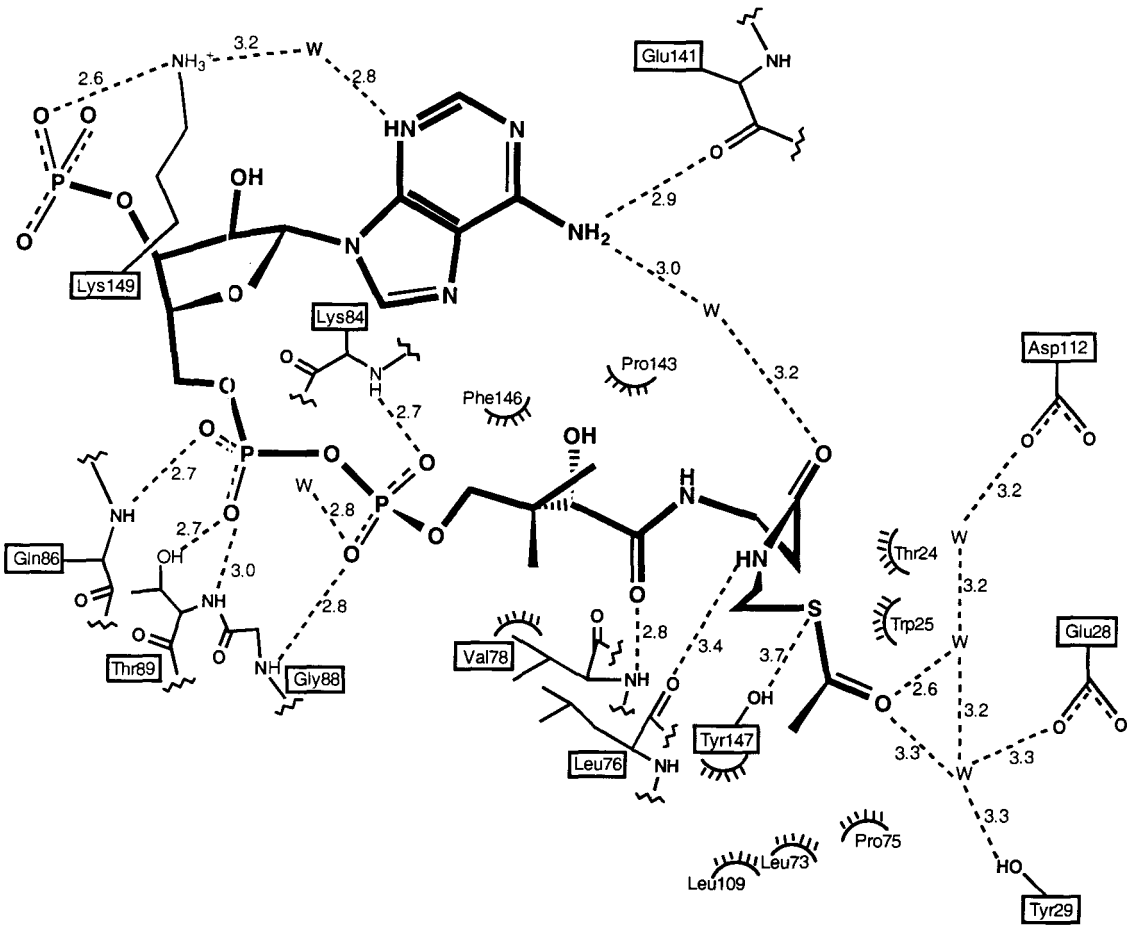

Figure 3.10 Interactions between AAC(6')-Ii and acetyl coenzyme A. The AcCoA molecule and residues forming interactions with it are drawn schematically, with dashed lines representing hydrogen bonds and semicircles indicating hydrophobic or Van der Waals interactions. Distances are given in Ångstroms.

The AAC(6')-Ii molecule appears to have a unique overall fold when compared to the crystal structures of various CoA binding proteins, as reviewed by Engel and Wierenga (1996). However, it does share some common features with these enzymes in the binding mode of CoA. For instance, consistent with the enzymes reviewed by Engel

and Wierenga, the 3'-phosphate group of the bound cofactor is solvent exposed while its adenine ring points towards the protein molecule. Furthermore, another characteristic of CoA binding proteins is that the adenine amino group is always hydrogen bonded to the protein, usually via main-chain atoms (Engel & Wierenga, 1996). This feature is observed in AAC(6')-Ii as well; the amino group of the adenine ring forms a hydrogen bond with the backbone carbonyl group of Glu141. In most CoA binding structures, at least one salt bridge and some hydrogen bonds with polar side-chains are observed between the protein and the phosphate groups (Engel & Wierenga, 1996). However, in AAC(6')-Ii, although one contact is observed between the 3'-phosphate and Lys149, the vast majority of hydrogen bonds with the pyrophosphate moiety are formed with main-chain amide groups (Figure 3.10). Until recently, this phenomenon had only been observed in succinyl-CoA synthetase (Engel & Wierenga, 1996). However, similar observations were recently reported for both histone acetyltransferase HAT1 (Dutnall et al., 1998) and *Serratia marcescens* aminoglycoside acetyltransferase(3)-Ia (Wolf et al., 1998) (see section 3.5).

As can be seen from Figure 1.3, the pantetheine arm of AcCoA incorporates two peptide groups. Interestingly, these groups form β-type hydrogen bonds with strand β4 of AAC(6')-Ii, thus creating an additional pseudo β strand and effectively extending the N-terminal β-sheet by one strand. This observation emphasizes the structural importance of the β bulge in strand β4; this feature affords adequate separation between strands β4 and

β5, thereby enabling an additional pseudo β strand to position itself between the N- and C-terminal arms of the protein. Here, the cofactor forms interactions with both arms of the enzyme, which may act to stabilize the protein by reducing the mobility of the upper portions of the two arms. This suggestion is consistent with protein NMR experiments which indicate that AAC(6')-Ii becomes more ordered upon binding of acetyl-CoA (Draker et al., 1999).

Despite the fact that the kinetic mechanism of AAC(6')-Ii has not yet been determined precisely, results indicate that substrate modification does not occur through an acyl-enzyme intermediate, but via a ternary complex (Wright & Ladak, 1997; Draker et al., 1999). The structure of AAC(6')-Ii in complex with AcCoA does not challenge this theory, given the lack of evidence for a covalent intermediate. Furthermore, the structure provides information as to the general location of the enzyme's active site. However, the exact residues involved in stabilizing the ternary complex and aminoglycoside acetylation can not be identified from this structure. In fact, even residues involved in positioning the reactive thioester in the active site can not be precisely identified since the position of the acyl moiety appears to be quite flexible, as indicated by its moderately high temperature factors (i.e. S:56.1, C:52.4, O:54.6, CH_3:53.1 $Å^2$).

Although definitive identification of the residues involved in aminoglycoside binding and acetylation will require structure determination of the ternary complex and

possibly mutagenesis studies, examination of the AAC(6')-Ii-AcCoA complex reveals the most likely site of aminoglycoside binding. First, the sulfur atom of AcCoA is positioned at the bottom of a cleft formed by N-terminal residues, specifically Trp25, Glu27, and Glu28, and C-terminal residues, like Thr111, Asp112, Leu114, Pro143, and Tyr147. Thus, the 6'-amino group of the aminoglycoside substrate must be positioned in this cleft. However, the size of the cleft is not large enough to accommodate the entire aminoglycoside substrate. This suggests that only the 6'-amino group will be positioned in this cleft, in agreement with the broad substrate specificity observed for AAC(6')-Ii (Wright & Ladak, 1997). Secondly, aminoglycoside antibiotics are invariably positively charged compounds due to the incorporation of numerous amino groups in their structure. In fact, the presence of these protonated amino groups has been shown to be important to binding, suggesting that electrostatic interactions are involved in the binding of AGAC antibiotics (Cox & Serpersu, 1997). Consequently, aminoglycosides are expected to bind a complementary charged surface, such as that provided by the front entrance to the cleft described above (Figure 3.11). The side-chains lining the wall of this front entrance are predominantly negatively charged (e.g. Glu27, Glu28, Glu36, Glu39, Glu72, Asp112, Asp115, and Asp168), thereby creating a negatively charged surface ideal for aminoglycoside binding. Similar negatively charged patches have been observed in other aminoglycoside modifying enzymes, such as APH(3')-IIIa (Hon et al., 1997) and AAC(3)-Ia (Wolf et al., 1998).

As mentioned earlier, mutagenesis experiments have indicated the importance of two regions that are relatively conserved across the three AAC(6') subfamilies. Specifically, residues 73-77 and 85-98 (AAC(6')-Ii numbering) are thought to influence aminoglycoside binding and specificity. Indeed, the structure of the AAC(6')-Ii•AcCoA complex reveals that a number of residues within these regions are involved in cofactor binding, such as Leu73, Pro75, Leu76, Gln86, Gly88, and Thr89 (Figures 3.10 & 3.12). However, the side-chains of both Leu76 and Leu91, which were specifically implicated by mutagenesis studies to be involved in aminoglycoside binding, are positioned within a large internal hydrophobic domain that exists between strands β1-β4 and helix α3 (Figure 3.12). It is possible that mutation of either of these large, hydrophobic side-chains to a small, polar group, such as that found in serine residues, could result in a disruption of this large hydrophobic pocket, thus altering the enzyme's active site and resistance profile. However, confirmation of such conformational changes and specific details regarding the extent to which residues 73-77 and 85-98 are involved in aminoglycoside binding will require determination of the three-dimensional structure of an aminoglycoside•AAC(6')•AcCoA complex.

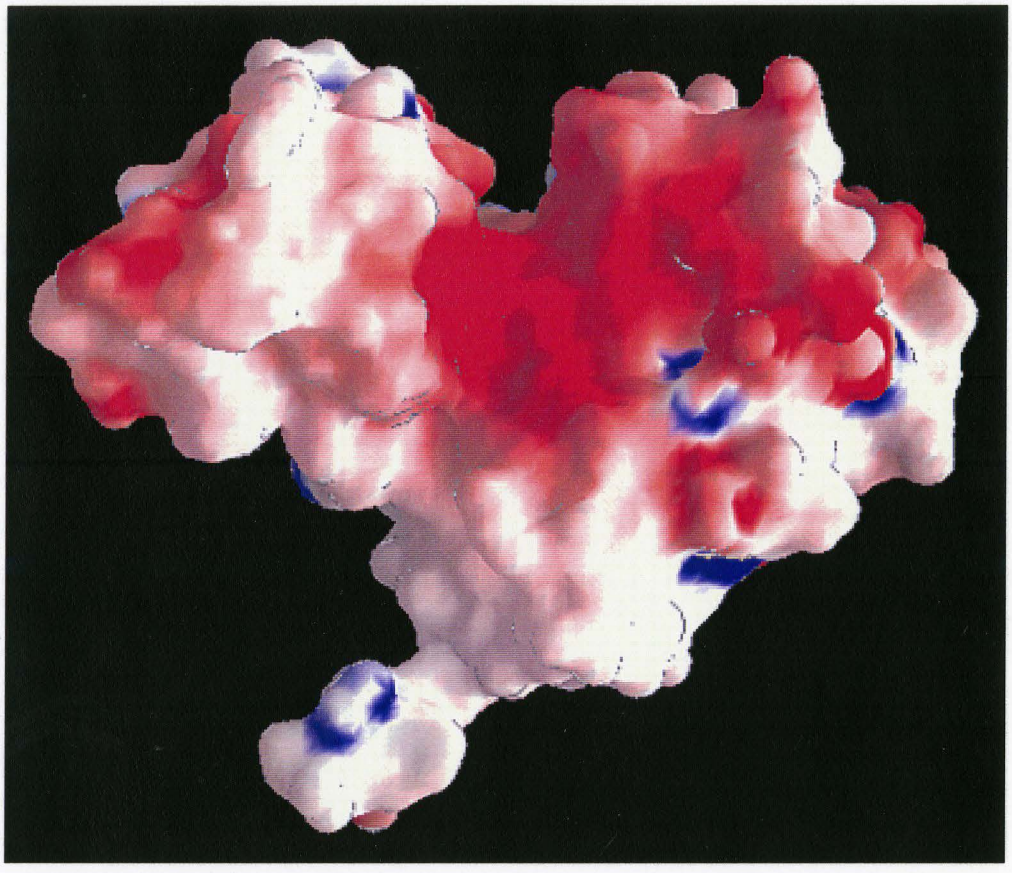

Figure 3.11 Putative aminoglycoside–binding site of AAC(6')–Ii–AcCoA complex. The molecular surface of the complex is coloured according to electrostatic potential, ranging from −15.0 to +15.0 k_BT (red to blue, respectively) as calculated by the program GRASP (Nicholls et al., 1991). The molecule is shown in the same orientation as that in the left panel of Figure 3.8.

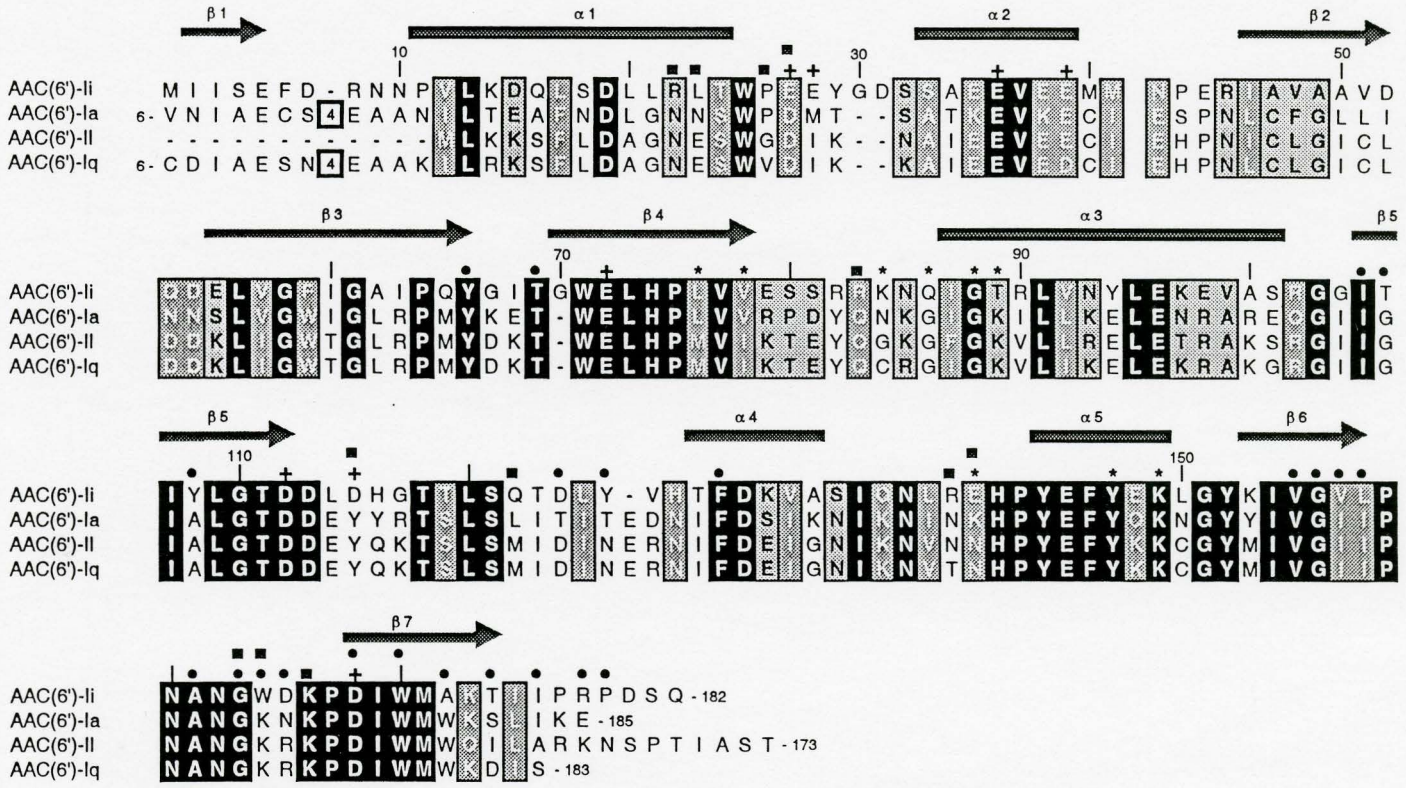

Figure 3.12 Sequence alignment of the four members of the AAC(6')-Ii subfamily, as aligned by ClustalW (Thompson et al., 1994). The secondary structure elements of AAC(6')-Ii are indicated, with α helices shown as solid boxes and arrows representing β strands. Identical residues are darkly shaded with white lettering, highly similar residues are lightly shaded with white lettering, and slightly similar residues are lightly shaded with black lettering.

Legend: * residue interacts with AcCoA; + putative aminoglycoside-binding residue;

■ forms intermolecular contact in dimer five; • forms intermolecular contact in dimer six.

3.3.4 Potential Aminoglycoside Acetyltransferase(6')-Ii Dimers

The AAC(6')-Ii enzyme packs as a monomer in the $I4_132$ crystal form, with only one molecule per asymmetric unit. However, analytical gel filtration experiments indicate that the enzyme is a dimer in solution (Wright & Ladak, 1997). Thus, it is very likely that the symmetry operator that relates the two molecules in the dimer corresponds with a crystallographic symmetry operator. Consequently, potential AAC(6')-Ii dimers were easily identified by using the *symmetry* options in the graphical program O (Jones et al., 1991). However, since the spacegroup $I4_132$ contains a high degree of symmetry, with 48 asymmetric units per unit cell, seven possible dimers were generated, six of which are unique and shown in Figure 3.13. As can be seen, a number of the dimer interfaces involve residues in the C-terminal tail of AAC(6')-Ii. In fact, both hydrogen bonds and Van der Waals contacts can be observed between specific residues of candidates one, two, and six and residues 176-180 of AAC(6')-Ii. As mentioned above, such stabilizing interactions likely reduce the mobility of the C-terminal tail, enabling it to be modeled.

In order to establish the most probable physiological dimer, the extent of dimer interface was measured by comparing the accessible surface area of two monomers to that of each dimer candidate (Figure 3.13, legend). These values, determined by the *build* and *calculate* options of the program GRASP (Graphical Representation and Analysis of Surface Properties) (Nicholls et al., 1991), implicated dimer candidates five and six as the most likely physiological dimers, since they resulted in the greatest reduction in the total

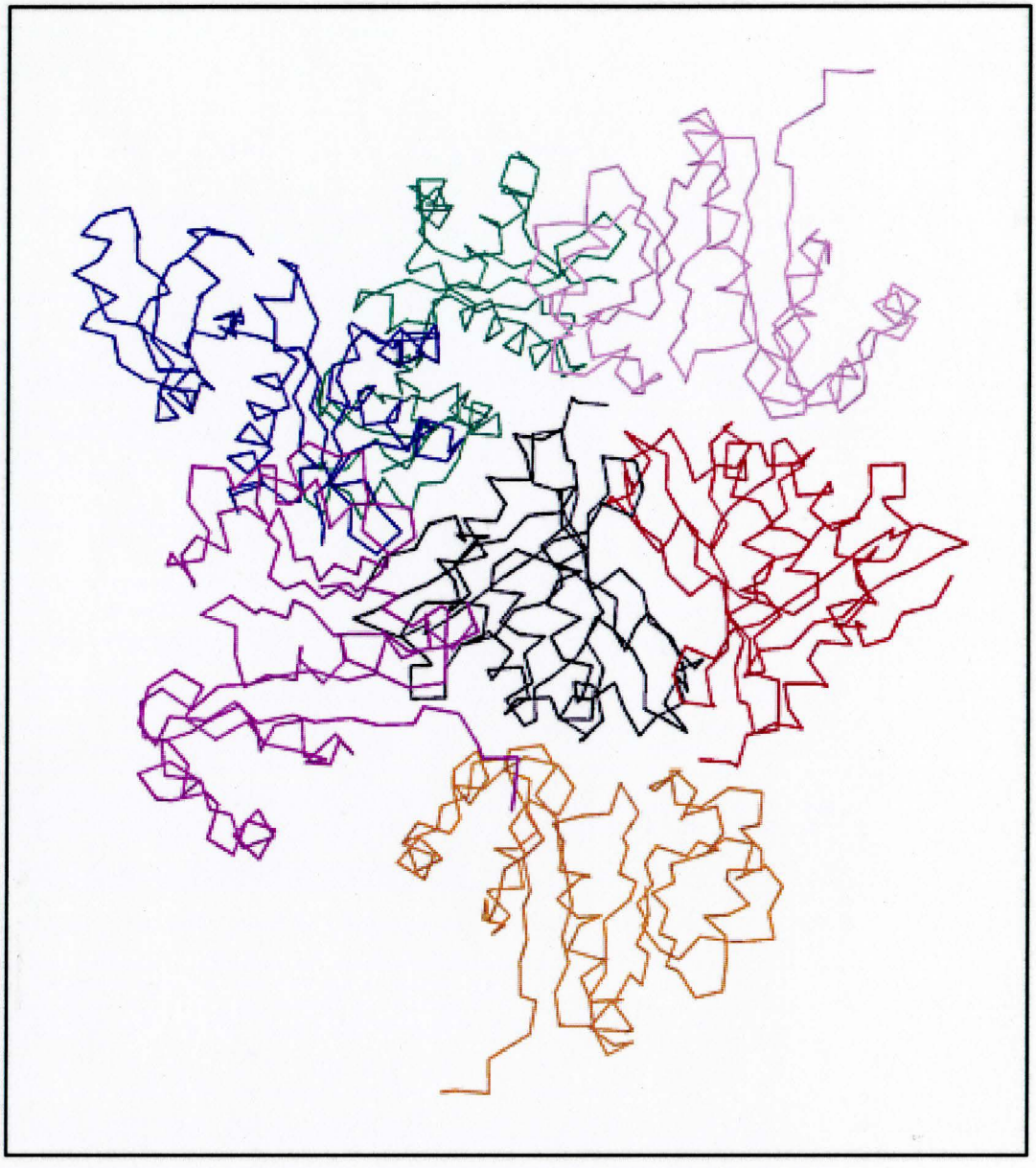

Figure 3.13 Schematic representation of potential AAC(6')–Ii dimers. Symmetry–related molecules were generated with respect to the black monomer using the graphical program O (Jones et al., 1991). Thus, the black monomer can be paired with any one coloured monomer to constitute a possible AAC(6')–Ii dimer. Dimer candidate numbers, colours, and interface areas (square angstroms) are as follows: (1) pink; 463, (2) green; 114, (3) blue; 1068, (4) purple; 1062, (5) orange; 1481, and (6) red; 2816. Areas of dimer interfaces were calculated with GRASP (Nicholls et al., 1991).

accessible surface area. In fact, only these two dimers exhibited an interface area of greater than 1400 $Å^2$, which is the accepted lower limit for dimer interfaces (Janin, 1995).

The dimer interface for candidate five involves the top portions of both the N-terminal and C-terminal arms of both monomers (Figure 3.14a). The majority of contacts between the two monomers involves residues located within loop regions of the enzyme; that is, loops α1α2, β4α3, β5α4, α4α5, and β6β7 (Figure 3.12). The monomers interact via hydrogen bonds, hydrophobic interactions, and Van der Waals contacts, as illustrated by a molecular surface drawing of the dimer coloured according to hydrophobic potential by residue (Figure 3.14b). Interactions between the monomers are reciprocated due to the symmetry of the interface; that is, if atom *n* of monomer A hydrogen bonds with atom *m* of monomer B, then atom *n* of monomer B also hydrogen bonds with atom *m* of monomer A. Each monomer appears to have a distinct active site, as indicated by the relatively large distance between the bound cofactors and the discrete negatively charged pockets that comprise the putative aminoglycoside binding sites (Figure 3.14).

The dimer interface of the other most probable physiological dimer, candidate six, involves mostly the C-terminal arms of both monomers (Figure 3.15a). The C-terminal strands, β5, β6, and β7, and loop regions β3β4, β5α4, and β6β7, as well as the C-terminal tail, are involved in both hydrophobic and hydrophilic interactions between the two monomers (Figure 3.15b). Again, two discrete active sites are observed (Figure 3.15). Of the two most probable physiological dimers, candidate six appears to be the

most likely for numerous reasons. First and foremost, the structure of this dimer candidate is more biochemically sound than candidate five is. For instance, the C-terminal tail appears to be unprotected in the monomer structure, despite the fact that it contains a number of large, hydrophobic residues. Whereas this region remains unprotected in dimer candidate five, it is stabilized in candidate six due to the formation of hydrogen bonds and Van der Waals interactions between the tail residues (176-181) of one monomer and residues in loops β5α4 and β6β7 of the other monomer. Consequently, the structure of dimer candidate six is much more compact and globular, which would likely result in better solubility. Furthermore, strand β6 from each monomer in dimer candidate six lay antiparallel to one another and form β-type hydrogen bonds with one another. In this way, the antiparallel β-sheets of each C-terminal arm merge into a larger, even more twisted, antiparallel β-sheet. Since most of the residues in strand β6 are hydrophobic in nature, extension of the β-sheet at this location would undoubtedly improve the stability and solubility of the enzyme. In contrast, this hydrophobic region remains exposed in dimer candidate five, making it a less likely candidate for the true physiological dimer. Secondly, a number of the residues that form strong interactions between the two monomers are identical for each member of the AAC(6')-Ii subfamily. For example, both Tyr66 and Asp168, whose side-chain atoms form a strong intermolecular hydrogen bond (distance 2.7 Å), are absolutely conserved (Figure 3.12). In addition, the aromatic side-chain of absolutely conserved Phe130 from one monomer stacks upon that of the second monomer at a distance of only 3.15 Å,

thereby creating a very strong intermolecular interaction. In contrast, although a number of the residues involved in the dimer interface for dimer five are functionally conserved, only two of the residues are absolutely conserved (Figure 3.12). The involvement of highly conserved residues in the dimer interface supports the physiological relevance of dimer six, since all members of the AAC(6')-Ii subfamily are expected to have similar structures based on their sequence homology. Finally, the dimer interface for candidate six occupies 2816 $Å^2$, while the area of interface for dimer candidate five is only 1481 $Å^2$ (Figure 3.13). This supports dimer candidate six as the true physiological dimer, since Janin observed that the area of a dimer interface is usually much larger than 1400 $Å^2$ (Janin, 1995). Thus, the structure of the physiological dimer of AAC(6')-Ii likely corresponds to that shown in Figure 3.15a, such that the two monomers are related to one another by the rotation operator –1 0 0, 0 –1 0, 0 0 1, followed by a translation of *a* and ½*b* (where $a = b = 146.96$ Å).

Although confirmation of the true physiological dimer of AAC(6')-Ii will require crystallization of the enzyme in another spacegroup and comparison of the potential dimers, it is important to note that all of the crystallographic dimers observed appear to contain two discrete active sites. This observation is consistent with the assumption made by Wright and Ladak that there is one active site per AAC(6')-Ii monomer (Wright & Ladak, 1997).

(a)

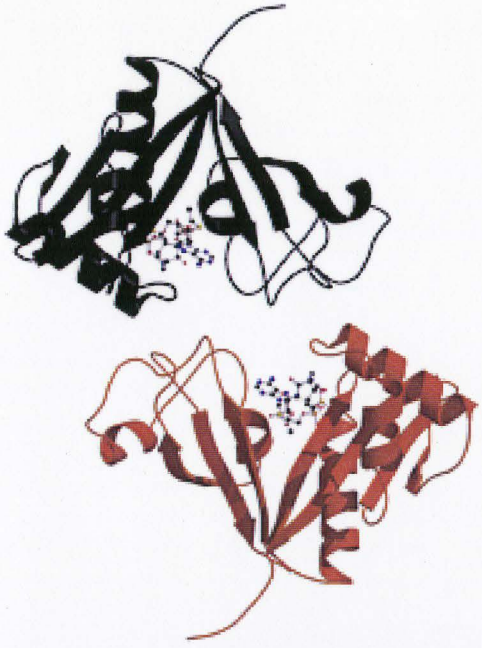

(b)

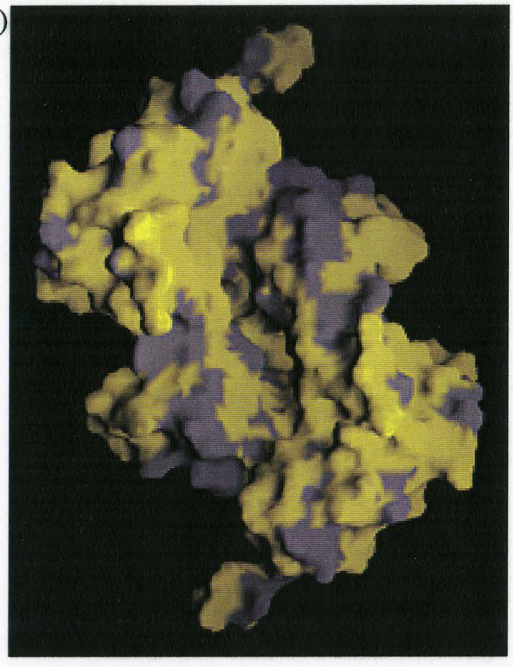

(c)

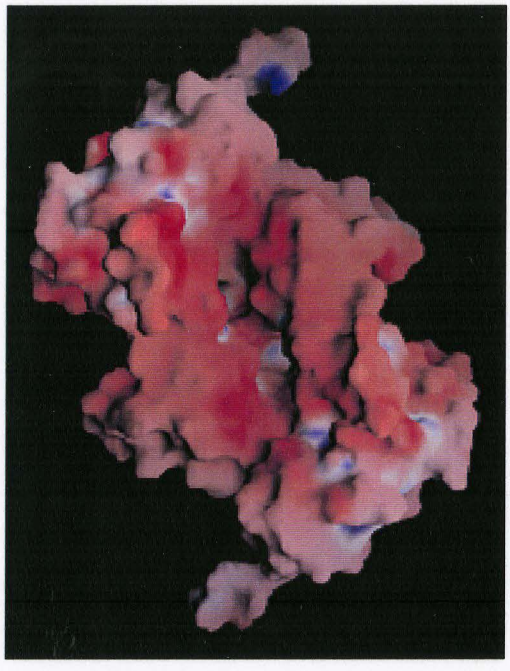

Figure 3.14 Representations of first potential AAC(6')–Ii–AcCoA dimer.

(a) Ribbon diagram of dimer, with colours corresponding to those in Figure 3.13 and bound AcCoA molecules in ball–and–stick representation.

(b) Molecular surface drawing of dimer, coloured according to hydrophobic potential by residue. Yellow regions are polar in nature, while grey areas are hydrophobic.

(c) Molecular surface drawing of dimer, coloured according to electrostatic potential, ranging from –25.0 to +25.0 kBT (red to blue, respectively).

Panels (b) and (c) were generated with GRASP via the GRASS Browser (http://honiglab.cpmc.columbia.edu/cgi–bin/GRASS/surfserv_enter.cgi).

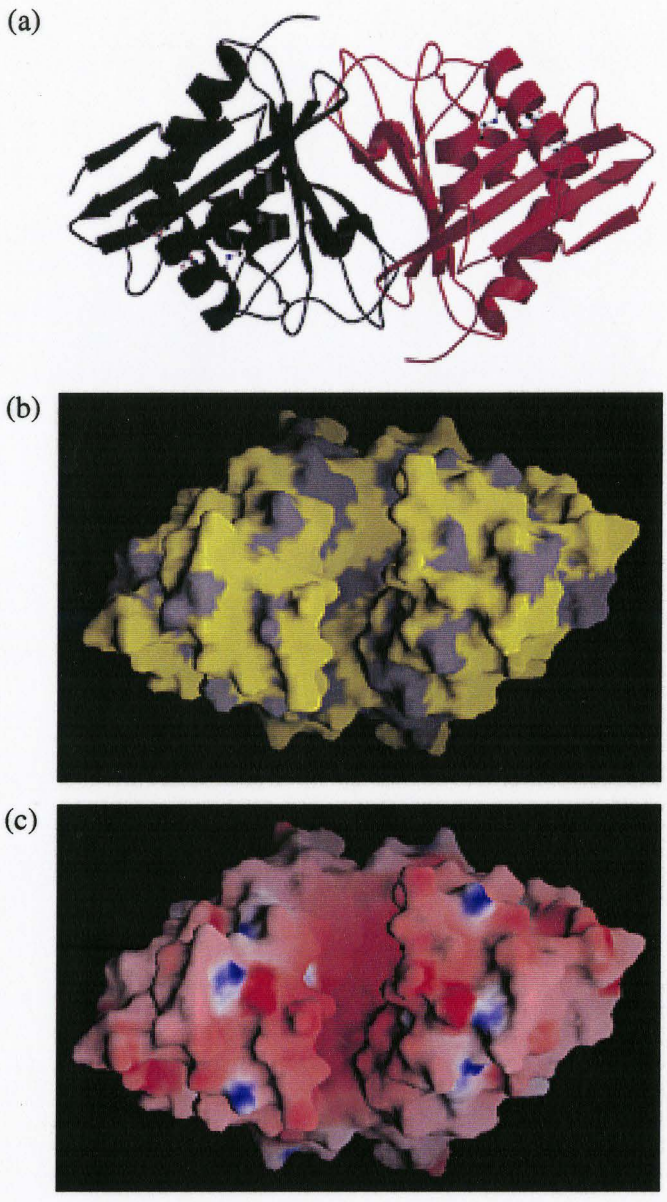

Figure 3.15 Schematic representations of second potential AAC(6')–Ii–AcCoA dimer. (a) Ribbon diagram of dimer, coloured as in Figure 3.13, with bound AcCoA molecules in ball–and–stick representation. (b) Molecular surface drawing of dimer coloured according to hydrophobic potential by residue. Yellow regions are polar in nature, while grey regions are hydrophobic. (c) Molecular surface drawing of dimer coloured according to electrostatic potential, ranging from –25.0 to +25.0 kBT (red to blue, respectively).

3.3.5 AAC(6')-Ii as a Member of the GCN5-Related *N*-Acetyltransferase Superfamily

GNAT Superfamily Fold

Determination of the crystal structure of the AAC(6')-Ii•AcCoA complex revealed the existence of another unique fold among CoA-binding proteins (Engel & Wierenga, 1996). Interestingly, part of this fold is seen in two structures that were published just after completion of the AAC(6')-Ii•AcCoA structure, namely histone acetyltransferase from *Saccharomyces cerevisiae* (yHAT1) (residues 1-320) in complex with acetyl-CoA (Dutnall et al., 1998) and *Serratia marcescens* AAC(3)-Ia (residues 1-168) in complex with CoA (Wolf et al., 1998) (Table 3.4). All three of these enzymes are members of an acetyl-CoA-dependent GCN5-related *N*-acetyltransferase or GNAT superfamily, which spans all kingdoms of life and has at least 140 members that often lack pairwise sequence similarity (Neuwald & Landsman, 1997). However, this lack of sequence homology is apparently not reflected in the three-dimensional structures of GNAT superfamily members. Indeed, 84 residues are structurally identical in AAC(6')-Ii, yHAT1, and AAC(3)-Ia, although only three of these residues are chemically identical (3.6%) and only nine are chemically similar (10.7%) (Figure 3.16). Thus, this expansive, functionally diverse superfamily appears to be characterized by a conserved fold that is unique among CoA-binding proteins.

Interestingly, the GNAT fold is also observed in *N*-myristoyltransferase (NMT) from *Candida albicans* (Weston et al., 1998; Modis & Wierenga, 1998), as well as in NMT1p from *Saccharomyces cerevisiae* (Bhatnagar et al., 1998). These two structures

are highly similar, with high sequence identity (Weston et al., 1998) and an rms difference in Cα positions of 1.35 Å (376 matched residues). Both enzymes exhibit internal two-fold symmetry, with each half of NMT adopting the same topology as that of the core domain of the GNAT family of enzymes (Modis & Wierenga, 1998). However, despite this topological similarity to GNAT members, NMT can not be identified as a true member of the GCN5-related *N*-acetyltransferase superfamily since it utilizes myristoyl-CoA to myristoylate the N-terminal glycine residue of its peptide substrates. These findings imply that the definition of the GNAT superfamily may have to be altered to include not just *N*-acetyltransferases, but any acyl-CoA binding transferase that contains the typical GNAT folding pattern. Given this extended definition, the structure of NMT must be included when analyzing the GNAT superfamily fold. Yet, considering the similarity between the *C. albicans* apo-enzyme structure and the *S. cerevisiae* ternary complex structure, only NMT1p will be included in the analysis presented here. Furthermore, since the N-terminal half of NMT1p contributes largely to the myristoyl-CoA binding site, while the C-terminal half contributes largely to the peptide binding site (Bhatnagar et al., 1998), only the former will be used for comparison.

According to Modis and Wierenga, both the AAC(3)-Ia monomer and each half of NMT(1p) share the same topology as the core domain of yHAT1, which consists of a β-sheet covered on both sides by α-helices (Modis & Wierenga, 1998). In agreement with this observation, comparison of AAC(6')-Ii to these three structures reveals that the N-terminal β-sheet β1-β4, helix α3, and strand β5 (AAC(6')-Ii nomenclature) are

Structure	PDB Code	Residues (missing)*	Resolution (Å)	R factor/ R free (%) (I/σ cutoff)	Reference
AAC(6')-Ii•AcCoA	1b87	1-182	2.7	18.8/23.4 (1)	Wybenga-Groot et al., 1999
YHAT1•AcCoA	1bob	1-320 (54 C-term)	2.3	20.4/26.9 (0)	Dutnall et al., 1998
AAC(3)-Ia•CoA	1bo4	1-168 (9 C-term)	2.3	20.4/25.1 (2)	Wolf et al., 1998
NMT	1nmt	1-451	2.8	21.4/27.9 (NR)†	Weston et al., 1998
NMT1p•analog of myristoyl CoA •peptidic inhibitor	2nmt	1-455	2.9	22.8/29.7 (1)	Bhatnagar et al., 1998

Table 3.4 Summary of structures of GNAT superfamily members. *Number in parentheses indicates number of residues missing from the original enzyme construct, and not those missing from the final structure due to eg. poor electron density. † NR indicates that the amplitude cutoff was not reported.

structurally well conserved (Figure 3.17). Helix α1 is generally well conserved as well, except for being partly unwound in the yHAT1 enzyme (Figure 3.17). The greatest degree of variation in the fold occurs between helix α1 and strand β2, where both the number and location of additional α helices differs for each enzyme (Figure 3.17). Slight variations in the length of loop regions also occurs, especially for loop β3β4 (Figure 3.17). However, the same core domain is generally shared among the available crystal structures of GNAT superfamily members, thus defining the GNAT fold.

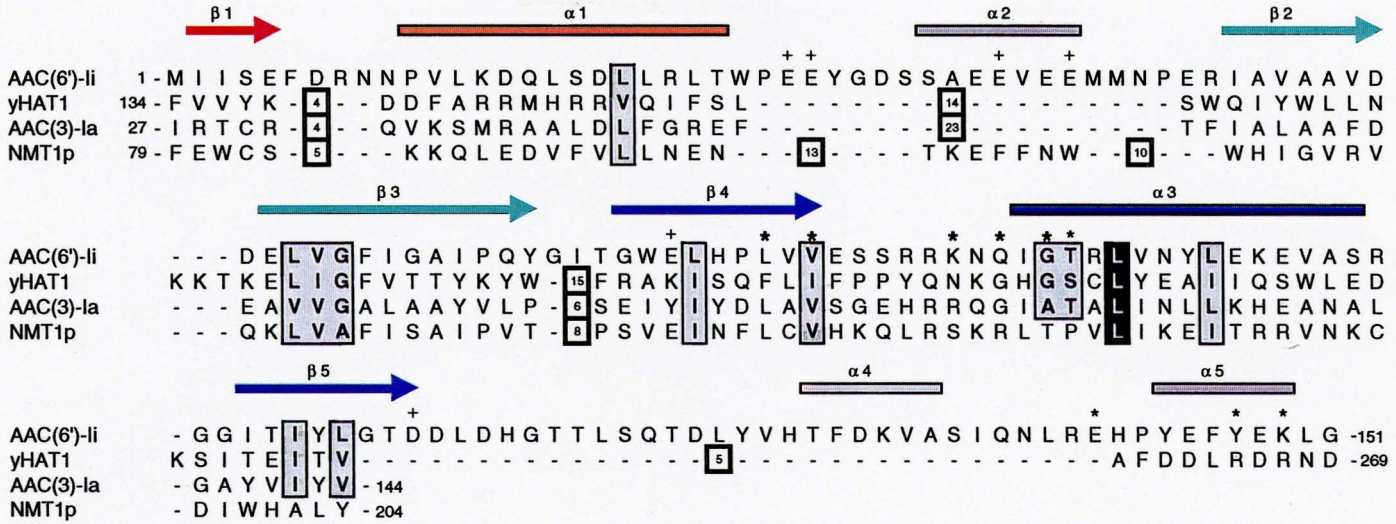

Figure 3.16 **Structure-based sequence alignment of the four unique GNAT superfamily members**, for which crystal structures have been determined. Residues that are functionally conserved are shown boxed with grey background and black lettering, while residues that are absolutely conserved within the superfamily are shown boxed with black background and white lettering. Inserts are shown as open boxes and the number displayed indicates the number of residues that are inserted at that location. The location of secondary structure elements (AAC(6')-Ii nomenclature) is indicated and the colour-coding scheme used follows that in Figure 3.17. Residues of AAC(6')-Ii that are known to interact with the cofactor are marked with an asterisk, and residues putatively implicated in substrate binding are indicated by a plus sign. Residues involved in main-chain hydrogen-bonds with the cofactor that are conserved within the GNAT family are marked by a larger asterisk.

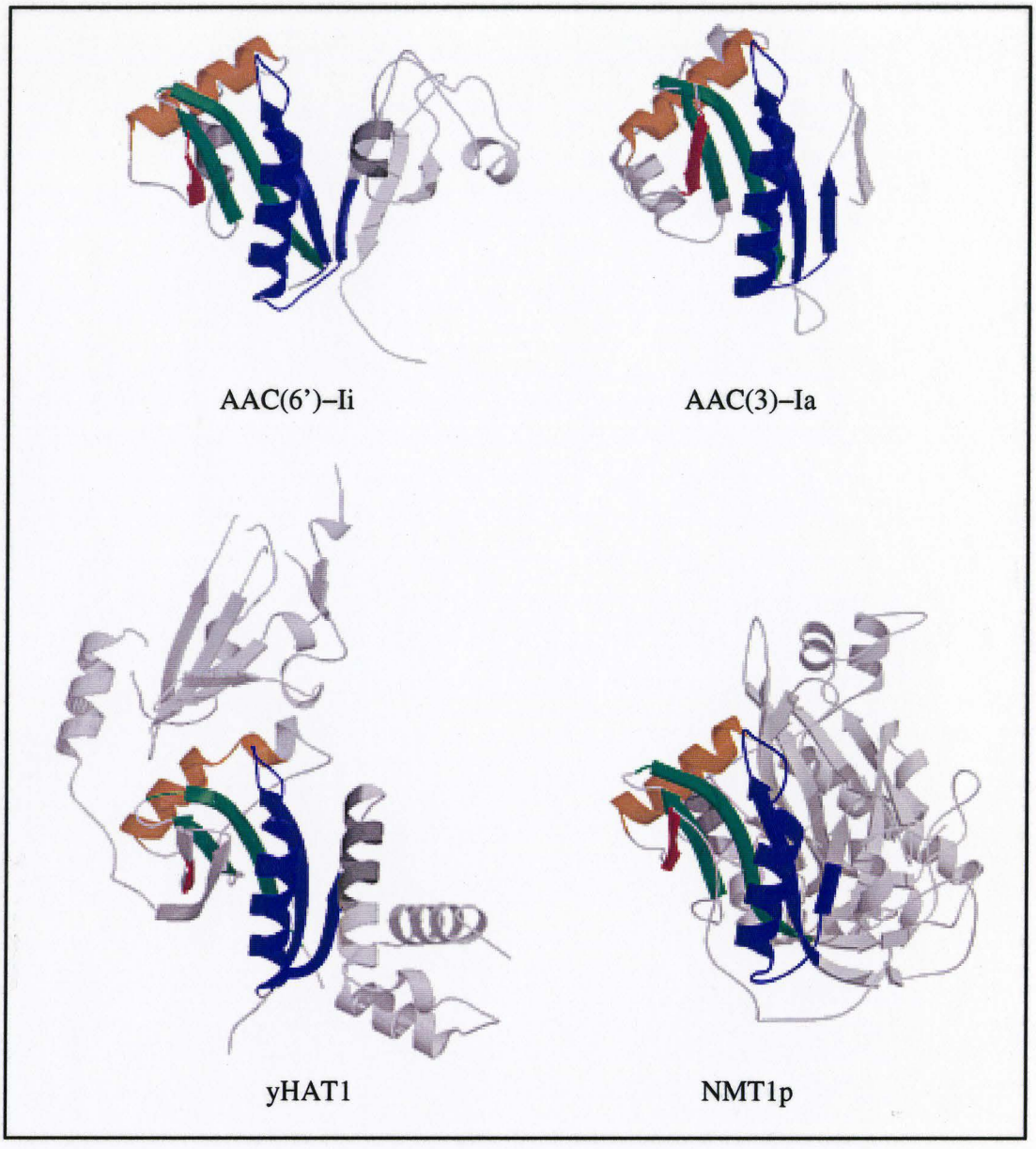

Figure 3.17 Structural comparison of GNAT superfamily members. The crystal structures of AAC(6')–Ii, AAC(3)–Ia, yHAT1, and NMT1p are shown so as to highlight the common fold shared among them. Regions that are structurally similar in all four structures are coloured the same and dissimilar parts of the protein structures are coloured light grey. Regions that are similar in two of the four structures are coloured dark grey. The colouring corresponds to that used in Figure 3.16. The figure was generated using Bobscript (Kraulis, 1991).

Coenzyme A Binding Site

The cofactor binding site of both yHAT1 and AAC(3)-Ia includes the βαβ unit at the end of the conserved β sheet (Dutnall et al., 1998; Wolf et al., 1998), which corresponds to β4α3β5 in AAC(6')-Ii. Likewise, residues within this region are involved in cofactor binding in both NMT1p (Bhatnagar et al., 1998) and in AAC(6')-Ii (Figure 3.16). Furthermore, the majority of hydrogen-bond interactions between the cofactor and all four proteins involve main-chain amino and carbonyl groups. In fact, five of the seven main-chain hydrogen bonds observed in AAC(6')-Ii are conserved in yHAT1, AAC(3)-Ia, and NMT1p (Figure 3.10, section 3.3.3; Figure 3.18). The exceptions are the Glu141 hydrogen bond to the adenine ring, which is not observed in any of the others, and the Thr89 amide interaction with the α-phosphate group, which is absent in both NMT1p and yHAT1. In contrast, the interactions formed with side-chain groups involve various residues from the four GNAT superfamily structures. Only the hydrogen bond seen between the hydroxyl group of residue Thr89 and the α-phosphate group is maintained in yHAT1 (Ser233) and AAC(3)-Ia (Thr124). However, this interaction is not observed in NMT1p, where the corresponding residue is Pro184. A number of the residues that contribute to the hydrophobic environment surrounding the β-methyl of the acetyl group in AAC(6')-Ii are conserved in both yHAT1 and NMT1p. For instance, the residues corresponding to Leu73 and Leu109 contribute to the hydrophobic pockets surrounding the β-methyl group in yHAT1 and the acyl chain of the cofactor in NMT1p (Dutnall et al., 1998; Bhatnagar et al., 1998).

The conformation of the CoA moiety is somewhat similar in the four GNAT superfamily structures in that the molecule binds in a bent conformation. However, the number of bends differs in the various cofactors. For instance, whereas a bend occurs around the PC6-PC7 positions in all four bound-cofactors, an additional sharp bend is located at the pyrophosphate group in AAC(6')-Ii and NMT1p. Consequently, the orientation of the adenine and ribose rings of the CoA moiety differs in the four structures (Figure 3.18). This diversity likely explains why interactions formed between a given protein and the 3'-phosphoadenosine moiety of its respective cofactor are not conserved among the four members. Indeed, neither yHAT1 nor AAC(3)-Ia appear to make intimate contact with either adenine base, distinguishing them from most CoA-binding proteins (Engel & Wierenga, 1996).

As mentioned, yHAT1, AAC(3)-Ia, and NMT1p employ a βαβ unit to bind the coenzyme A moiety, with the loop leading into the α helix of the unit involved in pyrophosphate binding (Dutnall et al., 1998, Wolf et al., 1998; Bhatnagar et al., 1998). AAC(6')-Ii binds its cofactor in a similar manner, with β4α3β5 comprising the βαβ unit. Interestingly, this mode of binding is similar to that observed for many nucleotide-binding proteins, which employ a βαβ Rossmann dinucleotide binding fold (Dutnall et al., 1998, Wolf et al., 1998; Rao and Rossmann, 1973). Although the CoA-binding domain of succinyl-CoA synthetase also contains a Rossman fold, the CoA chains point in opposite directions (reviewed in Modis & Wierenga, 1998). That is, "the relative position of the adenine moiety which is 'above' the sheet in yHAT1 (and AAC(3)-Ia,

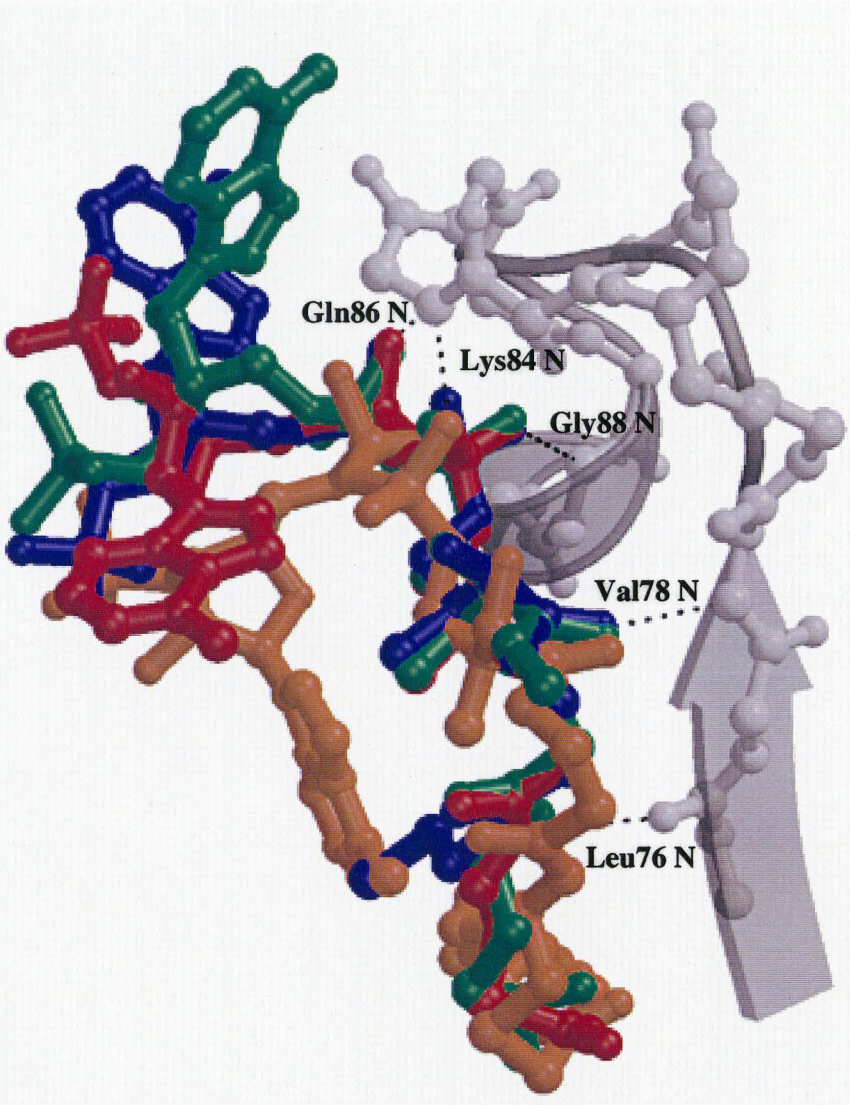

Figure 3.18 Cofactor conformations in GNAT superfamily members. The figure shows the AcCoA conformation observed in AAC(6')–Ii (red) and yHAT1 (green), the conformation of CoA seen in AAC(3)–Ia (blue), and the conformation of S–(2–oxo)pentadecylCoA observed in NMT1p (orange). Also indicated are the five conserved hydrogen–bond interactions present between the cofactor molecules and the main–chain atoms of the different acyltransferases. Only the main–chain atoms of AAC(6')–Ii are shown (in grey), overlayed with the secondary structure assignment as a transparent object.

NMT1p, and AAC(6')-Ii) is 'below' the sheet in the classical mode of binding" (Modis & Wierenga, 1998). Furthermore, whereas a tight turn typically exists between the first β strand and the α helix of the βαβ unit, this loop is somewhat longer in GNAT superfamily members (reviewed in Modis & Wierenga, 1998). Therefore, the topology seen in the CoA-dependent *N*-acylating enzymes is unique among CoA-binding proteins (Modis & Wierenga, 1998).

Since the ternary complex for only NMT1p has been determined, little information regarding the aminoglycoside binding site of AAC(6')-Ii can be obtained from comparing the GNAT superfamily members. However, it should be noted that the molecular surface of AAC(3)-Ia exhibits a narrow canyonlike feature with negative electrostatic potential that extends away from the AcCoA-binding surface (Wolf et al., 1998). The walls of this canyon are created by residues in the α1α2 loop (Asp53) and the β5β6 loop (Asp147 and Asp150) (Wolf et al., 1998). Interestingly, these negatively charged residues correspond to Glu27, Asp112, and Asp115, respectively, in AAC(6')-Ii, which line the wall of its putative aminoglycoside binding site. Furthermore, sequence analyses and homology modeling results indicate that the 2'-*N*-acetyltransferases also have negatively charged residues in their predicted α1α2 and β5β6 loops (Wolf et al., 1998). Therefore, it is likely that all three AACs use similar substrate binding strategies, which exploit a narrow, negatively charged slot in which to bind their polycationic aminoglycoside substrates (Wolf et al., 1998). Substrate specificity is likely dictated by the variation in topology that occurs in these two loop regions.

Reaction Mechanism

Comparison of the four GNAT superfamily structures does not provide a great deal of information regarding the residues involved in catalysis in AAC(6')-Ii. Of the 80 residues that are structurally identical in the four acyltransferases, only one is chemically identical and seven are chemically similar (Figure 3.16). Furthermore, all of these residues are hydrophobic, suggesting that they are important for cofactor binding or protein folding, and not catalysis. However, although specific catalytic residues may not be identified by comparing the four acyltransferase structures, information regarding the reaction mechanism of AAC(6')-Ii may be obtained from such an analysis.

Dutnall *et al.* suggest that the binding of AcCoA to yHAT1 produces a conformational change in the enzyme. This theory is based on the results of proteolysis experiments, the authors' inability to grow apo-crystals, and the structure of the binary complex, which seems to require that the cofactor bind to the enzyme first in order to set up the putative histone binding site (Dutnall et al., 1998). Furthermore, binding of the enzyme's peptide substrate does not appear to produce a change in the proteolysis pattern of yHAT1 (Dutnall et al., 1998). Both of these observations are in agreement with that observed for AAC(6')-Ii, thus supporting the hypothesis that ligand-binding produces a significant conformational change in AAC(6')-Ii.

The acetylation of a substrate by an AcCoA-dependent enzyme can either occur via an acetylated enzyme intermediate or by direct transfer to the free amine of the

substrate. Several pieces of evidence support the theory that the reaction catalyzed by GNAT superfamily members occurs via the second mechanism, whereby a direct nucleophilic attack on the carbonyl carbon of the acyl group takes place. First, whereas all of the structures indicate that the acyl-CoA molecule binds first, none of them gives evidence of an acetylated enzyme intermediate (reviewed in Modis & Wierenga, 1998). Secondly, the *N*-myristoylation reaction catalyzed by NMT proceeds through a sequential ordered Bi-Bi mechanism in which the apo-enzyme and myristoyl-CoA form a high affinity complex to which the substrate protein binds to form a ternary complex (Rudnick et al., 1991). Furthermore, a similar reaction mechanism was recently determined for serotonin acetyltransferase, another member of the GNAT superfamily (De Angelis et al., 1998). Kinetic experiments indicate that the enzyme binds acetyl-CoA first and then its substrate, thereby forming a ternary complex (De Angelis et al., 1998). This ordered binding also suggests that a conformational change in the protein occurs after acetyl-CoA binding, allowing the substrate binding site to become accessible (De Angelis et al., 1998). Following direct transfer of acetyl group, the product is released first, followed by CoASH (De Angelis et al., 1998). Since serotonin acetyltransferase is a member of the GNAT superfamily, it is likely that AAC(6')-Ii also obeys an ordered Bi-Bi ternary complex mechanism.

Determination of the ternary complex of NMT1p reveals how direct acyl transfer may typically be catalyzed in GNAT family members. First, in order for direct acyl transfer to occur, the carbonyl of the acetyl group should be polarized to facilitate

nucleophilic attack on the carbon. In NMT1p, polarization is achieved by positioning the carbonyl group near the main-chain amides of Phe170 and Leu171, thereby creating an "oxyanion hole" and resulting in a partial positive charge on the carbon (Bhatnagar et al., 1998). The construction of this oxyanion hole is facilitated by a kink in strand βe that causes the main-chain amide groups of Phe170 and Leu171 to present to the carbonyl (Bhatnagar et al., 1998). This kink is somewhat conserved in the other three GNAT superfamily members, although to a lesser extent. Instead, yHAT1, AAC(3)-Ia, and AAC(6')-Ii display a classic β bulge at this location, resulting in the orientation of only one main-chain amide group towards the carbonyl group (Leu76 N in AAC(6')-Ii). This suggests that polarization of the carbonyl in these GNAT structures may occur by a different mechanism than that observed for NMT1p. Nevertheless, it is possible that a conformational change occurs within this β strand upon substrate binding, causing the neighbouring backbone NH group to present to the carbonyl and thereby create an oxyanion hole. However, this mechanism of polarization remains unlikely in the case of AAC(6')-Ii, considering that its adjacent residue is a proline (Pro75) and thus void of an amide group altogether. Interestingly, while Pro75 is not observed in other aminoglycoside acetyltransferases or GNAT members, it is highly conserved within the AAC(6')-Ii subfamily (Shaw et al., 1993;Neuwald & Landsman, 1997). This implies that either polarization of the carbonyl of the acetyl group occurs by a different mechanism in AAC(6')-Ii subfamily members, or that the carbonyl bond is not as polarized in AAC(6')-Ii subfamily members as it is in other GNAT proteins. Either way, the efficiency of aminoglycoside acetyltransferase may be compromised. This is consistent with the

observation that AAC(6')-Ii is a relatively inefficient detoxifying catalyst (Wright & Ladak). Thus, although residues surrounding the β bulge in strand β4 of AAC(6')-Ii are likely involved in the enzyme's reaction mechanism, the precise means of carbonyl polarization and acyl transfer remain to be determined.

GNAT Superfamily Sequence Motifs

The GNAT superfamily was initially recognized from a multiple-alignment and database search that identified four relatively conserved motifs (A-D) in a number of *N*-acetyltransferases (Neuwald & Landsman, 1997). Of these four motifs, motif A is universally conserved, motifs B and D are usually present, and motif C is frequently predicted to be missing (Neuwald & Landsman, 1997). Given the recent determination of several structures belonging to this expansive family, the significance and structural location of these motifs can now be evaluated.

Mutagenesis experiments indicate that motif A is involved in the binding of acetyl CoA (reviewed in Neuwald & Landsman, 1997). In the midst of motif A lies an invariant Arg/Gln-X-X-Gly-X-Gly/Ala segment (where X is any amino acid) which appears to be critical to cofactor binding, since mutation of any of these conserved residues greatly reduces the enzyme's activity (reviewed in Wolf et al., 1998 and Dutnall et al., 1998). Accordingly, motif A corresponds to the first β strand and the α helix in the cofactor-binding βαβ unit. The R/Q-X-X-G-X-G/A motif forms a number of interactions with the cofactor's pyrophosphate group, explaining why its conservation is important to acetyl

CoA binding. However, it should be noted that some variation in this sequence is obviously tolerated, considering both AAC(6')-Ii and NMT1p exhibit at least one deviation in this motif.

Motif B was also predicted to be involved in cofactor binding (Neuwald & Landsman, 1997). Although this motif corresponds to loop α4α5, helix α5, and strand β6 in AAC(6')-Ii, its topology differs dramatically in the other GNAT structures. However, in all instances motif B remains close to the active-site pocket. Wolf *et al.* suggest that the function of motif B is to contribute acidic residues to the substrate-binding site (Wolf et al., 1998). In agreement with this hypothesis, a number of negatively charged residues in motif B of AAC(6')-Ii line a putative aminoglycoside-binding site. Thus, variation in the topology of motif B could be readily tolerated, and perhaps even exploited to achieve substrate specificity.

Finally, motifs C and D appear to be more related to the folding pattern than to catalysis (Modis & Wierenga, 1998). While motif C starts just after strand β1 and terminates at the end of helix α1, motif D starts halfway up strand β2 and terminates at the end of strand β3 (AAC(6')-Ii nomenclature). Residues of both motifs contribute mainly to the hydrophobic core of the GNAT fold (Modis & Wierenga, 1998). The presence of motif C in AAC(6')-Ii and yHAT1 was somewhat unexpected, since its existence was not predicted by Neuwald and Landsman (1997). This suggests that the

inability to detect a given motif does not necessarily indicate that the corresponding structural elements will be absent from the fold, but rather that the sequence homology is too low to be detected.

3.4 Summary

The three-dimensional structure of aminoglycoside acetyltransferase(6')-Ii in complex with the cofactor acetyl coenzyme A has been determined at 2.7 Å resolution. The final model displays good canonical properties and lacks only the last C-terminal residue. The cofactor is situated in a cleft between the N-terminal and C-terminal arms of the protein, binding in a novel manner that is reminiscent of the classical mode of binding of dinucleotides to the Rossmann fold. Although the protein packed as a monomer in the $I4_132$ spacegroup, the most probable physiological dimer was established. Residues from the C-terminal half of the protein, primarily those located within or C-terminal to strand β6, are likely involved in the dimer interface.

Comparison of the structure of AAC(6')-Ii with the structures of other members of the GCN5-related *N*-acetyltransferase superfamily reveals a common folding pattern, despite negligible sequence identity. Thus, AAC(6')-Ii is a structural homolog of protein acetylating enzymes like yeast histone acetyltransferase and *N*-myristoyl transferase. This supports the hypothesis that AAC(6')-Ii possesses another function in *E. faecium* other than aminoglycoside inactivation (Wright & Ladak, 1997). Consistent with this theory, AAC(6')-Ii has been shown to acetylate small basic proteins in a discriminate

fashion (Wybenga-Groot et al., 1999). The negatively charged cleft in the AAC(6')-Ii•AcCoA structure that comprises its putative aminoglycoside-binding site could likely accommodate both cationic AGACs and positively charged peptide substrates. However, the manner in which AAC(6')-Ii catalyzes *N*-acetyltransfer for either substrate remains to be determined.

Chapter 4 Determination of the AAC(6')-Ii•AcCoA Complex to 2.15 Å Resolution

4.1 Experimental Procedures

4.1.1 Crystallization

Wild-type aminoglycoside acetyltransferase(6')-Ii was crystallized by the hanging drop vapour diffusion technique in the presence of a five-fold molar excess of acetyl coenzyme A under similar conditions as those described previously (Wybenga, 1997) and for SeMet-AAC(6')-Ii (section 3.2.1). Reproducible, diffraction quality crystals were obtained by suspending a 6 μL drop, containing 9.8 mg/mL of protein (in 25 mM HEPES, 2 mM EDTA, pH 7.5 buffer), 2.5 mM acetyl CoA, 5% (w/v) D(+)-sucrose, and 0.6 M ammonium sulfate, over a 1 mL reservoir of 1.8 M ammonium sulfate. Again, cube-like crystals grew over one to three weeks at 22 °C, with one crystal growing to dimensions of ~0.11×0.13 mm over three weeks. The crystal belonged to the body-centered cubic spacegroup $I4_132$, with unit-cell dimensions of $a = b = c = 147.46$ Å, and one protein molecule per asymmetric unit (Matthews, 1968). A solution of 2.5 M ammonium sulfate saturated with D-glucose was used as a cryo-protectant for the crystals.

4.1.2 Data Collection and Processing

X-ray diffraction experiments were performed on the X8C beamline at the National Synchrotron Light Source, Brookhaven National Laboratory under cryogenic

conditions using a Mar Research 34.5 cm plate as detector. Data was collected at 1.0720 Å using the oscillation method, with oscillation angles of one degree. Forty-five frames of data were collected at a detector-crystal distance of 300.0 mm, resulting in an upper resolution limit of 2.15 Å. However, upon processing the data with the data reduction program Mosflm (Leslie, 1990) and programs from the CCP4 program suite (CCP4, 1994), it was discovered that the crystal had not been rotated properly for a significant portion of the data collection. Consequently, only 18 frames of data proved to be useful for processing, resulting in an overall completeness of ~67%. As expected, the redundancy or multiplicity of the data set is much lower than that of the SeMet data set, due to the reduced completeness of the data. The low redundancy of the data is reflected in the relatively high R_{sym} values of 9.8% overall, and 29.6% for the highest resolution bin. Fortunately, these values are within acceptable ranges, as are the values for $\langle I/\sigma \rangle$, thereby enabling use of the data for structure determination to a higher resolution. Pertinent statistics for data collection and processing are summarized in Table 4.1. As indicated, the mosaicity of the high-resolution crystal increased significantly from that of the SeMet crystal, despite utilization of highly similar crystal freezing and storage conditions.

4.1.3 Structure Determination and Refinement

Due to the insufficient amount of diffraction data, the high-resolution data set was merged with data collected at the peak wavelength during the MAD experiments (section 3.2). In preparation for combining the two data sets, the MAD data set was scaled and

	Native AAC(6')-Ii•AcCoA	SeMet AAC(6')-Ii•AcCoA
Space Group	$I4_132$	$I4_132$
Unit Cell Dimensions	$a = b = c = 147.46$ Å	$a = b = c = 146.96$ Å
Mosaicity (°)	0.75	0.2
Resolution Limit (Å)	2.15	2.70
Unique Reflections	9797	7725
Redundancy	1.6	6.4
Completeness (%) *	66.9 (63.5)	99.9 (100.0)
R_{sym} *†	0.098 (0.296)	0.080 (0.185)
$\langle I/\sigma \rangle$ *	5.5 (2.7)	8.6 (4.0)

Table 4.1 Summary of data collection statistics
* Numbers given in brackets refer to data for the highest resolution shell. † For definition of R_{sym}, see equation (7), section 3.2.2. Values were calculated with either Mosflm (Leslie, 1990) or Scala (CCP4, 1994).

merged again with Scala (CCP4, 1994), this time without refinement of B-factors. This scaling method produced statistics only slightly altered from those of the previous scaling procedure (compare Table 3.1 and Table 4.1). The first frame of the MAD data set was then used as a reference for scaling the high-resolution data set. Again, the B-factors were not refined, but instead the scale factors were allowed to vary across the detector in a restrained manner. Subsequently, the structure factor amplitudes of the two data sets were combined such that only reflections from the peak, SeMet data set were used to a resolution of 2.7 Å (61.8% of final data set), and only the native data was used above this resolution (38.2% of final data set). As indicated by a weighted R_{merge} value of 0.087 and an overall R_{merge} of 0.180 (from Scaleit, CCP4, 1994), the two data sets merged reasonably well. Although these values indicate that the two data sets are sufficiently isomorphous and thus can be merged with confidence, they are somewhat higher than expected considering the contents of the unit cells are identical bar four selenium atoms.

This suggests that very slight conformational changes may exist between the low-resolution and high-resolution structures, such as the movement of loop regions or the enzyme's C-terminal tail. Despite the slightly higher than expected R_{merge} values, large changes in the structure of the AAC(6')-Ii•AcCoA complex at higher resolution were not anticipated. Furthermore, in both data sets the complex crystallized in the same spacegroup, with nearly identical unit cell dimensions. Therefore, the model attained previously from MAD experiments (chapter 3) could be used as a phasing model for determination of the high resolution structure. Iterative model refinement and manual adjustment was performed as described in sections 2.4 and 3.2.4, with slight modifications. Data in the resolution range 40-2.15 Å with $F_{obs} > 1\sigma F_{obs}$ was used in refinement (i.e. 83.0% of all available data), with 10.3% of the data used for structure validation (Brünger, 1992a). B-factor refinement was performed with target sigma values of 1.5, 2.0, 2.0, and 2.5 for bonded backbone, angle-related backbone, bonded side-chain, and angle-related side-chain atoms, respectively. The final model contains 181 of the possible 182 residues, one AcCoA molecule, and 109 ordered solvent molecules.

4.2 Results and Discussion

4.2.1 Quality of High Resolution AAC(6')-Ii•AcCoA Model

The structure refined to a crystallographic R factor of 21.4% and an R free of 25.7% using data between 40.0 and 2.15 Å with $F_{obs} > 1\sigma F_{obs}$. These values are somewhat higher than the original SeMet structure, (R = 18.8%, R free = 23.4%), despite

the increase in both resolution and the number of ordered solvent molecules assigned (increased from 28 to 109) (Table 4.2). However, although the R factors appear to indicate that the 2.15 Å structure is less accurate than that solved at 2.7 Å resolution, the higher resolution structure displays stereochemical properties, temperature factor profiles, and rms deviations from ideality comparable to those of the lower resolution structure (Figures 4.1 and 4.2, and Table 4.2). Furthermore, the rms difference between the two structures is only 0.23 Å, which is slightly less than the average Luzzati estimated coordinate error for the 2.7 Å structure (0.24 Å). Thus, the structures are essentially identical, and therefore the higher resolution structure should be considered as more accurate.

The larger R factors exhibited for the high resolution structure may reflect the fact that a selenomethionyl data set was combined with a normal, sulfur containing data set in order to obtain a complete data set. Accordingly, the $|\mathbf{F}_{obs}|$ used during refinement were merged from the two different data sets. However, the parameter file utilized for refinement indicated that the structure consisted of only wild-type methionine residues. Consequently, crystallographic refinement may have been adversely affected, resulting in higher R factors than expected. Nevertheless, given the identity between the 2.7 Å and 2.15 Å structures, and the fact that the final R values are well within the acceptable range, the increase is not thought to present a concern.

Refinement Statistics		
Amplitude cutoff	$F_{obs} > 1\sigma F_{obs}$	
Number of reflections used in refinement	12496	
Resolution range (Å)	40-2.15	
Completeness (working + test) (%)	83.0	
R factor (%)[a]	21.4	
R free (%)[a]	25.7	
Number of non-hydrogen atoms used in refinement		
Protein atoms	1452	
AcCoA atoms	51	
Water molecules	109	
Number of atoms with occupancy set to zero	7	
Stereochemistry Statistics		
Rmsd in bond lengths (Å)	0.008	
Rmsd in bond angles (°)	1.4	
Rmsd in dihedral angles (°)	25.0	
Rmsd in improper angles (°)	1.22	
Residues in Ramachandran plot (%)[b]		
Most favourable region	84.0	
Additionally allowed region	15.4	
Generously allowed region	0.6	
Disallowed region	0.0	
	Working set	**Test set**
Luzzati estimated coordinate error (Å)[c]	0.26	0.32
Temperature Factors		
Overall mean B value (Å^2)	9.9	
Isotropic thermal model	Restrained	
Isotropic thermal factor restraints	**RMS**	**SIGMA**
Main-chain bond (Å^2)	1.68	1.50
Main-chain angle (Å^2)	2.38	2.00
Side-chain bond (Å^2)	2.85	2.00
Side-chain angle (Å^2)	3.91	2.50

Table 4.2 Statistics for the final model of the AAC(6')-Ii•AcCoA complex at 2.15 Å resolution. [a] For definitions of R factor and R free, see section 2.4, equation (1). [b]Values were calculated using Procheck (Laskowski, 1993). [c] Values were calculated by X-PLOR using Luzzati's method for estimating coordinate errors (Luzzati, 1952).

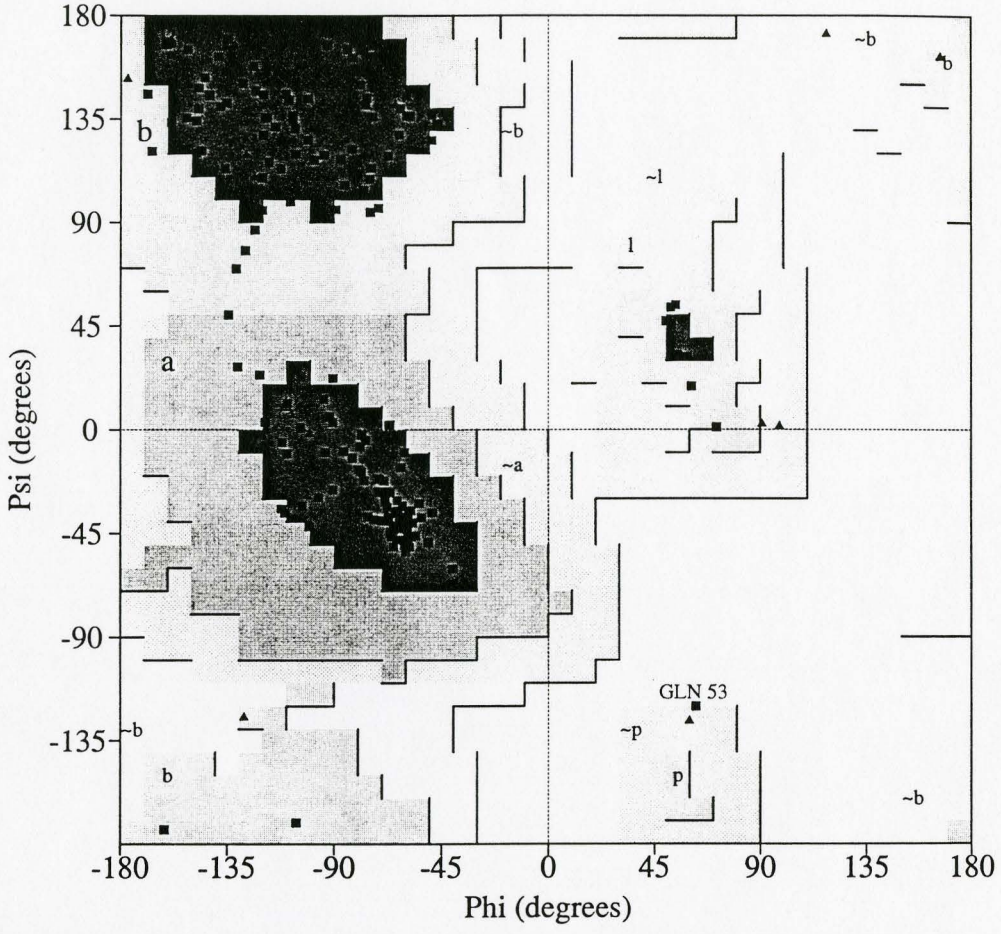

Figure 4.1 Ramachandran plot for high resolution AAC(6')-Ii•AcCoA structure. The main-chain torsional angle phi (N-C_α bond) is plotted against psi (Cα-C bond) for all residues of aminoglycoside acetyltransferase(6')-Ii. Glycine residues are represented by triangles; all other residues are shown as squares. The shaded or enclosed regions indicate sterically allowed angles, with the most favoured combinations in the darkest region, additionally allowed combinations in the next darkest region, and generously allowed angles in the least shaded region. Figure adapted from output of Procheck (Laskowski et al., 1993).

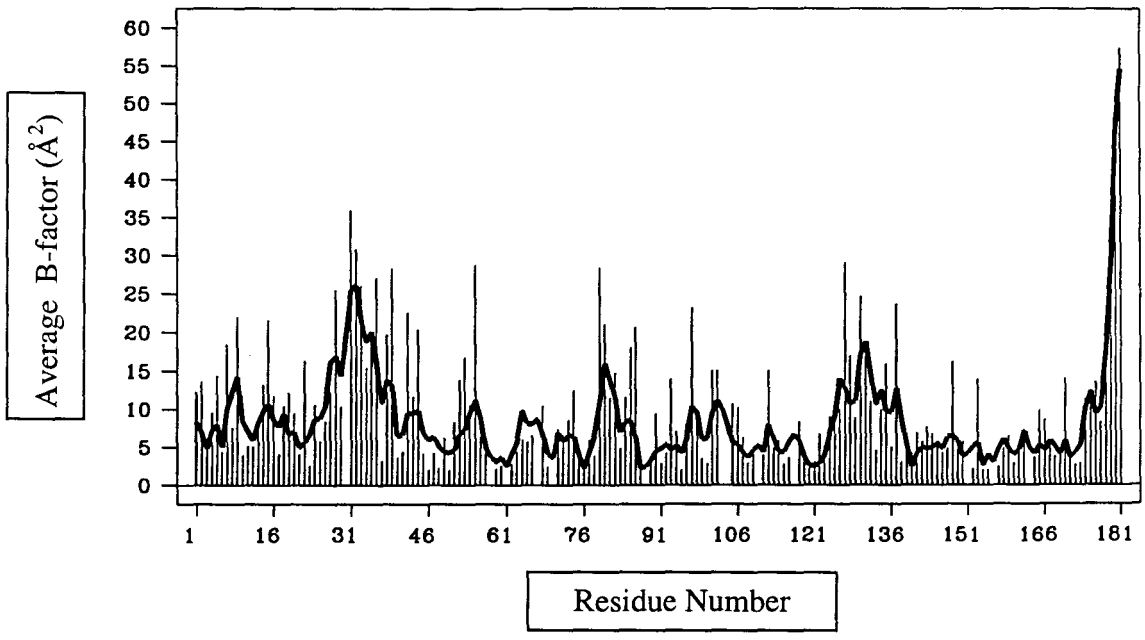

Figure 4.2 Mean values of the temperature factors for high resolution AAC(6')-Ii•AcCoA structure. Main-chain B values are indicated by the dark, thick line, while side-chain B-factors are represented by vertical spikes. Figure created by Bplot (CCP4, 1994).

4.2.2 High-Resolution Structure of the AAC(6')-Ii-AcCoA Complex

Careful examination of electron density maps for the high resolution structure failed to reveal any significant changes between the low resolution structure (2.7 Å) and the high resolution structure (2.15 Å). Density in the C-terminal region (residues 180-182) was somewhat better, such that the positions of residues Asp180 and Ser181 were altered slightly and the occupancy of Ser181 set to one instead of zero for all side-chain atoms. However, although some electron density was observed after Ser181, the final residue, Gln182, could still not be modeled with confidence. The location of the second peptide group in the pantetheine arm was also adjusted slightly to fit the electron density

better (Figure 4.3). The need for such an adjustment was suggested by the lower resolution data, considering the "awkwardness" of the hydrogen bond between the peptide's amide group and Leu76. However, whereas the lower resolution electron density map did not reveal how positioning of the cofactor could be improved, superior placement became apparent upon examination of the high-resolution data. Thus, it is not likely that the cofactor bound differently in the two crystals, but rather that the enhanced resolution of the data indicated a more accurate modeling of the molecule.

Alteration of the pantetheine moiety's position results in shortening of the hydrogen bond between the second peptide's amide group and the carbonyl oxygen of Leu76 from 3.4 Å to 3.0 Å (Figure 4.4). In addition, the distance between the peptide's carbonyl oxygen and a nearby water molecule is increased from 3.2 Å to 3.6 Å (Figure 4.4). Nevertheless, another water molecule is positioned only 3.1 Å away from the cofactor's carbonyl oxygen and 2.8 Å away from the first water molecule. Thus, the water-mediated interaction between the cofactor's adenine ring and its second peptide group appears to be maintained in the high resolution structure.

Refinement of the high resolution structure caused small adjustments in the distances between atoms involved in other protein-cofactor interactions as well. In general, these increases or decreases are minor, with distances changing by only ±0.1 Å in most instances (compare Figure 3.10 and Figure 4.4).

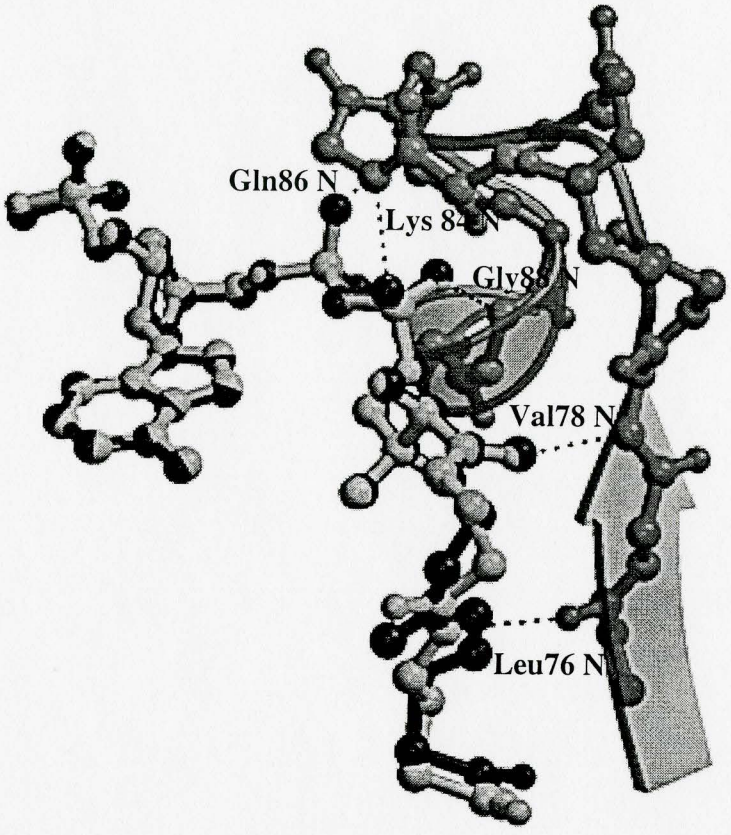

Figure 4.3 Comparison of cofactor conformation in 2.15 Å structure and 2.7 Å structure. The figure shows the slight change in conformation between the AcCoA molecule bound to the low resolution structure of AAC(6')-Ii (light grey) and that modeled for the high resolution complex (black). As in Figure 3.18, five conserved hydrogen-bonds are shown as dashed lines, and the main-chain atoms of the low resolution structure are shown (dark grey), overlayed with the secondary structure assignment.

Unfortunately, the location of the acyl moiety remains elusive even in the high-resolution structure. The temperature factors for the group remain relatively high (PS1:45.9, C:48.1, O:48.3, CH_3:48.4 $Å^2$), indicating that the group is very mobile. Furthermore, both conventional 2**F**o-**F**c maps and **F**o-**F**c omit maps show electron density near the hydroxyl group of Thr111 and the carbonyl oxygen of Gly110, as well as where the acyl moiety is presently modeled, suggesting that the acetyl tail assumes more than one conformation in the structure. This implies that the acyl group is flexible until an aminoglycoside substrate is bound, at which point the group would likely adopt a more fixed conformation, allowing transfer to occur. Due to the flexibility of this region, only water molecules found in this region for the lower resolution structure were modeled again despite the presence of additional peaks of electron density. Consequently, the distances between the carbonyl oxygen of the thioester and some nearby water molecules increased significantly, such that hydrogen bonding, and thereby stabilization of the thioester, appears to be lost (Figure 4.4). This is likely not the case, but merely a result of the inability to distinguish between density belonging to a water molecule, to the acetyl group itself, or to an interaction between two groups. Thus, it remains conceivable that the thioester is indeed stabilized by a water network and by water-mediated interactions in the absence of aminoglycoside substrate, as shown in Figure 3.10.

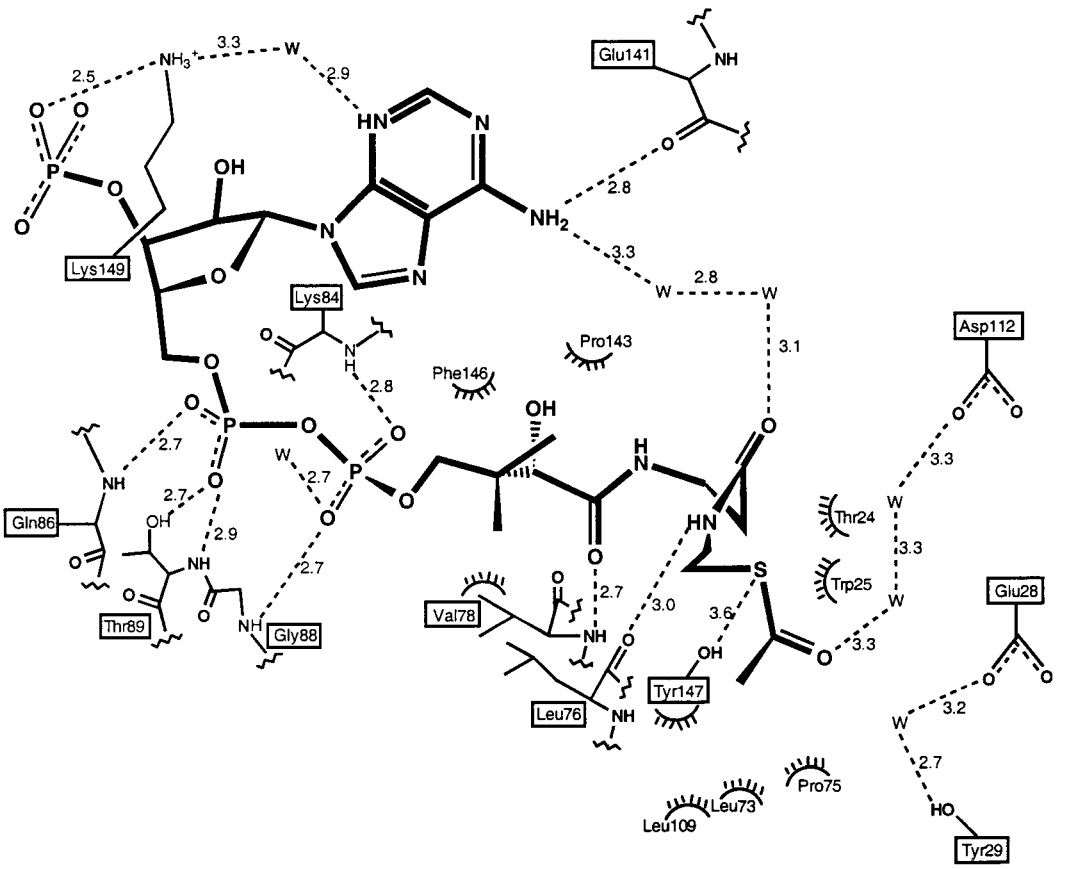

Figure 4.4 Interactions between AAC(6')-Ii and AcCoA for high resolution structure. The AcCoA molecule and residues forming interactions with it are drawn schematically, with dashed lines representing hydrogen bonds and semicircles indicating Van der Waals or hydrophobic interactions. Distances are given in Ångstroms.

Chapter 5 AAC(6')-Ii•AcCoA•Paromomycin Complex

5.1 Experimental Procedures

5.1.1 Crystallization

Wild-type aminoglycoside acetyltransferase(6')-Ii was crystallized by the hanging drop vapour diffusion technique in the presence of a five-fold molar excess of acetyl coenzyme A and a five-fold molar excess of paromomycin salt, an inhibitor of the enzyme. Cube-like crystals that were very similar in appearance to those grown in the presence of AcCoA only were obtained by suspending a 4 μL drop, containing 6 mg/mL of protein (in 25 mM HEPES, 2 mM EDTA, pH 7.5 buffer), 1.5 mM acetyl CoA, 1.5 mM paromomycin, 0.05 M Na citrate (pH 5.6), 0.05 M K/Na tartrate, and 0.8 M ammonium sulfate, over a 1 mL reservoir of 0.1 M Na citrate (pH 5.6), 0.1 M K/Na tartrate, and 1.6 M ammonium sulfate. Growth of the crystals under these conditions was not readily reproducible, given that only one well out of 24 grew crystals. The crystal belonged to the body-centered cubic spacegroup $I4_132$, with unit-cell dimensions of $a = b = c =$ 147.22 Å, and one protein molecule per asymmetric unit (Matthews, 1968). A solution of 0.1 M Na citrate (pH 5.6), 0.1 M Na/K tartrate, and 2.2 M ammonium sulfate saturated with D-glucose was used as a cryo-protectant for the crystals.

5.1.2 Data Collection and Processing

X-ray diffraction experiments were performed on the X8C beamline at the National Synchrotron Light Source, Brookhaven National Laboratory under cryogenic conditions using a Mar Research 34.5 cm scanner. Data was collected at 1.0720 Å using the oscillation method, with oscillation angles of one degree and a detector-crystal distance of 350.0 mm. Diffraction images thus obtained were processed to a resolution of 2.4 Å with the data reduction program Mosflm (Leslie, 1990) and programs from the CCP4 program suite (CCP4, 1994). Three rings of data, 3.91-3.88 Å, 3.68-3.65 Å, and 3.45-3.43 Å, were excluded from processing due to the presence of three ice rings at these resolutions. All the pertinent statistics for data collection and processing were found to be acceptable, with very high completeness, good data redundancy, and an $\langle I/\sigma \rangle$ value of 3.8 in the highest resolution bin (Table 5.1).

Space Group	$I4_132$
Unit Cell Dimensions	$a = b = c = 147.22$ Å
Mosaicity (°)	0.65
Resolution Limit (Å)	2.40
Unique Reflections	10585
Redundancy	3.8
Completeness (%) *	97.0 (99.2)
R_{sym} *†	0.079 (0.207)
$\langle I/\sigma \rangle$ *	9.3 (3.8)

Table 5.1 Summary of data dollection statistics for AAC(6')-Ii•AcCoA• paromomycin complex. * Numbers given in brackets refer to data for the highest resolution shell. † For definition of R_{sym}, see equation (7) section 3.2.2. Values were calculated with either Mosflm (Leslie, 1990) or Scala (CCP4, 1994).

5.1.3 Structure Determination and Refinement

The high resolution structure of AAC(6')-Ii•AcCoA was used as a phasing model for determination of the AAC(6')-Ii•AcCoA•paromomycin ternary complex by molecular replacement. Since the ternary complex crystallized in the same space group as the binary complex, and with very similar unit cell dimensions, the orientation of the protein molecule in the unit cell was already known, thus eliminating the need for rotation and translation searches. The 2.15 Å structure lacking all ordered solvent molecules was used as a phasing model for the initial round of refinement with X-PLOR version 3.843 as described above (sections 2.4 and 3.2.4). Initial refinement without solvent molecules was thought to be necessary since the aminoglycoside substrate was expected to displace some of the solvent molecules in the active site. Ordered solvent molecules were added to the structure after the first cycle of refinement.

Data in the resolution range 40-2.4 Å with $F_{obs} > 1\sigma F_{obs}$ was included in refinement (i.e. 96.3% of all available data), with 10.3% used for structure validation (Brünger, 1992a). B-factor refinement was performed with target sigma values of 1.5, 2.0, 2.0, and 2.5 for bonded backbone, angle-related backbone, bonded side-chain, and angle-related side-chain atoms, respectively. The final model contains 181 of the possible 182 residues, one AcCoA molecule, and 68 ordered solvent molecules.

5.2 Results and Discussion

The AAC(6')-Ii•AcCoA•paromomycin model refined readily, resulting in an R factor of 20.5% and an R free of 25.1% ($F_{obs} > 1\sigma F_{obs}$) after only two cycles of refinement with X-PLOR. However, at this point of refinement the electron density near the thioester group of the cofactor remained weak in conventional **F**o-**F**c, 2**F**o-**F**c, and 3**F**o-2**F**c maps. In fact, the density observed was similar to that observed for the high resolution structure, suggesting that the density could be due to ordered solvent molecules or noise instead of the paromomycin molecule. Regardless, the paromomycin substrate could not be modeled with confidence, and thus is missing from the final model.

Several possible explanations exist as to why the paromomycin molecule can not be observed in the crystal structure. First, the antibiotic may be too flexible in its bound state due to rotation about its three glycosidic bonds, so that it is too disordered to be observed. Second, paromomycin may adopt more than one conformation when binding to the active site of the AAC(6')-Ii•AcCoA complex, as has been observed for isepamicin (DiGiammarino et al., 1998). This too may result in disordered electron density that can not be interpreted. Finally, the paromomycin molecule may not actually be present in the crystal. This explanation seems the most likely, given that careful examination of electron density maps for the ternary complex structure fails to reveal any significant changes from the binary complex structure. In fact, the rms difference between the two structures is only 0.13 Å, with acetyl coenzyme A adopting the same conformation in both structures. In addition, the dimensions and spacegroup of the unit cell for the

ternary complex crystal are nearly identical to those of the binary complex, despite the presumed incorporation of a moderately large substrate. Furthermore, subtilisin digestion and NMR experiments indicate that a conformational change occurs upon formation of the ternary complex (Draker et al., 1999). Since even the slightest conformational change would likely affect crystal packing, it seems feasible that the paromomycin molecule was not incorporated into the crystal.

Concluding Remarks

In summary, the three-dimensional structure of aminoglycoside acetyltransferase(6')-Ii in complex with its cofactor, acetyl coenzyme A, was solved at 2.15 Å resolution. Despite negligible sequence similarity, AAC(6')-Ii shares a common folding pattern with members of an expansive GCN5-related *N*-acetyltransferase superfamily, namely yeast histone acetyltransferase HAT1, *N*-myristoyl transferase, and aminoglycoside acetyltransferase(3)-Ia. This establishes AAC(6')-Ii as a structural homolog of protein acylating enzymes, supporting the hypothesis that the enzyme has a physiological role other than antibiotic modification. Furthermore, given the number of different CoA-binding folds determined thus far (reviewed in Engel & Wierenga, 1996), the structural similarity between the CoA-binding site of bacterial aminoglycoside acetyltransferases and that of eukaryotic protein acetyltransferases supports the hypothesis that these enzymes share a common evolutionary origin.

The GNAT superfamily fold represents a novel CoA-binding fold, binding the cofactor in a manner similar to that seen in many nucleotide-binding proteins, but with the orientation of the adenine moiety reversed. Interestingly, the cofactor is bound by numerous hydrogen-bonds involving main-chain atoms of AAC(6')-Ii. In fact, main-chain atoms are thought to facilitate polarization of the carbonyl group during catalysis in

the ternary complex of NMT1p. However, at present, there is no evidence for such a reaction mechanism in AAC(6')-Ii.

The crystal structure of the AAC(6')-Ii•AcCoA complex is consistent with information obtained from previous structural studies. For instance, the cofactor is situated in a cleft between the N- and C-terminal arms of the protein, forming numerous interactions with both arms. This likely affects the mobility of the enzyme, which is consistent with the finding that AAC(6')-Ii becomes more ordered upon ligand-binding. Furthermore, the hydrophobic pocket surrounding the β-methyl of the acetyl group appears deep enough to accommodate propionyl CoA, which has been shown to be a suitable alternative cofactor for AAC(6')-Ii. In addition, the sulfur atom of AcCoA is positioned at the bottom of a cleft that appears to be large enough to accommodate only the 6'-amino group of an aminoglycoside substrate. This is in agreement with the broad substrate specificity observed for AAC(6')-Ii.

Due to the failure to determine the crystal structure of the AAC(6')-Ii•AcCoA•paromomycin complex and the high mobility of the cofactor's acetyl group in the binary complex, little information regarding the specific reaction mechanism employed by AAC(6')-Ii has been obtained. Two other members of the GNAT superfamily, serotonin acetyltransferase and NMT, have been shown to catalyze acyltransfer via an ordered Bi-Bi ternary complex mechanism, with acetyl CoA binding first. Given the lack of evidence for an acyl-intermediate for AAC(6')-Ii and its

structural homology to GNAT superfamily members, it is likely that the acetylation reaction catalyzed by AAC(6')-Ii also proceeds through a sequential Bi-Bi mechanism.

The next stage of the structural analysis of AAC(6')-Ii should undoubtedly be determination of the enzyme's ternary complex. In order to design a potent inhibitor of the enzyme, information regarding the reaction mechanism of the protein must be obtained. From a practical point of view, crystallization of AAC(6')-Ii in the presence of propionyl CoA, and in the presence of CoA and its minimum substrate neamine may provide the most useful information. First, the additional CH_2 group on propionyl CoA may help elucidate the exact positions of the carbonyl and β-methyl groups of the acetyl moiety, thus providing information as to which residues stabilize the moiety. Secondly, neamine contains only two sugar rings and thus may exhibit less mobility or flexibility in the aminoglycoside binding site, allowing it to be modeled. Such specific information regarding the reaction mechanism of AAC(6')-Ii is crucial to the structure-based drug design process, especially given the structural similarity between AAC(6')-Ii and many important eukaryotic enzymes.

References

Abrahams, J.P., and Leslie, A.G.W. (1996) Methods used in the structure determination of bovine mitochondrial F_1 ATPase. *Acta Crystallographica D***52**:30-42.

Bhatnagar, R.S., *et al.* (1998) Structure of N-myristoyltransferase with bound myristoylCoA and peptide substrate analogs. *Nature Structural Biology* **5(12)**:1091-1097.

Brünger, A.T. (1992a) Free R value: a novel statistical quantity for assessing the accuracy of crystal structures. *Nature* **355**:472-474.

Brünger, A.T. (1992b) X-PLOR Version 3.1 A system for x-ray crystallography and NMR. Yale University Press, New Haven, CT.

Brünger, A.T. (1993) Assessment of phase accuracy by cross validation: the free R value. Methods and applications. *Acta Crystallographica D***49**:24-36.

Brünger, A.T., Krukowski, A., and Erickson, J.W. (1990) Slow-cooling protocols for crystallographic refinement by simulated annealing. *Acta Crystallographica A***46**:585-593.

Brünger, A.T., Kuriyan, J., and Karplus, M. (1987) Crystallographic R factor refinement by molecular dynamics. *Science* **235**:458-460.

Centron, D., and Roy, P.H. (1998) Characterization of the 6'-N-aminoglycoside acetyltransferase gene aac(6')-Iq from the integron of a natural multiresistance plasmid. *Antimicrobial Agents and Chemotherapy* **42(6)**:1506-1508.

Chen, H.Y., and Williams, J.D. (1985) Transferable resistance and aminoglycoside-modifying enzymes in enterococci. *Journal of Medical Microbiology* **20**:187-196.

Cohen, M.L. (1992) Epidemiology of drug resistance: implications for a post-antimicrobial era. *Science* **257**:1050-1055.

Collaborative Computational Project, Number 4 (1994). *Acta Crystallographica D***50**:760-763.

Costa, Y., Galimand, M., Leclercq, R., Duval, J., and Courvalin, P. (1993) Characterization of the chromosomal *aac(6')-Ii* gene specific for *Enterococcus faecium*. *Antimicrobial Agents and Chemotherapy* **37**:1896-1903.

Courvalin, P.M., Shaw, W.V., and Jacob, A.E. (1978) Plasmid-mediated mechanisms of resistance to aminoglycoside-aminocyclitol antibiotics and to chloramphenicol in group D streptococci. *Antimicrobial Agents and Chemotherapy* **13**:716-725.

Cox, J.R., and Serpersu, E.H. (1997) Biologically important conformations of aminoglycoside antibiotics bound to an aminoglycoside 3'-phosphotransferase as determined by transferred nuclear Overhauser effect spectroscopy. *Biochemistry* **36**:2353-2359.

Davies, J.E. (1991) Aminoglycoside-aminocyclitol antibiotics and their modifying enzymes. In *Antibiotics in Laboratory Medicine*, 3rd ed. Lorian, V., ed. Williams and Wilkins, Baltimore, Maryland, pp.691-713.

Davies, J., Gilbert, W., and Gorini, L. (1964) Streptomycin, suppression, and the code. *Proceedings of the National Academy of Sciences* **51**:883-890.

Davis, B.D. (1988) Leading article; the lethal action of aminoglycosides. *Journal of Antimicrobial Chemotherapy* **22**:1-3.

De Angelis, J., Gastel, J., Klein, D.C., and Cole, P.A. (1998) Kinetic analysis of the catalytic mechanism of serotonin *N*-acetyltransferase (EC 2.3.1.87) *The Journal of Biological Chemistry* 273:3045-3050.

de La Fortelle, E., and Bricogne, G. (1997) Maximum-likelihood heavy-atom parameter refinement for multiple isomorphous replacement and multiwavelength anomalous diffraction methods. *Methods in Enzymology* **276**:472-494.

DiGiammarino, E.L., Draker, K., Wright, G.D., and Serpersu, E.H. (1998) Solution studies of isepamicin and conformational comparisons between isepamicin and butirosin A when bound to an aminoglycoside 6'-*N*-acetyltransferase determined by NMR spectroscopy. *Biochemistry* **37**:3638-3644.

Draker, K., Gardner, K.H., and Wright, G.D. (1999) Ligand effects on an aminoglycoside antibiotic resistance enzyme, AAC(6')-Ii: conformational changes detected by partial proteolysis, circular dichroism, protein NMR, and Trp fluorescence. Unpublished.

Drenth, J. (1994) Principles of Protein X-ray Crystallography. Springer-Verlag New York, Inc., New York, NY, pp.153-157, 205-209.

Dubin, D.T., Hancock, R., and Davis, B.D. (1963) The sequence of some effects of streptomycin in *Escherichia coli. Biochimica et Biophysica Acta* **74**:476-489.

Dutnall, R.N., Tafrov, S.T., Sternglanz, R., and Ramakrishnan, V. (1998) Structure of the histone acetyltransferase Hat1: a paradigm for the GCN5-related N-acetyltransferase superfamily. *Cell* **94**:427-438.

Eliopoulos, G.M., Wennersten, C., Zighelboim-Daum, S., Reiszner, E., Goldmann, D., and Moellering, R.C., Jr. (1988) High-level resistance to gentamicin in clinical isolates of *Streptococcus* (*Enterococcus*) *faecium. Antimicrobial Agents and Chemotherapy* **32**:1528-1532.

Engel, C., and Wierenga, R. (1996) The diverse world of coenzyme A binding proteins. *Current Opinion in Structural Biology* **6**:790-797.

Gorini, L. (1974) In *Ribosomes.* Nomura, M., Tissieres, A., and Lengyel, P., eds. Cold Spring Harbor Laboratory, Cold Spring Harbor, NY, pp.791-803.

Haley, R.W., Hightower, A.W., Khabbaz, R.F., Thornsberry, C., Martone, W.J., Allen, J.R., and Hughes, J.M. (1982) The emergence of methicillin-resistant *Staphylococcus aureus* infections in United States hospitals. *Annals of Internal Medicine* **97**:297-308.

Hannecart-Pokorni, E., Depuydt, F., De Wit, L., Van Bossuyt, E., Content, J., and VanHoof, R. (1997) Characterization of the 6'-*N*-aminoglycoside acetyltransferase gene *aac(6')-Il* associated with a *sulI*-type integron. *Antimicrobial Agents and Chemother*apy **41**:314-318.

Hendrickson, W.A. (1991) Determination of macromolecular structures from anomalous diffraction of synchrotron radiation. *Science* **254**:51-58.

Hendrickson, W.A., and Ogata, C.M. (1997) Phase determination from multiwavelength anomalous diffraction measurements. *Methods in Enzymology* **276**:494-523.

Hinshaw, H.C., and Feldman, W.H. (1945) Streptomycin in treatment of clinical tuberculosis: a preliminary report. *Proceedings of the Staff Meetings of the Mayo Clinic* **20**:313-318.

Ho, J.L., and Barza, M. (1987) Role of aminoglycoside antibiotics in the treatment of intra-abdominal infection. *Antimicrobial Agents and Chemother*apy **31**:485-491.

Hoffmann, S.A. and Moellering, R.C., Jr. (1987) The Enterococcus: "Putting the bug in our ears". *Annals of Internal Medicine* **106**:757-761.

Hon, W.-C., McKay, G.A., Thompson, P.R., Sweet, R.M., Yang, D.S.C., Wright, G.D., and Berghuis, A.M. (1997) Structure of an enzyme required for aminoglycoside antibiotic resistance reveals homology to eukaryotic protein kinases. *Cell* **89**:887-895.

Horodniceanu, T., Bougueleret, L., El-Solh, N., Bieth, G., and Delbos, F. (1979) High-level, plasmid-borne resistance to gentamicin in *Streptococcus faecalis* subsp. *Zymogenes. Antimicrobial Agents and Chemother*apy **16**:686-689.

Hunter, T.H. (1947) Use of streptomycin in the treatment of bacterial endocarditis. *American Journal of Medicine* **2**:436-442.

Jacoby, G.A. (1996) Antimicrobial-resistant pathogens in the 1990s. *Annu. Rev. Med.* **47**:169-179.

Janin, J. (1995) Principles of protein-protein recognition from structure to thermodynamics. *Biochimie* **77**:497-505.

Jawetz, E., Gunnison, J.B., and Coleman, V.R. (1950) The combined action of penicillin with streptomycin or chloromycetin on enterococci *in vitro. Science* **111**:254-256.

Jiang, J.-S., and Brünger, A.T. (1994) Protein hydration observed by x-ray diffraction; solvation properties of penicillopepsin and neuraminidase crystal structures. *Journal of Molecular Biology* **243**:100-115.

Jones, T.A., Zou, J.-Y., Cowan, S.W., and Kjeldgaard, M. (1991) Improved methods for building protein models in electron density maps and the location of errors in these models. *Acta crystallographica A***47**:110-119.

Jones, W.G., Barie, P.S., Yurt, R.W., and Goodwin, C.W. (1986) Enterococcal burn sepsis. *Archives of Surgery* **121**:649-653.

Kabsch, W., and Sander, C. (1983) Dictionary of protein secondary structure: pattern recognition of hydrogen-bonded and geometrical features. *Biopolymers* **22**:2577-2637.

Kaji, H., and Kaji, A. (1965) Specific binding of sRNA to ribosomes: effect of streptomycin. *Proceedings of the National Academy of Sciences* **54**:213-219.

Kingman, S. (1994) Resistance a European problem, too. *Science* **264**:363-365.

Kleywegt, G.J., and Brünger, A.T. (1996) Checking your imagination: applications of the free R value. *Structure* **4**:897-904.

Kraulis, P.J. (1991) MOLSCRIPT: a program to produce both detailed and schematic plots of protein structures. *Journal of Applied Crystallography* **24**:946-950.

Krogstad, D.J., Korfhagen, T.R., Moellering, R.C., Jr., Wennersten, C., and Swartz, M.N. (1978a) Plasmid-mediated resistance to antibiotic synergism in enterococci. *Journal of Clinical Investigation* **61**:1645-1653.

Krogstad, D.J., Korfhagen, T.R., Moellering, R.C., Jr., Wennersten, C., Swartz, M.N., Perzynski, S., and Davies, J. (1978b) Aminoglycoside-inactivating enzymes in clinical isolates of *Streptococcus faecalis*. *Journal of Clinical Investigation* **62**:480-486.

Laskowski, R.A., MacArthur, M.W., Moss, D.S., and Thornton, J.M. (1993) PROCHECK: a program to check the stereochemical quality of protein structures. *Journal of Applied Crystallography* **26**:283-290.

LeMaster, D.M., and Richards, F.M. (1985) ^{1}H-^{15}N heteronuclear NMR studies of *Escherichia coli* thioredoxin in samples isotopically labeled by residue type. *Biochemistry* **24**:7263-7268.

Leslie, A.G.W. (1990) Macromolecular data processing. In *Crystallographic Computing*. Moras, V.D., Podjarny, A.D., and Thierry, J.C., eds. Oxford University Press, Oxford, UK, pp. 27-38.

Lovering, A.M., Bywater, M.J., Holt, H.A., Champion, H.M., and Reeves, D.S. (1988) Resistance of bacterial pathogens to four aminoglycosides and six other antibacterials and prevalence of aminoglycoside modifying enzymes, in 20 UK centres. *Journal of Antimicrobial Chemotherapy* **22**:823-839.

Luzzati, V. (1952) Statistical treatment of errors in the determination of crystal structures. *Acta crystallographica* **5**:802-810.

Mandell, G.L., Kaye, D., Levison, M.E., and Hook, E.W. (1970) Enterococcal endocarditis. *Archives of Internal Medicine* **125**:258-264.

Matthews, B.W. (1968) Solvent content of protein crystals. *Journal of Molecular Biology* **33**:491-497.

Merritt, E.A., and Murphy, M.E.P. (1994) *Raster3D* version 2.0. A program for photorealistic molecular graphics. *Acta crystallographica D***50**:869-873.

Miller, G.H., et al. (1997) The most frequent aminoglycoside resistance mechanisms – changes with time and geographic area: a reflection of aminoglycoside usage patterns? *Clinical Infectious Diseases* **24(Suppl. 1)**:S46-S62.

Moazed, D., and Noller, H.F. (1987) Interaction of antibiotics with functional sites in 16S ribosomal RNA. *Nature* **327**:389-394.

Modis, Y., and Wierenga, R. (1998) Two crystal structures of N-acetyltransferases reveal a new fold for CoA-dependent enzymes. *Structure* **6**:1345-1350.

Moellering, R., Weinberg, A., Zimmermann, R., and Wennersten, C. (1970) Antibiotic synergism against group D streptococci (abstract). *Clinical Research* **18**:445.

Moellering, R.C., Jr. (1991) The enterococcus: a classic example of the impact of antimicrobial resistance on therapeutic options. *Journal of Antimicrobial Chemotherapy* **28**:1-12.

Moellering, R.C., Jr., Korzeniowski, O.M., Sande, M.A., Wennersten, C.B. (1979) Species-specific resistance to antimicrobial synergism in *Streptococcus faecium* and *Streptococcus faecalis*. *The Journal of Infectious Diseases* **140**:203-208.

Moellering, R.C., Jr., Murray, B.E., Schoenbaum, S.C., Adler, J., and Wennersten, C.B. (1980) A novel mechanism of resistance to penicillin-gentamicin synergism in *Streptococcus faecalis*. *The Journal of Infectious Diseases* **141**:81-86.

Moellering, R.C., Jr., and Weinberg, A.N. (1971a) Studies on antibiotic synergism against enterococci. II. Effect of various antibiotics on the uptake of ^{14}C-labeled streptomycin by enterococci. *Journal of Clinical Investigation* **50**:2580-2584.

Moellering, R.C., Jr., Wennersten, C., Medrek, T., and Weinberg, A.N. (1971b) Prevalence of high-level resistance to aminoglycosides in clinical isolates of enterococci. *Antimicrobial Agents and Chemotherapy* **1970**:335-340.

Moellering, R.C., Jr., Wennersten, C., and Weinberg, A.N. (1971c) Studies on antibiotic synergism against enterococci. I. Bacteriologic studies. *The Journal of Laboratory and Clinical Medicine.* **77**:821-828.

Moellering, R.C., Jr., Wennersten, C., and Weinstein, A.J. (1973) Penicillin-tobramycin synergism against enterococci: a comparison with penicillin and gentamicin. *Antimicrobial Agents and Chemotherapy* **3**:526-529.

Murray, B.E. (1990) The life and times of the enterococcus. *Clinical Microbiology Reviews* **3**:46-65.

Musser, J.M. (1995) Antimicrobial agent resistance in mycobacteria: molecular genetic insights. *Clinical Microbiology Reviews* **8**:496-514.

Navia, M.A., and Peattie, D.A. (1993) Structure-based drug design: applications in immunopharmacology and immunosuppression. *Trends in Pharmacological Sciences (TiPs)* **14**:189-195.

Neu, H.C. (1992) The crisis in antibiotic resistance. *Science* **257**:1064-1073.

Neuwald, A.F., Landsman, D. (1997) GCN5-related histone *N*-acetyltransferases belong to a diverse superfamily that includes the yeast SPT10 protein. *Trends in Biochemical Sciences* **22**:154-155.

Nicholls, A., Sharp, K., and Honig, B. (1991) Protein folding and association: insights from the interfacial and thermodynamic properties of hydrocarbons. *Proteins* **11**:281-296.

Piepersberg, W., Distler, J., Heinzel, P., and Perez-Gonzalez, J.-A. (1988) Antibiotic resistance by modification: many resistance genes could be derived from cellular control genes in Actinomycetes – a hypothesis. *Actinomycetologica* **2**:83-98.

Powell, M.J.D. (1977) Restart procedures for the conjugate gradient method. *Mathematical Programming* **12**:241-254.

Price, K.E. (1986) Aminoglycoside research 1975-1985: prospects for development of improved agents. *Antimicrobial Agents and Chemotherapy* **29**:543-548.

Radika, K., and Northrop, D.B. (1984) Correlation of antibiotic resistance with V_{max}/K_m ratio of enzymatic modification of aminoglycosides by kanamycin acetyltransferase. *Antimicrobial Agents and Chemotherapy* **25**:479-482.

Rather, P.N., Munayyer, H., Mann, P.A., Hare, R.S., Miller, G.H., and Shaw, K.J. (1992) Genetic analysis of bacterial acetyltransferases: identification of amino acids determining the specificities of the aminoglycoside 6'-*N*-acetyltransferase Ib and IIa proteins. *Journal of Bacteriology* **174**:3196-3203.

Read, R.J. (1986) Improved Fourier coefficients for maps using phases from partial structures with errors. *Acta Crystallographica A***42**:140-149.

Rhodes, G. (1993) *Crystallography Made Crystal Clear: A Guide for Users of Macromolecular Models.* Academic Press, Inc., San Diego, CA.

Richardson, J.S., Getzoff, E.D., and Richardson, D.C. (1978) The β bulge: a common small unit of nonrepetitive protein structure. *Proceedings of the National Academy of Science USA* **75**:2574-2578.

Rudnick, D.A., et al. (1991) Kinetic and structural evidence for a sequential ordered Bi Bi mechanism of catalysis by Saccharomyces cerevisiae myristoyl-CoA:protein N-myristoyl transferase. *Journal of Biological Chemistry* **266**:9732-9739.

Schaberg, D.R., Alford, R.H., Anderson, R., Farmer, J.J., III, Melly, M.A., and Schaffner, W. (1976) An outbreak of nosocomial infection due to multiply resistant *Serratia marcescens*: evidence of interhospital spread. *The Journal of Infectious Diseases* **134**:181-188.

Schaberg, D.R., Culver, D.H., and Gaynes, R.P. (1991) Major trends in the microbial etiology of nosocomial infection. *The American Journal of Medicine* **91(3B)**:72S-75S.

Schatz, A., Bugie, E., and Waksman, S.A. (1944) Streptomycin, a substance exhibiting antibiotic activity against gram-positive and gram-negative bacteria. *Proceedings of the Society for Experimental Biology and Medicine* **55**:66-69.

Shaw, K.J., Rather, P.N., Hare, R.S., and Miller, G.H. (1993) Molecular genetics of aminoglycoside resistance genes and familial relationships of the aminoglycoside-modifying enzymes. *Microbiological Reviews* **57**:138-163.

Spera, R.V., Jr., and Farber, B.F. (1992) Multiply-resistant *Enterococcus faecium*; the nosocomial pathogen of the 1990s. *JAMA* **268**:2563-2564.

Spera, R.V., Jr., and Farber, B.F. (1994) Multidrug-resistant *Enterococcus faecium*; an untreatable nosocomial pathogen. *Drugs* **48(5)**:678-688.

Standiford, H.D., de Maine, J.B., and Kirby, W.M.M. (1970) Antibiotic synergism of enterococci; relation to inhibitory concentrations. *Archives of Internal Medicine* **126**:255-259.

Terán, F.J., Alvarez, M., Suárez, J.E., and Mendoza, M.C. (1991) Characterization of two aminoglycoside-(3)-*N*-acetyltransferase genes and assay as epidemiological probes. *Journal of Antimicrobial Chemotherapy* **28**:333-346.

Terwilliger, T.C. (1997) Multiwavelength anomalous diffraction phasing of macromolecular structures: analysis of MAD data as single isomorphous replacement with anomalous scattering data using the MADMRG program. In *Methods in Enzymology* **276**:530-537. Also see http://www.solve.lanl.gov

Thompson, J.D., Higgins, D.G., and Gibson, T.J. (1994) CLUSTAL W: improving the sensitivity of progressive multiple sequence alignment through sequence weighting, position-specific gap penalties and weight matrix choice. *Nucleic Acids Research* **22**:4673-4680.

Toala, P., McDonald, A., Wilcox, C., and Finland, M. (1969) Susceptibility of group D streptococcus (enterococcus) to 21 antibiotics *in vitro*, with special reference to species differences. *The American Journal of the Medical Sciences* **258**:416

Travers, A. (1999) Chromatin modification: how to put a HAT on the histones. *Current Biology* **9**:R23-R25.

Travis, J. (1994) Reviving the antibiotic miracle? *Science* **26**:360-362.

Weinstein, A.J., and Moellering, R.C., Jr. (1973) Penicillin and gentamicin therapy for enterococcal infections. *JAMA* **223**:1030-1032.

Weinstein, R.A., and Kabins, S.A. (1981) Strategies for prevention and control of multiple drug-resistant nosocomial infection. *American Journal of Medicine* **70**:449-454.

Wennersten, C.B., and Moellering, R.C., Jr. (1980) Mechanism of resistance to penicillin-aminoglycoside synergism in *Streptococcus faecium.* In *Current Chemotherapy and Infectious Diseases*, vol.1. Nelson, J.D, and Grassi, C., eds. American Society for Microbiology, Washington, D.C., pp.710-712.

Weston, S.A., *et al.* (1998) Crystal structure of the anti-fungal target N-myristoyltransferase. *Nature Structural Biology* **5(3)**:213-21.

Williams, J.W., and Northrop, D.B. (1978) Kinetic mechanisms of gentamicin acetyltransferase I. *The Journal of Biological Chemistry* **253**:5902-5907.

Williams, R.J., and Heymann, D.L. (1998) Containment of antibiotic resistance. *Science* **279**:1153-1154.

Wolf, E., Vassilev, A., Makino, Y., Sali, A., Nakatani, Y., and Burley, S.K. (1998) Crystal structure of a GCN5-related N-acetyltransferase: *Serratia marcescens* aminoglycoside 3-N-acetyltransferase. *Cell* **94**:439-449.

Woodcock, J., Moazed, D., Cannon, M., Davies, J., and Noller, H.F. (1991) Interaction of antibiotics with A- and P-site specific bases in 16S ribosomal RNA. *The EMBO Journal* **10**:3099-3103.

Wright, G.D., Berghuis, A.M., and Mobashery, S. (1999) Aminoglycoside antibiotics: structures, functions, and resistance. In *Resolving the Antibiotic Paradox: Progress in Drug Design and Resistance.* Rosen, B.P. and Mobashery, S., eds. Plenum Publishing Corporation, New York, New York, pp. 27-69.

Wright, G.D., and Ladak, P. (1997) Overexpression and characterization of the chromosomal aminoglycoside 6'-*N*-acetyltransferase from *Enterococcus faecium. Antimicrobial Agents and Chemotherapy* **41**:956-960.

Wybenga, L. (1997) Structural analysis of aminoglycoside acetyltransferase(6')-Ii and the flavoprotein domain of nitric oxide synthase 2 by crystallographic techniques. Biochemistry 4B06 Thesis, Department of Biochemistry, McMaster University.

Wybenga-Groot, L.E., Draker, K., Wright, G.D., and Berghuis, A.M. (1999) Crystal structure of an aminoglycoside 6'-*N*-acetyltransferase: defining the GCN5-related *N*-acetyltransferase superfamily fold. *Structure* **7**:497-507.

Zervos, M.J., Kauffman, C.A., Therasse, P.M., Bergman, A.G., Mikesell, T.S., and Schaberg, D.R. (1987) Nosocomial infection by gentamicin-resistant *Streptococcus faecalis. Annals of Internal Medicine* **106**:687-691.

Zimmermann, R.A., Moellering, R.C., Jr., and Weinberg, A.N. (1971) Mechanism of resistance to antibiotic synergism in enterococci. *Journal of Bacteriology* **105**:873-879.

Appendix 1

Enzyme Activity Assay

1. Mix 600 uL Assay Buffer, 80 uL DTDP (20 mM stock in Assay Buffer), 80 uL AcCoA (0.7 mM stock in Assay Buffer), and 20 uL kanamycin A (1.0 mM stock in Assay Buffer) in a 1 mL plastic cuvette.
2. Preincubate samples at 37°C for 2-5 minutes. Monitor at 324 nm for one minute, then add 20 uL protein sample (use buffer only as a negative control).
3. Monitor for about five minutes to get a good slope; record slope.

Enzyme Purification Protocol

1. Inoculate 1 mL of LB medium supplemented with 100 μg/mL ampicillin with a single colony of *E.coli* W3110/pPLaac. Grow in a rotary shaker at 250 rpm, 37 °C overday.
2. Inoculate 25 mL of LB medium (100 μg/mL amp) with 1 mL overday and grow overnight in a rotary shaker at 250 rpm, 37 °C.
3. Inoculate 1 L of LB broth (100 μg/mL amp) with overnight and grow at 250 rpm, 37 °C until the optical density at 590 nm (OD_{590}) reaches ~0.6 as measured on a UV-Visible Spectrophotometer. At this point, induce overexpression by adding isopropyl-β-D-thiogalactopyranoside (IPTG) to a final concentration of 1 mM and allowing cells to continue growing at 250 rpm, 37 °C.
4. Once the OD_{590} measures ~1.6, the cells are harvested by centrifugation (GSA rotor, 7500 rpm, 15 min) in a Sorvall RC-5B Refrigerated Superspeed Centrifuge.

The following steps should be performed at 4 °C or on ice:

5. The cell pellet was washed with 0.85% NaCl and spun down (GSA rotor, 7500 rpm, 15 min) in a Sorvall RC-5B Refrigerated Superspeed Centrifuge. **Note**: At this stage the cell pellet can either be frozen or lysed immediately.
6. The pellet was resuspended (by shaking) in ice-cold Lysis Buffer (< 40 mL) and passed through a French Pressure Cell Press (20,000 psi) 2-3 times to ensure complete lysis of the cells.
7. The suspension was centrifuged (SS-34 rotor, 10,000 rpm, 10 min) and the supernatant stored on ice. The cell pellet was resuspended in a small volume of Lysis Buffer (< 10 mL), centrifuged (SS-34 rotor, 10,000 rpm, 10 min), and the supernatant pooled with that of the first spin.
8. The pooled sample was loaded onto a 2.5 x 16 cm column of Q-Sepharose (~75 mL bed volume) equilibrated with Buffer A, connected to a GradiFrac System from Pharmacia Biotech AB. The protein was eluted at a flow rate of 0.5 mL/min with the following program:

Volume (mL)	Concentration of Buffer B (%)	Fraction Size (mL)
0	0	0
300	0	6
350	10	6
400	10	6
550	40	6
625	40	6
725	70	6
726	100	0
850	100	0

9. The OD_{280} of every second fraction was measured in quartz cuvettes and every second or third fraction within the protein peaks monitored for activity by the assay described above. Active fractions were pooled and the final sample concentrated to ~10 mL using a nitrogen concentrator from Amicon (P_{max} =75 psi) fitted with a PM10 Diaflo ultrafiltration membrane (Amicon, Beverly, Massachusetts). The concentrating cell and filter were rinsed with 2-3 mL of Buffer A and the rinse pooled with the concentrated sample.
10. The sample was then loaded onto a 2.5 x 113 cm column of Sephadex G100 (610 mL bed volume) equilibrated with Buffer A, connected to a peristaltic pump. The protein was eluted with Buffer A at a flow rate of 0.5 mL/min and the absorbance/activity of the fractions monitored as in step 9.
11. The pooled fractions were applied to a 2.5 x 33 cm column of Gent-Agarose equilibrated with Buffer A, connected to a GradiFrac System. (The gentamicin-Affi-Gel was prepared by other members of the lab as previously described by Van Pelt and Northrop (1984) using gentamicin C as ligand.) The protein was eluted at a flow rate of 0.5 mL/min with the following program:

Volume (mL)	Concentration of Buffer B (%)	Fraction Size (mL)
0	0	0
275	0	6
450	30	6
500	30	6
675	60	6
725	60	6
800	100	6
900	100	0
1000	0	0

12. The absorbance/activity of the fractions were monitored as in step 9. Active fractions were prepared for sodium dodecyl sulfate polyacrylamide gel electrophoresis (SDS-PAGE) by mixing 20 μL of sample with 20 μL of loading buffer and boiling the mixture for ~10 min. Samples were run on a 12% SDS-PAGE gel and stained by a standard silver staining protocol. Standard protocols for SDS-PAGE and silver staining were obtained from the "Wright Lab Standard Protocol" binder.
13. Samples that gave a single band by silver staining were pooled and the volume reduced to ~1-2 mL using Centriprep 10 concentrators and Centricon 10 concentrators, both from Amicon. The sample was then dialyzed overnight against 1 L of Buffer A (Spectra/Por molecularporous membrane tubing, 12-14,000 MWCO, VWR Scientific or SnakeSkin, 10,000 MWCO, Pierce).
14. The sample's protein concentration was determined by the Bradford assay (Bradford, 1976), using bovine serum albumin as the standard and reagents purchased from Bio-Rad. The appropriate concentration was achieved either through further concentrating or by dilution with Buffer A.
15. The final sample was filtered with a Sterile Acrodisc, 0.2 μm (Gelman Sciences) and stored in sterile eppendorf tubes at 4 °C.

References

Bradford, M.M. (1976) *Analytical Biochemistry* **72**:248-254.

Van Pelt and Northrop (1984) *Biochem. Biophys.* **230**:250.